





Instituto de Bioquímica Vegetal y Fotosíntesis,  
cicCartuja, Universidad de Sevilla – CSIC

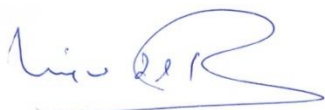


## **REDOX BIOINTERACTOME OF CYTOCHROMES IN RESPIRATION AND PHOTOSYNTHESIS**

Trabajo presentado por el Licenciado **D. José Blas Moreno Beltrán** para  
optar al título de Doctor en Bioquímica por la Universidad de Sevilla con  
la acreditación de Mención Internacional

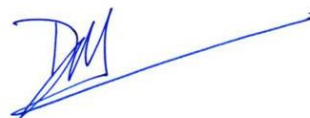
Sevilla, 2015

Directores



**Dr. D. Miguel Ángel  
De la Rosa Acosta**

Catedrático de  
Universidad de Sevilla



**Dra. Dña. Irene  
Díaz Moreno**

Profesora Titular de  
Universidad de Sevilla



*A mis abuelos*



# AGRADECIMIENTOS

---

Quiero expresar mi agradecimiento a quienes han contribuido en la realización de esta tesis y me han apoyado durante todos estos años.

En primer lugar, me voy a dirigir a mis directores de tesis, a quienes agradezco la oportunidad que me han brindado de realizar los estudios de doctorado en el grupo de Biointeractómica. La dedicación al mundo científico por parte de Miguel Ángel e Irene es encomiable. Me han servido de referencia continua durante estos años.

Agradezco a Miguel Ángel sus conocimientos y paciencia. Su experiencia y consejos han sido muy valiosos para afrontar los vaivenes de esta etapa.

Agradezco a Irene su compromiso, perseverancia en los momentos difíciles y haberme abierto las puertas en el fascinante mundo de la resonancia magnética nuclear. Sus numerosas enseñanzas, ayuda prestada y consejos científicos han sido decisivos para la realización de esta tesis. Estoy muy agradecido por el apoyo recibido durante todos estos años.

En segundo lugar, me dirijo a Antonio Díaz Quintana, quien me introdujo en la biología estructural y del que he aprendido una capacidad crítica sin precedentes. Su apoyo en computación unido a sus consejos y continua predisposición han sido muy importantes.

En tercer lugar, mi agradecimiento a mis compañeros de laboratorio, en especial a Jonathan, Isabel, Alejandra, Kati y Carlos, con los que he compartido numerosas aventuras científicas y vivencias. Muchas gracias también a Estrella, Rafa, Silvia, Sofía y Curro. Os agradezco haberme sentido muy arropado y querido por vosotros, a quienes animo a que sigáis con esa motivación extra que hace falta para estar entre los mejores. Os voy a echar mucho de menos.

A continuación, también agradezco a aquellos colaboradores cuya aportación ha sido decisiva para mi formación y el desarrollo de esta tesis doctoral:

Al Prof. Marcellus Ubink (*Leiden Institute of Chemistry*, Universidad de Leiden, Holanda), por la estancia realizada en 2011 y por la formación recibida en resonancia paramagnética y cálculos de “docking” para complejos transitorios. Sus estudios en los últimos años sobre complejos transitorios de metaloproteínas han servido de referencia para nuestras aproximaciones experimentales y posteriores discusiones.

A la Prof. Paola Turano y a la Dr. Rebecca Del Conte (*CERM - Centro di Ricerca di Risonanze Magnetiche*, Universidad de Florencia, Italia), por la formación recibida en 2012-2013 en el CERM, el laboratorio de referencia mundial de metaloproteínas. Estoy muy agradecido a la “familia del CERM” por haberme acogido y arropado como uno más. Mi paso por el Sesto

Fiorentino ha dejado muy buenos momentos y amigos. Mil gracias a todo el personal del CERM.

A la Dr. Louise Bird (*OPPF – Oxford Protein Production Facility*, Universidad de Oxford, Reino Unido), por la estancia realizada en 2015 y la formación recibida en biología molecular.

Al Dr. Adrián Velázquez Campoy (Universidad de Zaragoza, España), y al Dr. Pedro M. Nieto Mesa (Instituto de Investigaciones Químicas, Universidad de Sevilla - CSIC, España), por sus discusiones científicas en los campos de calorimetría isotérmica de valoración y resonancia magnética nuclear, respectivamente.

Agradezco a las siguientes fuentes de financiación:

Ministerio de Educación de España – Beca FPU (AP2009-4092) y estancia dentro del programa de movilidad FPU (AP2009-4092-2011).

Ministerio de Economía y Competitividad de España – Proyecto BFU (BFU2012-31670/BMC), que me ha financiado con un contrato de 4 meses para finalizar la resolución de los estudios estructurales.

Proyecto Europeo BioNMR – Proyecto BIO-NMR-00130 y beca de viaje destinada a jóvenes biólogos estructurales (BIO-NMR-00130-2012).

Junta de Andalucía – Incentivo al grupo de investigación (BIO-198).

cicCartuja – Servicios generales y Plataforma de Biointeractividad.

Proyecto Europeo Instruct – Proyecto Instruct Proposal ID 1163.

Sociedad Española de Bioquímica y Biología Molecular; Grupo de Resonancia Magnética Nuclear de la Real Sociedad Española de Química – Bolsas de viaje para la asistencia a cursos y congresos.

Finalmente,

A mis padres, que se han sacrificado y me hicieron amar el mundo académico. Esta tesis doctoral está dedicada a la memoria de mis abuelos, que superaron las enormes dificultades que se encontraron cuando jóvenes con una vida de trabajo, esfuerzo y sacrificio. La realización de esta tesis doctoral coincidió con el fallecimiento de dos abuelos (justo al comenzarla y en la etapa final). Mis padres me han transmitido ese ideal de superación.

A mis hermanos, por su sincera amistad e incansables ánimos.

A María Isabel, por su cariño, paciencia y apoyo.







# CONTENTS

---

<b>I. FOREWORD .....</b>	<b>1</b>
<b>II. ABBREVIATIONS .....</b>	<b>5</b>
<b>III. LIST OF PUBLICATIONS .....</b>	<b>11</b>
<b>IV. SUMMARY .....</b>	<b>17</b>
<b>V. INTRODUCTION .....</b>	<b>21</b>
V.1. Transient protein-protein redox interactions .....	23
V.2. Cellular respiration .....	24
V.2.1. Oxidative phosphorylation .....	25
V.2.2. Fluid and solid models of the mitochondrial respiratory chain .....	27
V.2.3. Cytochrome <i>c</i> signalosome .....	33
V.2.4. Respiratory complex III .....	36
V.2.5. Respiratory complex IV .....	38
V.2.6. L-galactono-1,4-lactone dehydrogenase .....	39
V.3. Photosynthesis .....	39
V.3.1. Photosynthetic electron chain .....	40
V.3.2. Photosynthetic supercomplexes .....	43
V.3.3. Plastocyanin and cytochrome <i>c</i> <sub>6</sub> .....	46
V.3.4. Cytochrome <i>b</i> <sub>6</sub> <i>f</i> .....	48
V.4. Methods based on solution Nuclear Magnetic Resonance to study transient protein-protein interactions and structural determination .....	50

V.4.1. Diamagnetic chemical-shift perturbations and surface mapping .....	50
V.4.2. Paramagnetic relaxation enhancement .....	53
V.4.3. Nuclear Magnetic Resonance restrained-driven docking computations .....	57
V.4.4. Nuclear Magnetic Resonance structure calculation ..	59
V.5. Isothermal Titration Calorimetry experiments .....	61
<b>VI. OBJECTIVES.....</b>	<b>63</b>
<b>VII. RESULTS AND DISCUSSION .....</b>	<b>67</b>
VII.1. Electron transfer complexes as examples of short-lived complexes.....	69
VII.2. Promiscuity and binding surfaces.....	70
VII.3. Stoichiometry and binding affinity.....	72
VII.4. From the encounter ensemble to the well-defined complex .....	74
VII.5. Electron transfer pathways within respiratory supercomplexes .....	77
VII.6. Post-translational regulation .....	77
<b>VIII. CONCLUSIONS .....</b>	<b>81</b>
<b>IX. GENERAL REFERENCES.....</b>	<b>85</b>
<b>X. APPENDIX I.....</b>	<b>105</b>
<b>XI. APPENDIX II.....</b>	<b>269</b>
<b>XII. APPENDIX III.....</b>	<b>305</b>

# **I. FOREWORD**



---

# I. FOREWORD

---

The current document has been prepared by following the guidelines required by the University of Seville to submit the PhD thesis as a collection of journal papers and book chapters. It consists of the following sections:

II. The list of Abbreviations.

III. The list of Publications and merits of the PhD candidate.

IV. A brief Summary of the PhD thesis.

V. An Introduction and the state-of-the-art.

VI. A section covering the Objectives of the PhD thesis.

VII. A brief description of the Results and Discussion, including main achievements and outcomes.

VIII. The global Conclusions.

IX. The list of References which have been cited in previous sections.

X. The Appendix I, containing the published journal papers and an accepted book chapter, on which the PhD thesis is based. All papers were published in scientific journals indexed in Journal Citation Reports (JCR) database.

XI. The Appendix II, containing an additional manuscript in preparation focused on the structure and dynamics of a phosphomimetic variant of cytochrome *c*.

XII. The Appendix III, including three datasets deposited in the Biological Magnetic Resonance Data Bank (BMRB) and the Protein Data Bank (PDB).





## **II. ABBREVIATIONS**



---

## II. ABBREVIATIONS

---

ADP	Adenosine 5'-diphosphate
AIRs	Ambiguous Interaction Restraints
ATP	Adenosine 5'-triphosphate
<i>b<sub>6</sub>f</i>	Cytochrome <i>b<sub>6</sub>f</i> complex
BMRB	Biological Magnetic Resonance Data Bank
BN-PAGE	Blue Native Polyacrylamide Gel Electrophoresis
C11orf83	Chromosome 11 open reading frame 83
<i>Cbc<sub>1</sub></i>	Cytochrome <i>bc<sub>1</sub></i> complex
<i>Cc</i>	Cytochrome <i>c</i>
<i>Cc<sub>1</sub></i>	Cytochrome <i>c<sub>1</sub></i>
<i>Cc<sub>6</sub></i>	Cytochrome <i>c<sub>6</sub></i>
<i>CcO</i>	Cytochrome <i>c</i> oxidase
CSP	Chemical-Shift Perturbations
cI	complex I
cII	complex II
cIII	complex III
cIV	complex IV
cV	complex V
<i>Em</i>	Mid-point redox potential
ET	Electron Transfer
Fd	Ferredoxin
FNR	Ferredoxin-NADP Reductase
Fv	Flavodoxin
GALDH	L-GAlactono-1,4-Lactone DeHydrogenase
HADDOCK	High Ambiguity Driven biomolecular DOCKing

HetNOE	Heteronuclear NOE
HIG1	Hypoxia-Inducible Genes
HSQC	Heteronuclear Single-Quantum Correlation
ITC	Isothermal Titration Calorimetry
JCR	Journal Citation Reports
$K_D$	Equilibrium dissociation constant
$k_{\text{off}}$	Dissociation rate constant
$k_{\text{on}}$	Association rate constants
LHCI	PSI light-harvesting antenna complexes
LHCII	PSII light-harvesting antenna complexes
n	stoichiometry
NADH	Reduced Nicotinamide Adenine Dinucleotide
NADPH	Reduced Nicotinamide Adenine Dinucleotide Phosphate
NDH	NADH dehydrogenase
NMR	Nuclear Magnetic Resonance
NOE	Nuclear Overhauser Effect
NOESY	NOE spectroscopy
OXPHOS	Oxidative phosphorylation
Pc	Plastocyanin
PCD	Programmed Cell Death
<i>p</i> CMF	<i>p</i> -carboxymethyl-L-phenylalanine
PCS	Pseudo-Contact Shifts
PDB	Protein Data Bank
PQ	Plastoquinone
PRE	Paramagnetic Relaxation Enhancement
PSI	Photosystem I
PSII	Photosystem II

---

Q	Coenzyme Q <sub>10</sub>
R <sub>1</sub>	Longitudinal relaxation rate constant
R <sub>2</sub>	Transverse relaxation rate constant
RDC	Residual Dipolar Couplings
RMD	Restrained Molecular Dynamics
RNOS	Reactive Nitrogen and Oxygen Species
SC	respiratory SuperComplex
SPR	Surface Plasmon Resonance
$\Delta G$	Gibbs energy
$\Delta H$	Binding enthalpy
$\Delta S$	Binding entropy
$\Delta\delta_{\text{avg}}$	Average CSP values



## **III. LIST OF PUBLICATIONS**





---

### III. LIST OF PUBLICATIONS

---

In the following list, the publications and achievements of the PhD candidate are enumerated as follows:

#### 1. Journal Papers:

- González-Arzola, K, Díaz-Moreno, I, Cano-González, A, Díaz-Quintana, A, Velázquez-Campoy, A, **Moreno-Beltrán, B**, López-Rivas, A and De la Rosa, MA. (2015) Structural basis of SET/TAF- $\beta$  inhibition by cytochrome *c*. *Proc. Natl. Acad. Sci. U.S.A.*, under review.
- **Moreno-Beltrán, B**, Díaz-Moreno, I, González-Arzola, K, Guerra-Castellano, A, Velázquez-Campoy, A, De la Rosa, MA and Díaz-Quintana, A. (2015) Respiratory complexes III and IV can each bind two molecules of cytochrome *c* at low ionic strength. *FEBS Lett.*, 589, 476-483.
- **Moreno-Beltrán, B**, Díaz-Quintana, A, González-Arzola, K, Velázquez-Campoy, A, De la Rosa, MA and Díaz-Moreno, I. (2014) Cytochrome  $c_1$  exhibits two binding sites for cytochrome *c* in plants. *Biochim. Biophys. Acta – Bioenergetics*, 1837, 1717-1729.
- Díaz-Moreno, I, Hulsker, R, Skubak, P, Foerster, JM, Cavazzini, D, Finiguerra, MG, Díaz-Quintana, A, **Moreno-Beltrán, B**, Rossi, G, Ullmann, GM, Pannu, NS, De la Rosa, MA and Ubbink, M. (2014) The dynamic complex of cytochrome  $c_6$  and cytochrome *f* studied

### III. List of Publications

---

with paramagnetic NMR spectroscopy. *Biochim. Biophys. Acta – Bioenergetics*, 1837, 1305-1315.

- Olloqui-Sariego, JL, **Moreno-Beltrán, B**, Díaz-Quintana, A, De la Rosa, MA, Calvente, JJ and Andreu, R. (2014) Temperature-driven changeover in the electron-transfer mechanism of a thermophilic plastocyanin. *J. Phys. Chem. Lett.*, 5, 910-914.
- Hervás, M, Bashir, Q, Leferink, NG, Ferreira, P, **Moreno-Beltrán, B**, Westphal, AH, Díaz-Moreno, I, Medina, M, De la Rosa, MA, Ubbink, M, Navarro, JA and van Berkel, WJ. (2013) Communication between (L)-galactono-1,4-lactone dehydrogenase and cytochrome *c*. *FEBS J.*, 280, 1830-1840.

#### 2. Book Chapter:

- **Moreno-Beltrán, B\***, González-Arzola, K\*, Martínez-Fábregas, J, Díaz-Moreno, I and De la Rosa, MA (2015). Cytochrome *c*-based signalosome. In *Redox proteins in supercomplexes and signalosomes*, Editors: R.O. Louro and I. Díaz-Moreno. Taylor and Francis Editorial Group. ISBN: 978-1-4822-5110-4.

\*These authors have equally contributed.

#### 3. Oral Communications:

- A ‘Floating Boat Bridge’ of cytochrome *c* molecules in plant respirasome.  
**Moreno-Beltrán, B**, González-Arzola, K, Díaz-Quintana, A, Velázquez-Campoy, A, De la Rosa, MA, Díaz-Moreno, I.

14<sup>th</sup> FEBS Young Scientists' Forum. August 27<sup>th</sup>-30<sup>th</sup>, 2014, Paris (France).

- NMR as a tool to analyze the structural basis for the different functional properties of phosphorylated cytochrome *c*.

**Moreno-Beltrán, B.**

3<sup>rd</sup> Bio-NMR Annual User-Meeting: NMR in protein dynamics and structural biology. June 10<sup>th</sup>-13<sup>th</sup>, 2013, Budapest (Hungary).

#### **4. International Research Training:**

- Oxford Protein Production Facility (OPPF), Division of Structural Biology, University of Oxford, United Kingdom. 2 weeks, 2015.  
Supervisor: Dr. Louise Bird.
- Magnetic Resonance Center (CERM), Department of Chemistry, University of Florence, Italy. 16 weeks, 2012-2014.  
Supervisors: Prof. Paola Turano and Dr. Rebecca Del Conte
- Leiden Institute of Chemistry, Department of Protein Chemistry, University of Leiden, The Netherlands. 16 weeks, 2011.  
Supervisor: Prof. Marcellus Ubbink

#### **5. Awards:**

- The Finn Wold Travel Award of The Protein Society. 2015.
- Second Place of the Roche Prize to the Best Poster at the XXXVII SEBBM Congress. Title: How redox proteins form transient complexes in photosynthesis and respiration. 2014.
- 14<sup>th</sup> FEBS Young Scientists' Forum Award. 2014.

### III. List of Publications

---

- Short-Term Travelling Fellowship for Structural Biologists of European Bio-NMR Project (BIO-NMR-00130). 2012.
- Short-Term Fellowship of International Exchange Program of Spanish Ministry of Education (AP2009-4092-2011). 2011.
- Graduated Research PhD Fellowship of Spanish Ministry of Education (AP2009-4092). 2010.

## **IV. SUMMARY**



---

## IV. SUMMARY

---

Protein complex formation is at least a two-step process in which the formation of a final, well-defined complex entails the initial formation of a dynamic encounter complex. Highly transient complexes, with lifetimes in the order of microseconds-milliseconds, exhibit moderate or low binding affinities, with dissociation constants in the micromolar-millimolar range. Electron transfer reactions mediated by soluble redox proteins exchanging electrons between large membrane complexes in respiration and photosynthesis are excellent examples of transient interactions.

Here, experimental approaches based on diamagnetic and paramagnetic Nuclear Magnetic Resonance (NMR) spectroscopy and/or Isothermal Titration Calorimetry, combined with computational methods, have been used to study the molecular recognition processes of particular redox complexes involved in respiration and photosynthesis.

The studies presented in this PhD thesis go into detail about the structural and biophysical basis of the following redox complexes: cytochrome *c*-cytochrome *c*<sub>1</sub>, cytochrome *c*-cytochrome *c* oxidase and cytochrome *c*-galactonolactone dehydrogenase interactions in respiration and the cytochrome *c*<sub>6</sub>-cytochrome *f* adduct in photosynthesis. All these ET ensembles exhibit proper coupling between the redox centers although they differ in their dynamic behavior, which can be ascribed to its distinct functionality depending on the organism and its biological context. Moreover, post-translational regulation can alter the usual mechanisms of such proteins. In this work, the structure determination of

a phosphomimetic mutant of cytochrome *c* has also been addressed by means of solution NMR.

Needless to say, such a multidisciplinary methodology, combining experimental and computational methods, opens new perspectives in our understanding of the dynamic, transient adducts formed between proteins beyond the model systems herein analyzed.



## **V. INTRODUCTION**



---

## V. INTRODUCTION

---

Electron transfer (ET) processes are of great importance in many of the metabolic pathways of living organisms. They are essential for, among other processes, cellular respiration and photosynthesis, in which biochemical energy obtained from the oxidation of nutrients or from capturing light is converted into adenosine 5'-triphosphate (ATP). In these two processes, small and soluble redox proteins facilitate ET between large membrane-embedded complexes via transient contacts (Hervás *et al.*, 2003; Lenaz and Genova, 2010; Hasan and Cramer, 2012).

General aspects of transient protein-protein redox interactions, cellular respiration and photosynthesis are presented in this section, as well as the fundamentals of the more relevant experimental and computational methodologies used.

### V.1 TRANSIENT PROTEIN-PROTEIN REDOX INTERACTIONS

Transient inter-protein complexes exhibit high a turnover and usually involve proteins that interact with several partners: *e.g.* ET chains in cellular respiration and photosynthesis or signal transduction cascades (Bashir *et al.*, 2011; Díaz-Moreno and De la Rosa, 2011; Schilder and Ubbink, 2013). Due to the interest in intermolecular ET, studies of interactions between redox proteins have provided a large amount of knowledge on transient complexes (Crowley and Ubbink, 2003; Prudêncio and Ubbink, 2004; Díaz-Quintana *et al.*, 2015).

To sustain the high turnover rates required for several biological processes, some proteins need to interact transiently. This phenomenon is achieved by a high dissociation rate constant ( $k_{\text{off}} \geq 10^3 \text{ s}^{-1}$ ). The association rate constants ( $k_{\text{on}}$ ) for such transient protein-protein complexes often vary from  $10^7$  to  $10^9 \text{ M}^{-1}\cdot\text{s}^{-1}$ . The binding affinity between two proteins that interact reversibly is defined by the equilibrium dissociation constant ( $K_{\text{D}}$ ), which is calculated as the ratio between  $k_{\text{off}}$  and  $k_{\text{on}}$ . Thus, the  $K_{\text{D}}$  values are generally in the  $\mu\text{M}$ - $\text{mM}$  range for transient contacts. The length of such interactions is significantly short, yielding complex lifetimes in the microsecond-millisecond time-scale. The lifetime of such complexes is calculated as the ratio between  $\text{Ln}2$  and the  $k_{\text{off}}$  value (Crowley and Ubbink, 2003; Prudêncio and Ubbink, 2004; Kastritis and Bonvin, 2013; Díaz-Quintana *et al.*, 2015).

## V.2 CELLULAR RESPIRATION

In eukaryotes, cellular respiration is based on a series of energy transformations and metabolic processes that take place in the cytoplasmic and mitochondrial compartments to convert biochemical energy from nutrients into ATP.

Mitochondrial or nuclear genetic defects involving enzymes acting in this process impair cellular respiration. In particular, tissues with a high energy demand are vulnerable to deficiencies in or damage to cellular respiration. Such mitochondrial dysfunctions are implicated in several diseases in humans such as Parkinson's disease, Alzheimer's disease, diabetes and cancer (DiMauro, 2004; Koopman *et al.*, 2012; Pinto and Moraes, 2014).

The following topics about eukaryotic cellular respiration are commented on in-depth below: oxidative phosphorylation, solid and fluid models of the mitochondrial electron chain, cytochrome *c* signalosome, respiratory complexes III and IV, along with the galactono-lactone dehydrogenase.

## V.2.1 OXIDATIVE PHOSPHORYLATION

Oxidative phosphorylation (OXPHOS) is the metabolic culmination of aerobic cellular respiration in the mitochondrial electron transport chain, in which proton translocations are coupled to ET reactions. The resulting electrochemical proton gradient is used for the generation of ATP molecules from adenosine 5'-diphosphate (ADP) and inorganic phosphate (Figure 1).

First, metabolites are oxidized in the Krebs cycle in the mitochondrial matrix to produce electrons with high transfer potential. Then, this so generated electron-motive force is converted into a proton-motive force in the mitochondrial electron transport chain and, finally, transformed into phosphoryl transfer potential, generating ATP molecules.

The transformation of the electron-motive force into the proton-motive force is performed by three respiratory multisubunit enzymes that act as electron-driven proton pumps: complex I (cI, reduced nicotinamide adenine dinucleotide (NADH) oxidoreductase); complex III, (cIII, cytochrome *c* oxidoreductase, also called cytochrome *bc*<sub>1</sub> complex; *Cbc*<sub>1</sub>); and complex IV (cIV, cytochrome *c* oxidase; *CcO*). These large transmembrane complexes contain multiple redox centers, including

hemes, iron-sulfur clusters, copper ions and flavins (Lenaz and Genova, 2010).

In addition, coenzyme Q<sub>10</sub> (Q) and cytochrome *c* (Cc) work as freely diffusible electron carriers in the mitochondrial electron chain, being required for ET between transmembrane complexes. Whereas Q is a lipid-soluble carrier, Cc is a water-soluble protein.

Electrons from NADH are transferred to cI, which, in turn, transfers electrons to cIII by means of Q molecules. The Q pool also receives electrons from complex II (cII, succinate dehydrogenase). In addition, Cc molecules are involved in the ET from cIII to cIV. Electrons are finally transferred from the latter cIV to molecular oxygen and, with the addition of protons, water molecules are formed. The final phase of OXPHOS is carried out by complex V (cV, ATP synthase), an ATP-synthesizing assembly that is driven by the electrochemical proton gradient (Figure 1). The OXPHOS pathway is a highly efficient way of releasing ATP molecules, compared to alternative fermentation processes, such as anaerobic glycolysis (Lenaz and Genova, 2010).

The traditional scheme of OXPHOS that includes the core proton-translocating complexes (cI, cIII and cIV), the auxiliary cII and the ATP-synthesizing cV, can be complemented with other auxiliary enzymes of the respiratory chain, such as the electron-transferring flavoprotein Q oxidoreductase, glycerophosphate dehydrogenase and dihydroorotate dehydrogenase (Lenaz and Genova, 2010). It is worth noting that the organization and dynamics of the respiratory complexes in the inner mitochondrial membrane are currently a matter of intense debate, for

which two opposite models have been proposed: the fluid and solid models (Acín-Perez and Enriquez, 2014).

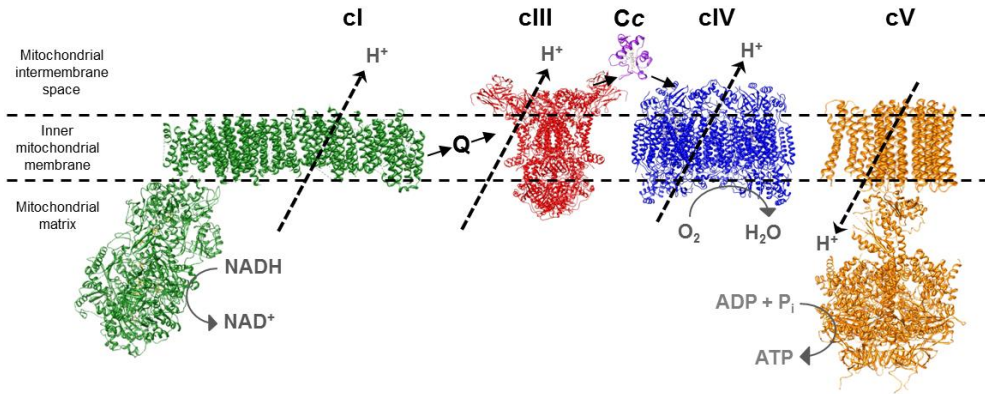


**Figure 1. Mitochondrial electron transport chain.** Respiratory complexes I, III, IV and V constitute the basis for eukaryotic OXPHOS. Water- and lipid-soluble redox carriers are necessary for the ET between respiratory complexes. The proton translocations are coupled to the ET reactions, and the resulting proton gradient is used for energy production by cV. PDB coordinates were taken from X-ray structures of the mentioned complexes (PDB entries: 3M9S and 3RKO for cI, 1KY0 for cIII, 1OCC for cIV and 2XND for cV) and the NMR structure of human Cc (PDB entry 1J3S). This figure was generated with Chimera (Pettersen *et al.*, 2004).

## V.2.2 FLUID AND SOLID MODELS OF THE MITOCHONDRIAL RESPIRATORY CHAIN

In the fluid model, all membrane proteins and redox components catalyzing electron transport and ATP synthesis in the mitochondrial respiratory chain are in constant and independent diffusional motion (Hackenbrock *et al.*, 1986). By contrast, the solid model of the membrane is based on specific interactions between individual respiratory

complexes to form stable assemblies of them, named supercomplexes (SCs; Chance and Williams, 1955; Acín-Pérez *et al.*, 2008).

The proposal of the fluid model, also known as the random collision model, is based on the fact that all redox components are independent lateral diffusants, and the ET reactions between large respiratory complexes occur during multicollisional, long-range kinetic processes (Hackenbrock *et al.*, 1986). Such respiratory enzymes would not be in close contact with each other, excluding any solid state organization of the respiratory chain components. Thus, this model states that each complex would act as an individual entity. These observations are mainly supported by the existence of lateral diffusion of respiratory complexes and by the occupancy of only one half of the membrane surface by proteins (Sowers and Hackenbrock, 1981; Gupte *et al.*, 1984).

By contrast, the solid model has received strong support since the discovery of detergent-based strategies for the isolation and solubilization of respiratory SCs. The finding of distinct compositions and stoichiometries of SCs has come mainly from studies of co-migrations in Blue native polyacrylamide gel electrophoresis (BN-PAGE) and co-purifications by sucrose gradient centrifugations (Schägger and Pfeiffer, 2000; Eubel *et al.*, 2004; Krause *et al.*, 2004).

Notably, plant and mammalian SCs comprising cI, cIII and cIV, have been shown to autonomously transfer electrons from NADH to molecular oxygen in the presence of Q and Cc, the so-called respirasome (Schägger and Pfeiffer, 2000; Acín-Pérez *et al.*, 2008). Such respirasomes are SCs that contain the necessary respiratory chain complexes to accomplish reduced equivalent ET to molecular oxygen. More evidence suggesting



functional supramolecular associations in the OXPHOS systems have also been provided by flux control analysis, questioning the hypothesis of the random diffusion model (Bianchi *et al.*, 2004; Trouillard *et al.*, 2011).

The fundamental features of the supramolecular organization of the respiratory chain have been revealed in several eukaryotic organisms, being the best characterized those from plant and mammalian mitochondria (Schägger and Pfeiffer, 2000; Eubel *et al.*, 2003). These assemblies are present in multiple forms, and four copies have even been found of cIV (Schägger and Pfeiffer, 2000). Thus, cI, cIII and cIV assemble into cI+cIII<sub>2</sub>, cI+cIII<sub>2</sub>+cIV<sub>1-4</sub> and cIII<sub>2</sub>+cIV<sub>1-2</sub> SCs (Krause *et al.*, 2004; Bultema *et al.*, 2009). In addition to them, several modules of these larger assemblies and other different SCs organizations have also been described in plant and mammalian mitochondria (Genova and Lenaz, 2014). For example, cII has been found to be associated in SCs only in the mitochondria of mice. This finding could be explained due to the participation of cII in the Krebs cycle (Acín-Pérez *et al.*, 2008; Genova and Lenaz, 2014).

The first structural insight into a cI<sub>1</sub>+cIII<sub>2</sub>+cIV<sub>1</sub> respirasome was carried out by transmission electron microscopy from mammalian mitochondria (Schäfer *et al.*, 2007). Since then, more refined investigations have been performed not only in mammals but also in plants and other organisms, as with recent studies by single particle cryo-electron microscopy and tomography (Figure 2; Bultema *et al.*, 2009; Althoff *et al.*, 2011; Dudkina *et al.*, 2011). From all these studies, it can be inferred that cytochrome *b* and Rieske Fe-S protein subunits of cIII are in close proximity to subunits III, VIa and VIIa of cIV, while the productive soluble Cc binding sites on both complexes appear to face each other at a

distance of 11 nm, facilitating a putative electron pathway or gliding mechanism between both complexes, as has been proposed in plants and in humans (Genova and Lenaz, 2013; De March *et al.*, 2014).

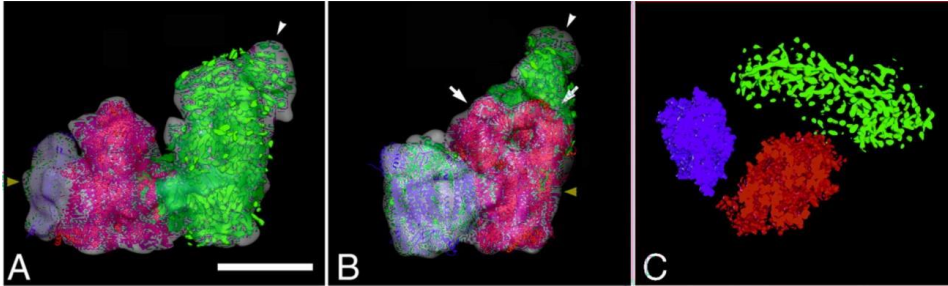


**Figure 2. Electron cryomicroscopy structure of the respirasome  $cI_1+cIII_2+cIV_1$ .** a) Side view of the fitting of the high- and medium-resolution structures of cI, cIII and cIV to the cryo-electron microscopy map. White arrowhead points to flavoproteins of cI and the olive one to the position of detergent micelles. Scale bar stands for 10 nm. b) A second side view of the respirasome, arrows point to some subunits of cIII. White and olive arrowheads point to flavoproteins of cI and the position of detergent micelles, respectively. c) Above view of the SC, showing the gaps between the complexes. This figure has been adapted from Dudkina *et al.* (2011).

Due to the observed variations in the amount and composition of SCs between different cell types, a new scenario for the membrane called the plasticity model has been proposed, wherein these SCs can likely co-exist with free complexes and that a variable combination of SCs and free complexes seems to exist under diverse physiological conditions, as a consequence of the cell type or the physiological state encountered (Figure 3; Lapuente-Brun *et al.*, 2013; Genova and Lenaz, 2014). In accordance with this model, SC composition in plant and mammalian mitochondria has been shown to vary due to several factors, such as pH

and oxygen availability (Ramírez-Aguilar *et al.*, 2011). Such diversity in the arrangement of the respiratory complexes may modulate the capability of cells to respond to diverse environmental conditions as the respirasome could quickly drive electrons from NADH to molecular oxygen in the presence of Q and Cc (Lapuente-Brun *et al.*, 2013).

The organization in SCs is predicted to provide functional advantages in the mitochondrial respiratory function (Lapuente-Brun *et al.*, 2013; Genova and Lenaz, 2014). In addition, the tighter organization in the SCs may protect auto-oxidizable prosthetic groups, hampering their reaction with molecular oxygen and protecting them from reactive nitrogen and oxygen species (RNOS) damage (Panov *et al.*, 2007; Maranzana *et al.* 2013). At the same time, cI seems to be stabilized within the SCs to preserve its structural integrity and activity (Schägger and Pfeiffer, 2001). Nowadays, the role of several integral membrane proteins involved in the SC assembly, stability and regulation of its activity is being investigated in-depth. Such extra membrane proteins have been named as SC assembly factors and can be critical for the optimization of the electron flow and the minimization of ROS production under stress conditions. For example, yeast respiratory supercomplex factors 1 and 2, known as Rcf1 and Rcf2, have been reported to be relevant for cIII<sub>2</sub>+cIV<sub>1</sub> SC assembly and for the optimal activity of cIV (Chen *et al.*, 2012; Strogolova *et al.*, 2012; Vukotic *et al.*, 2012). Rcf proteins are highly conserved in eukaryotes and belong to the hypoxia-inducible genes family (HIG1 family). Their mammalian homologues, known as Rcf or HIG1 factors, have been also described to be critical for the assembly and function of SCs (Chen *et al.*, 2012; Hayashi *et al.*, 2015). Proteins from the HIG1 family are helical bundles composed of two conserved

transmembrane crossing segments, which can be preceded by an additional, amphiphilic N-terminal  $\alpha$ -helix (Klammt *et al.*, 2012). In addition, another SC assembly factor, named chromosome 11 open reading frame 83 (C11orf83), has been reported in mammals (Desmurs *et al.*, 2015). C11orf83 directly interacts with cIII and is involved in the stabilization of cIII-containing SCs, especially the cIII<sub>2</sub>+cIV SC. The sequence of C11orf83 is highly conserved in mammals, presenting an N-terminal  $\alpha$ -helix which is anchored to the membrane (Desmurs *et al.*, 2015).

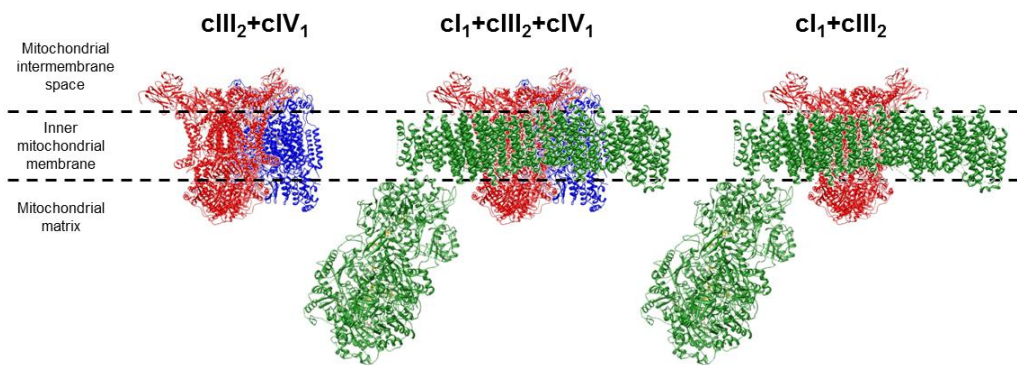


**Figure 3. Plasticity model of the mitochondrial electron chain.** Respiratory complexes and SCs coexist in the membrane. Fluid and solid models can be considered as extremes of a more dynamic situation in which the respirasome cI+cIII<sub>2</sub>+cIV<sub>1</sub>, other SCs (cI+cIII<sub>2</sub> and cIII<sub>2</sub>+cIV<sub>1</sub>) and free respiratory complex populations cohabit. PDB coordinates were taken from the sources mentioned in the Figure 1 legend. This figure was generated with Chimera (Pettersen *et al.*, 2004).

### V.2.3 CYTOCHROME C SIGNALOSOME

Cc provides a clear example of the connections that exist between supercomplexes of redox proteins that may be called respirasomes and those that form the so-called signalosomes. Indeed, Cc roles in the mitochondrial electron chain and the beginning of apoptosis, which form part of cell life and cell death signalosomes, respectively, are directly connected with the working and disruption of SCs.

Cc is a positively-charged heme-protein located in the intermembrane mitochondrial space under homeostatic conditions in eukaryotes. Cc has a nearly spherical shape and its overall fold is mainly  $\alpha$ -helical, with several regions with a coiled structure located between the helices. Cc contains four helices: the N-terminal, 50's helix, 60's helix and C-terminal. The buried hydrophobic residues making up the hydrophobic core, as well as most of the polar residues in contact with the porphyrin moiety, are conserved within highly evolved organisms. The structure is anchored through an interaction between the N- and C-terminal helices via conserved side chains present in each of the helices. The heme binding motif is essential for proper 3D folding, which is stabilized by hydrophobic and aromatic interactions with the heme. Two cysteine residues are required for the covalent attachment of the heme cofactor to the amino acid chain. The heme contains an iron ion that has two physiologically relevant low-spin oxidation states, Fe(II) and Fe(III). The heme is diamagnetic in the reduced form and paramagnetic in the oxidized state. In addition, histidine and methionine residues act as axial ligands of the iron, being the heme iron six-coordinated (Figure 4; Keilin and Hartree, 1955; Baistrocchi *et al.*, 1996; Banci *et al.*, 1997).

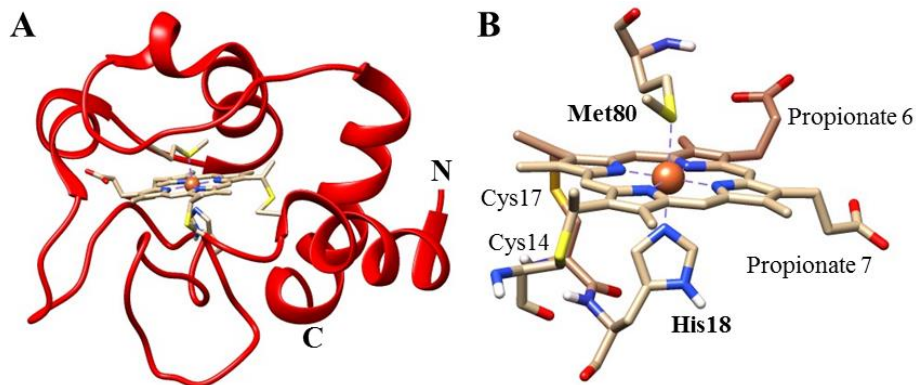


**Figure 4. Three-dimensional structure of human cytochrome *c*.** A) Overall fold of the protein. The heme is shown in sticks. Protein ends are indicated by the labels. B) His18 and Met80 axial ligands of the iron are shown (bold labels). Cys14 and Cys17 covalently bound to the heme group are also indicated in the figure, as well as the propionates of the heme. PDB coordinates were taken from the NMR structure of human *Cc* (PDB entry 1J3S). This figure was generated with Chimera (Pettersen *et al.*, 2004).

The cellular role of *Cc*, which was first described as a long-distance redox carrier from cIII to cIV (Keilin and Hartree, 1955), has been continuously revisited. In the mitochondrial electron chain, *Cc* receives electrons from the cytochrome  $c_1$  ( $Cc_1$ ) of the cIII via a heme-to-heme ET reaction. The globular, water-soluble domain of  $Cc_1$  is responsible for the ET to *Cc*.  $Cc_1$  is bound to the membrane through a C-terminal  $\alpha$ -helix. Once *Cc* is reduced, electrons are transferred from *Cc* to the binuclear copper center of cIV, called  $Cu_A$  (Lange and Hunte, 2002; Sakamoto *et al.*, 2011; Díaz-Moreno *et al.*, 2011).

Since the discovery of the respiratory function of *Cc* in the mitochondrial electron transport chain, several other mitochondrial *Cc* partners have been reported, including the flavoenzyme L-galactono-1,4-lactone dehydrogenase (GALDH) in plants. GALDH is required for the

correct assembly of cI and catalyzes the terminal step of L-ascorbate biosynthesis (Leferink *et al.*, 2008).

In the context of SCs, it has been proposed that *Cc* glides between cIII and cIV to shuttle electrons instead of carrying them by long-distance random diffusion, which is in agreement with the metabolic channeling model proposed by Kholodenko and Westerhoff (1993). Within this framework, the channeling would imply gliding mechanisms of *Cc* molecules on the surface of respiratory complexes, impairing its release to the bulk phase but providing a diffusion path between its redox partners (Genova and Lenaz, 2013; De March *et al.*, 2014). This idea demands a detailed structural and functional analysis of the interactions between *Cc* and its respiratory partners cIII and cIV, whose behavior in plant and mammalian SCs remains obscure from a structural point of view.

In addition, it has been demonstrated that *Cc* is capable of interacting with several protein and/or lipid targets not only under homeostatic conditions but also in the cytoplasm and even in the nucleus under programmed cell death conditions (Díaz-Moreno *et al.*, 2011; Martínez-Fábregas *et al.*, 2013; Martínez-Fábregas *et al.*, 2014a). Notably, *Cc*-mediated peroxidation of cardiolipin is accepted as one of the early signals of apoptosis in the cell death signalosome. Such oxidative modification of cardiolipin leads to the disruption of mitochondrial supercomplexes and consequent increase in RNOS formation (Lenaz *et al.*, 2010). Thus, the impairing of supercomplexes can be linked with the participation of *Cc* in the cell death signalosome.

A further step of complexity in these networks of interconnected molecules is added by post-translational modifications of eukaryotic Cc, which drastically alter the binding patterns and, then regulate cell signaling mechanisms of Cc. Post-translational modifications, such as phosphorylation, of mammalian Cc could open up another level of regulation of Cc activity. Indeed, phosphorylated Cc has been shown to cause partial inhibition of the oxidative phosphorylation process, and in turn, has been linked to some pathological situations, such as ischemia or reperfusion injury (Yu *et al.*, 2008; Pecina *et al.*, 2010; Hüttemann *et al.*, 2012a). On the other hand, experiments with a phosphomimetic substitution of Tyr48 in human Cc have suggested functional effects on programmed cell death (PCD; Hüttemann *et al.*, 2011; Hüttemann *et al.*, 2012b; Sanderson *et al.*, 2013). The possibility that phosphorylation of human Cc regulates PCD has potentially important therapeutic implications for diseases like cancer, in which PCD is inhibited (Hüttemann *et al.*, 2012b).

### **V.2.4 RESPIRATORY COMPLEX III**

Respiratory cIII is a homodimeric multisubunit membrane enzyme with a molecular mass close to 500 kDa. Each monomer contains three redox-active subunits: cytochrome *b* with two *b*-type heme groups, Cc<sub>1</sub> with a *c*-type heme, and the Rieske protein containing a [2Fe–2S] cluster (Figure 5). The enzyme operates via a mechanism called the Q cycle, in which it couples ET from Q to Cc, with the net translocation of protons across the membrane. Key features of the mechanism are: the bifurcated ET upon Q oxidation at the Q<sub>o</sub> catalytic site, a spatially separated second catalytic site for Q reduction (Q<sub>i</sub> site), and the large-scale domain



movement of the Rieske protein, which facilitates ET from the Qo site to subunit  $Cc_1$ .  $Cc$  docks on the latter subunit to accept the electron (Lange and Hunte, 2002; Lenaz and Genova, 2010).

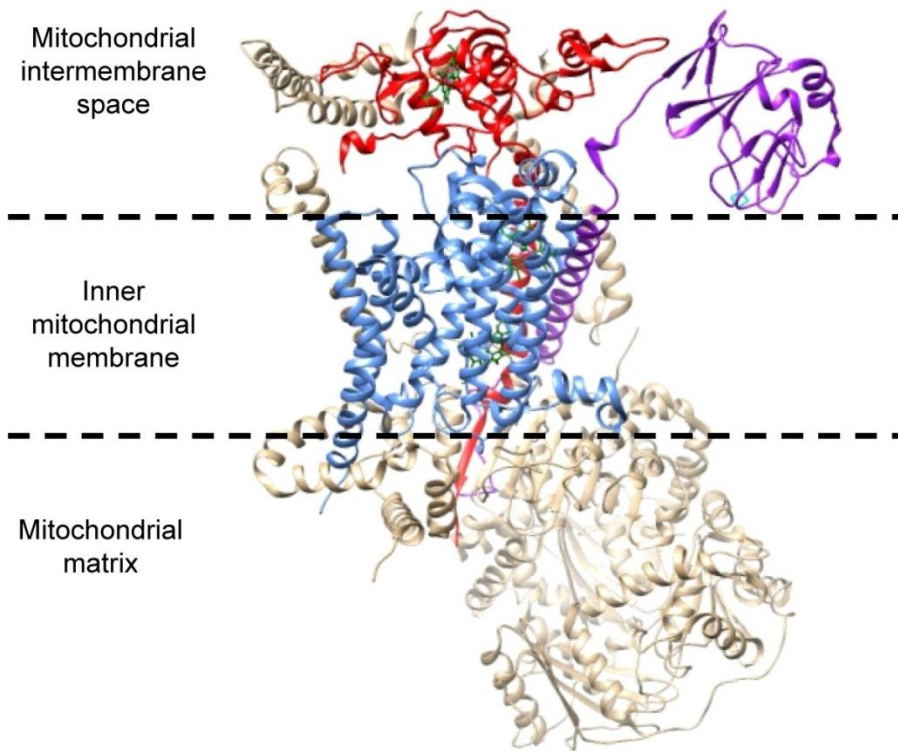


**Figure 5. Structural monomer of eukaryotic respiratory complex III.** Model of the structural monomer of cIII based on the dimeric structure of this complex from yeast (PDB entry 1KYO). The cytochrome  $b$  subunit is colored in blue, the Rieske subunit in purple and the cytochrome  $c_1$  subunit in red. Other yeast cIII subunits are colored in tan. Heme cofactors are in green and the iron-sulfur cluster is in cyan. This figure was generated with Chimera (Pettersen *et al.*, 2004).

## V.2.5 RESPIRATORY COMPLEX IV

Respiratory cIV is another multisubunit enzyme that is usually present in its monomeric form, with a molecular mass close to 200 kDa. This enzyme contains several metallic cofactors required for ET reactions including low-spin hemes and copper centers (Figure 6). ET through cIV occurs from  $C_c$  to the  $Cu_A$  center (which acts as a single-electron receptor). Then, ET is conducted to the heme  $a$ , and in turn, onto the bimetallic center heme  $a_3$ - $Cu_B$ . Finally, electrons and protons are transferred to oxygen bound to heme  $a_3$ , generating water molecules (Lenaz and Genova, 2010; Sakamoto *et al.*, 2011).

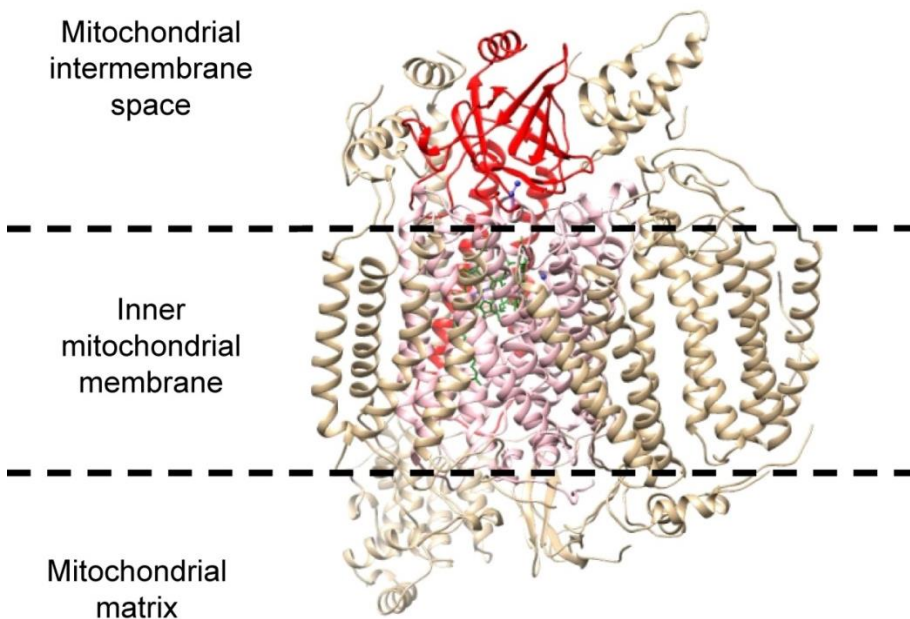


**Figure 6. Structural monomer of eukaryotic respiratory complex IV.** Model of the structural monomer of cIV based on the dimeric structure of this complex from bovine (PDB entry 1OCC). The cytochrome  $c$  oxidase subunit containing the binuclear copper site is colored in red, whereas the subunit that contains the

*a*-type hemes and the mononuclear copper center is in pink. Other bovine cIV subunits are colored in tan. Heme cofactors are in green and the copper atoms are in blue. This figure was generated with Chimera (Pettersen *et al.*, 2004).

## **II.2.6 L-GALACTONO-1,4-LACTONE DEHYDROGENASE**

L-galactono-1,4-lactone dehydrogenase, namely GALDH, catalyzes the oxidation of L-galactono-1,4-lactone to L-ascorbate with the concomitant reduction of *Cc*. GALDH is presumed to be an integral membrane protein of the inner mitochondrial membrane where it shuttles electrons into the mitochondrial electron transport chain via *Cc*. Although GALDH has been isolated from the mitochondria of several plants, it has been poorly characterized. Most aldonolactone oxidoreductases contain a covalently bound FAD, but plant GALDH binds the FAD cofactor in a non-covalent manner. Little information is known about the active site and 3D structures of plant GALDH are not available to date (Leferink *et al.*, 2008).

## **V.3 PHOTOSYNTHESIS**

Photosynthesis takes place on the thylakoid membranes in plants, algae and cyanobacteria. It is a fundamental biochemical process, through which light energy is converted into chemical energy, stored in ATP and reduced nicotinamide adenine dinucleotide phosphate (NADPH) molecules. These compounds provide the energy and reducing power for biosynthetic pathways, including carbon assimilation. The production of ATP using the energy of sunlight is known as photophosphorylation.

Molecular oxygen is produced as a waste product (Hasan and Cramer, 2012).

Cyanobacterial thylakoids are topologically rather different from those of algae and plant chloroplasts. Thylakoids of the latter organisms contain prominent structures known as grana, which are formed by multiple stacked layers of thylakoid disks linked by intergrana thylakoids, also known as stroma thylakoids or lamellae. Cyanobacterial thylakoid membranes lack grana and they are much more homogeneous than chloroplast thylakoids. Notably, cyanobacteria carry out both respiration and photosynthesis in the thylakoid membranes. In the absence of light, the respiratory consumption of stored photosynthesis products is essential for maintaining cell functions. In contrast to algae and plants, the majority of respiratory electron transport in cyanobacteria occurs in the thylakoid membrane, in close proximity to the photosynthetic apparatus. The proximity of both photosynthetic and respiratory systems opens up several possibilities for “hybrid” modes of electron transport involving electron exchange between photosynthetic and respiratory complexes (Bailey *et al.*, 2008; Lea-Smith *et al.*, 2013).

The following topics about photosynthesis are commented on in detail below: photosynthesis electron chain, photosynthetic supercomplexes, and cytochrome  $c_6$  and plastocyanin.

### **V.3.1 PHOTOSYNTHETIC ELECTRON CHAIN**

The photosynthetic electron chain machinery consists of membrane-bound protein complexes and mobile partners, which accomplish the ET process coupled with proton translocations in the thylakoid space. The fundamentals of the photosynthesis process present a high degree of

similarity with that described for OXPHOS systems, in which proton translocations are coupled to ET steps and soluble carriers transfer electrons between large multi-subunit enzymes (Figure 7). These large transmembrane complexes contain multiple redox centers, including hemes, iron-sulfur clusters, manganese centers, phyloquinones, pheophytins, chlorophylls and carotenoids (Hasan and Cramer, 2012).

The photosynthetic ET transport in oxygen-evolving photosynthesis is mediated by two photochemical reactions, carried out by photosystem II (PSII) and photosystem I (PSI). When light photoexcites the P680 reaction center of PSII (directly or indirectly via the light-harvesting antenna complexes, which are presented in the following section), PSII converts this energy into the electrochemical potential energy required for ET reactions through PSII redox centers to plastoquinone (PQ) molecules, energizing the electrons coming from the water splitting. The P680 reaction center is composed of a chlorophyll dimer. The mechanism of water splitting is carried out by the manganese center of PSII and generates molecular oxygen and proton molecules in the thylakoid space. This mechanism and the basic subunit structure of the PSII core are highly conserved from cyanobacteria to flowering plants, constituting the source of nearly all the oxygen in the atmosphere (Umena *et al.*, 2011). However, some peripheral subunits of PSII differ among oxygenic photosynthetic organisms (Ifuku *et al.*, 2011).

From PSII, electrons are transferred through the membrane to the cytochrome  $b_6f$  complex ( $b_6f$ ) with the help of the lipid-soluble PQ. The Q cycle is a mechanism for coupling the ET through  $b_6f$  with proton translocation across the thylakoid membrane. The membrane proton gradient is the driving force for ATP production. Then, a mobile water-

soluble carrier named plastocyanin (Pc), carries out the ET from  $b_6f$  to PSI at the lumen side. Finally, electrons are transferred from PSI to ferredoxin-NADP reductase (FNR) via ferredoxin (Fd) on the stromal side for the production of NADPH. The latter step culminates the linear photosynthetic ET from water splitting to NADPH production by FNR. Photoexcitation on the P700 reaction center of PSI, which contains two chlorophyll molecules, is required to generate the electrochemical potential energy required for ET reactions towards Fd. NADPH and ATP are the first stable products of photosynthesis and are used in  $\text{CO}_2$  fixation (Hasan and Cramer, 2012).

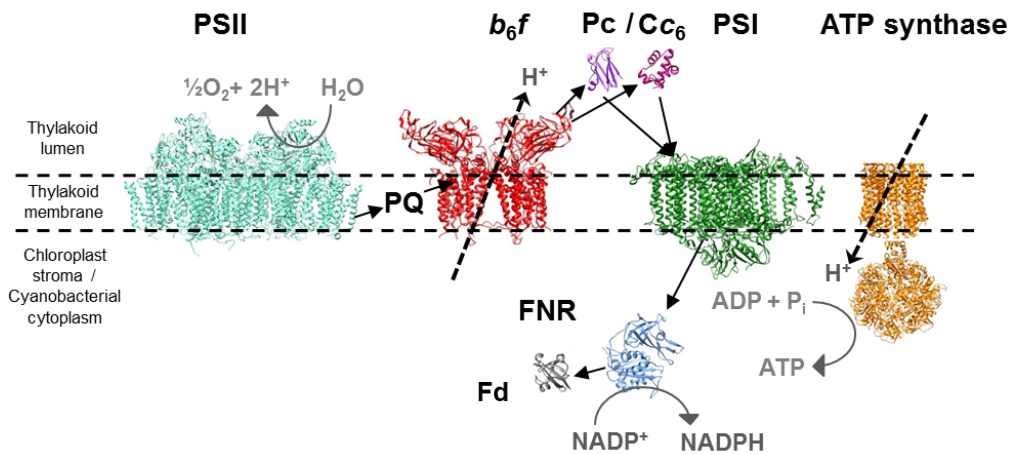


**Figure 7. Oxygen-evolving photosynthetic electron transport chain.**

Formation of the transmembrane proton gradient by the linear electron transport chain, which extends from the water oxidation site of PSII to the reduction of NADP molecules in the chloroplast stroma or cyanobacterial cytoplasm. Water- and lipid-soluble redox carriers are necessary for the ET between multi-subunit enzymes. A proton gradient is formed by the action of the PSII reaction center and  $b_6f$ . The ATP synthase use this gradient for the formation of energy. PDB coordinates were taken from X-ray structures of mentioned complexes (PDB entries: 1S5L for PSII, 2ZT9 for  $b_6f$ , 1PCS for Pc, 4GYD for  $Cc_6$ , 1JB0 for PSI,

2W5J and 1FX0 for ATP synthase and 2XND for FNR and Fd). This figure was generated with Chimera (Pettersen *et al.*, 2004).

In addition, cyclic ET can occur in photophosphorylation. In this process, electrons are transferred from Fd to the PQ pool. Flavodoxin (Fv) plays the same ET role as Fd. The goal of the cyclic photosynthetic ET is ATP production, whereas the lineal ET generates ATP and NADPH molecules (Hasan and Cramer, 2012).

An excess of reducing power generated by ET induces the production of ROS. Light intensity fluctuations are normal under natural conditions. To avoid photoinhibition by excessive light energy, the most efficient strategy is the dissipation of absorbed light energy from PSII safely as heat, but there are other strategies that can involve inactive state transitions or disassemblies of the components of the photosynthetic electron chain. The dissipation of this excess light energy can be monitored as non-photochemical quenching of chlorophyll fluorescence (Horton *et al.*, 1996; Murata *et al.*, 2007; Tikkanen and Aro, 2014).

In addition, to sustain an efficient performance and satisfy the light reactions, photosynthetic protein complexes alter their structure and activity dynamically, forming photosynthetic supercomplexes.

### **V.3.2 PHOTOSYNTHETIC SUPERCOMPLEXES**

The traditional models of the photosynthetic electron chain are incomplete, giving us an inadequate understanding of the ability of photosynthetic organisms to adapt to fluctuating light environments. However, technical innovations have enabled us to reconsider the

molecular mechanisms for the regulation of photosynthesis as the dynamic interaction of thylakoid membrane complexes.

In plants and green algae, the PSII core complex is associated with the membrane-embedded light-harvesting antenna complexes, named LHCII, containing multiple pigments, *e.g.* carotenoides and chlorophylls. LHCII forms large macromolecular complexes, namely the PSII-LHCII supercomplexes (Croce and van Amerongen, 2014). Such an organization of supercomplexes has been visualized by electron microscopy and single particle analysis (Dekker and Boekema, 2005; Caffarri *et al.*, 2009; Pagliano *et al.*, 2014). The LHCII trimers associated with the PSII core are categorized into three types on the basis of their affinity with the PSII supercomplex, namely those that have a strong (S), moderate (M), or loose (L) association with the PSII core (C). These LHCII trimers consist of different combinations of three LHCII proteins (Caffarri *et al.*, 2009).

In addition, the PSI core complex in the mentioned organisms is also associated with the membrane-embedded light-harvesting antenna complexes, known as LHCI. The structure of the PSI-LHCI complex depends on the organism (Busch and Hippler, 2011). For example, in flowering plants, the PSI-LHCI supercomplex consists of a PSI core and one copy each of four major LHCI molecules (Amunts *et al.*, 2007; Amunts *et al.*, 2010). In contrast, in *Chlamydomonas*, it is composed of a single PSI core complex and nine LHCI proteins (Drop *et al.*, 2011). In addition to these major LHCI molecules, some organisms encode minor LHCI molecules, but they are necessary in order for the organism to function properly (Wientjes *et al.*, 2009).



Nowadays, the assembly of reaction centers forming antenna complexes in photosynthetic supercomplexes is well accepted. However, the composition of such photosynthetic supercomplexes may involve further proteins, such as a large multisubunit complex named NADH dehydrogenase (NDH, NDH complex), which is quite similar to the respiratory cI (Shikanai, 2007). The latter enzyme can be distinguished from respiratory cI according to structural and functional differences. In fact, in flowering plants, NDH forms a supercomplex with PSI and LHCI components (Shikanai, 2014). A single particle analysis has allowed for the identification of the supercomplex consisting of a single NDH sandwiched by two copies of the PSI-LHCI supercomplexes, although several versions of such NDH-PSI-LHCI supercomplexes have been recognized (Kouril *et al.*, 2014). Other proteins have been discovered to be essential for supercomplex associations, such as the PGR5 and PGRL1 proteins, which promote the cyclic ET around PSI in the LHCI-LHCII-FNR-*b<sub>6</sub>f*-PGRL1-PGR5 supercomplex (Iwai *et al.*, 2010). Notably, the formation and dissociation of the latter supercomplex not only switches the mode of photosynthetic electron flow, but also controls the energy balance of the two photosystems (Iwai *et al.*, 2010).

The variability of photosynthetic supercomplexes is quite high among distinct organisms and conditions, in which distinct supercomplex associations and additional proteins can be involved, such as the PGR5/PGRL1 machinery (Shikanai, 2014). Despite the conservation of the plant and green algae core subunits of PSII and PSI, the light-harvesting systems are rather divergent in distinct organisms, suggesting different strategies for adapting to different light environments. Notably, there is no strong evidence to date for electron transport supercomplexes

in cyanobacteria, in which the role of the soluble electron carriers seems to be critical to understand the adequate working of the ET transport.

### **V.3.3 PLASTOCYANIN AND CYTOCHROME $c_6$**

In some cyanobacteria and green algae, the copper protein Pc can be substituted by the hemeprotein cytochrome  $c_6$  ( $Cc_6$ ) to perform the same function. Although the two small and soluble proteins have no structural similarities, their interaction surfaces seem to be evolutionarily correlated. Such surfaces are proposed to be iso-functional, presenting a conserved hydrophobic region around the redox centers, as well as a relevant contribution of charge residues (Hervás *et al.*, 1995). In addition, their heme mid-point redox potential ( $Em$ ) and isoelectric points are quite similar when comparing proteins from the same organism, varying their values among distinct species (Howe *et al.*, 2006; Worrall *et al.*, 2008).

Pc is a blue copper protein with a type-I redox center, showing the immunoglobulin fold composed of eight  $\beta$ -strands along with a small  $\alpha$ -helix. The metal atom is buried in a hydrophobic pocket close to the helix, and it is coordinated by two histidines, one methionine and one cysteine. The copper binding site features a distorted trigonal pyramid. One of the histidine residues, called HisC, is the only copper ligand that is solvent-exposed, thus making this group the most likely physiological ET port to its partners (Canters and Gilardi, 1993; Gong *et al.*, 2000).

Opposite to Pc, the structure of  $Cc_6$  consists mainly of  $\alpha$ -helices, typical of a *c*-type cytochrome (Figure 8). The heme is thus covalently linked by two thioether bonds to two cysteine residues, which are part of a conserved CXXCH motif near the N-terminus. A histidine and a

methionine are coordinating the iron atom of  $Cc_6$  (Worrall *et al.*, 2007; Bialek *et al.*, 2009).

It has been proposed that the alternative expression of the genes coding for the Pc and  $Cc_6$  proteins depends on the relative environmental abundance of copper and iron (Hervás *et al.*, 1995). In this way, cyanobacteria and green algae are able to adapt to chemically different environments. In recent years, a number of new *c*-type cytochromes have been identified in plants (cytochrome  $c_{6A}$ ), cyanobacteria (cytochrome  $c_{6B}$ ) and algae (cytochrome  $c_{6C}$ ). They have structural features similar to  $Cc_6$  but their function has not been yet elucidated, although their low *Em* excludes a possible functional analogy between  $Cc_6$  and Pc (Mason *et al.*, 2012).

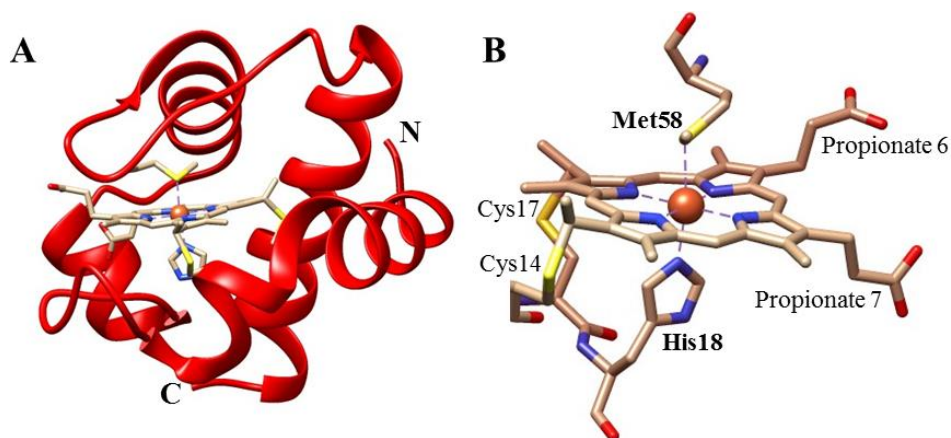


**Figure 8. Three-dimensional structure of cytochrome  $c_6$  from *Nostoc*.** A) Overall fold of the protein. The heme group is shown as sticks. Protein ends are indicated by the labels. B) The axial ligands are shown (bold labels) as well as the Cys residues covalently bound to the heme and the heme propionates. PDB coordinates were taken from the X-ray structure of *Nostoc Cc<sub>6</sub>*. (PDB entry 4GYD). This figure was generated with Chimera (Pettersen *et al.*, 2004).

The possibility of inter-exchange between Pc and Cc<sub>6</sub>, depending on the copper availability in the medium, within the photosynthetic chain in some cyanobacteria and green algae underlines the importance of the transient and dynamic nature of the complexes formed by Pc and Cc<sub>6</sub> with both *b<sub>6</sub>f* and PSI.

### V.3.4 CYTOCHROME *b<sub>6</sub>f*

The multisubunit enzyme *b<sub>6</sub>f*, known as cytochrome *b<sub>6</sub>f* complex, is composed of several catalytic subunits (Figure 9). The Rieske protein and the *Cf* form the so-called high-potential path, whereas the two hemes of cytochrome *b<sub>6</sub>*, located on the opposite side of the membrane, form the low-potential path. Two Q binding sites are located on the two sides of the membrane. This complex takes up two electrons from a Q bound at the luminal Q<sub>o</sub> site and results in the release of two protons in the aqueous lumen. *Cf* is anchored in the thylakoid membrane by hydrophobic residues. Interestingly, the structure of *Cf* has an elongated shape and is mainly made up of  $\beta$ -sheets. It is composed of a small and a large domain joined by a hinge region, the latter domain houses the heme group. A histidine acts as the fifth ligand to the iron, whereas the N-terminal Tyr1 is the sixth ligand.

A comparison of the X-ray structures of *b<sub>6</sub>f* from diverse organisms with the reported respiratory cIII, the mitochondrial homologue of the *b<sub>6</sub>f*, suggest that the transmembrane parts are quite similar, confirming the structural homology inferred from sequence analysis (Breyton, 2000; Baniulis *et al.*, 2008). Indeed, the same type of large-scale domain movement of the Rieske protein is observed in the *b<sub>6</sub>f* as it is in the mitochondrial cIII upon the binding of the quinol analogue stigmatellin

(Breyton, 2000). X-ray data also suggest other specific movements of the transmembrane domains of the  $b_6f$  required for intermediate states in the ET reaction (Breyton, 2000; Baniulis *et al.*, 2008). On the other hand, the soluble domains of the  $b_6f$  exhibit significant divergences between distinct species that can be correlated with an evolutionary adaptation for efficient ET in different photosynthetic organisms (Baniulis *et al.*, 2008).

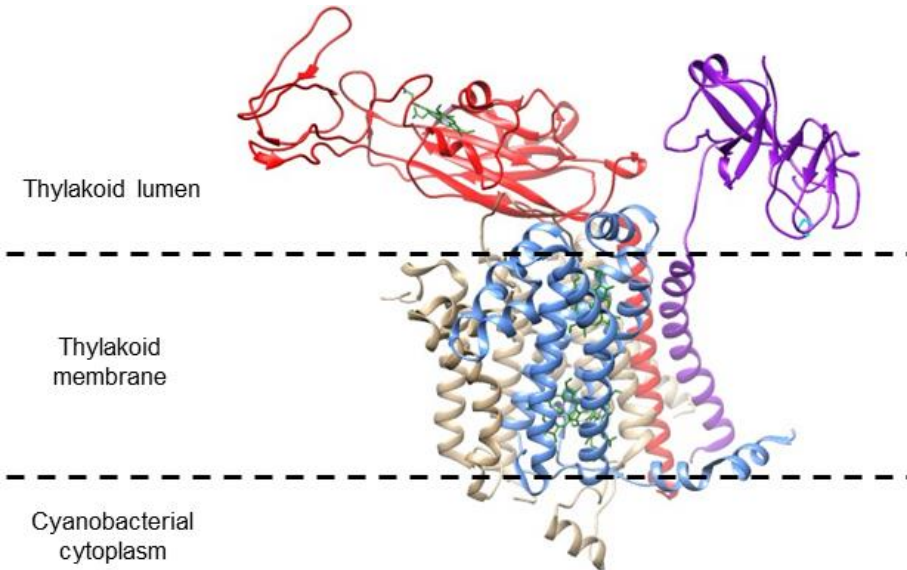


**Figure 9. Structure of the cytochrome  $b_6f$  complex monomer from *Nostoc* cyanobacterium.**

Model of the structural monomer of cytochrome  $b_6f$  based on the dimeric structure of this complex from *Nostoc* (PDB entry 2ZT9). The cytochrome  $b_6$  subunit is colored in blue, the Rieske subunit in purple and the cytochrome  $f$  subunit in red. Other *Nostoc* cytochrome  $b_6f$  subunits are colored in tan. Heme cofactors are in green and the iron-sulfur cluster is in cyan. This figure was generated with Chimera (Pettersen *et al.*, 2004).

## **V.4 METHODS BASED ON SOLUTION NUCLEAR MAGNETIC RESONANCE TO STUDY TRANSIENT PROTEIN-PROTEIN INTERACTIONS AND STRUCTURAL DETERMINATION**

Solution NMR spectroscopy is a powerful technique for the characterization and structural determination of protein-protein transient complexes, as well as for the elucidation of protein structure and dynamics in solution, with a resolution at the atomic level.

The NMR parameters measured in this PhD thesis were, mainly, diamagnetic chemical-shift perturbations (CSP) and paramagnetic relaxation enhancement (PRE). All of them were included in NMR-driven docking models. Besides this, Nuclear Overhauser Effect (NOE) techniques for protein structure and dynamics characterizations in solution have also been tackled in another section.

### **V.4.1 DIAMAGNETIC CHEMICAL-SHIFT PERTURBATIONS AND SURFACE MAPPING**

Protein interface mapping by CSP is a well-established procedure to study weak complexes by NMR.  $^{15}\text{N}$  labeling of proteins allows us to perform 2D [ $^{15}\text{N}$ - $^1\text{H}$ ] Heteronuclear Single-Quantum Correlation (HSQC) experiments. The [ $^{15}\text{N}$ - $^1\text{H}$ ] HSQC spectrum gives a fingerprint of protein structure. Indeed, this spectrum provides precise information about the folding state of the protein, the presence of disordered regions,

and even degradation or aggregation phenomena. Each [ $^{15}\text{N}$ - $^1\text{H}$ ] HSQC cross-peak represents an amide group, correlating the chemical-shift of the amide proton with the chemical-shift of the attached amide nitrogen of a particular  $^{15}\text{N}$  labeled residue (Figure 10).

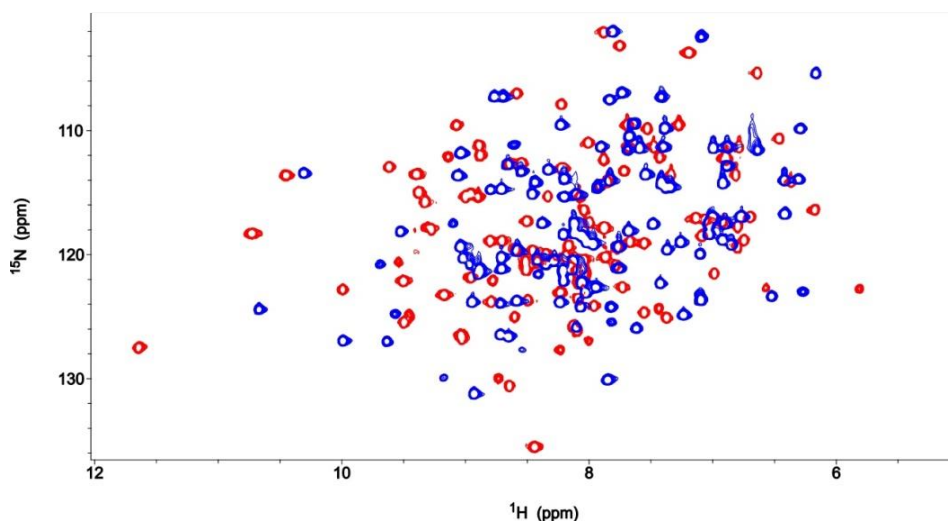


**Figure 10.** [ $^{15}\text{N}$ - $^1\text{H}$ ] HSQC spectra of reduced and oxidized human Cc. Reduced Cc amide groups are colored in blue, whereas oxidized Cc resonances are in red.

The assignment of the [ $^{15}\text{N}$ - $^1\text{H}$ ] HSQC spectrum requires other experiments, ideally triple resonance experiments with  $^{15}\text{N}$  and  $^{13}\text{C}$ -labeled proteins that provide sequential connectivities between residues. Thus, amide groups can be linked to particular residues and sequentially assigned. The assignment of the spectrum is essential for a meaningful interpretation of more advanced NMR experiments such as binding experiments, structure determination and relaxation analysis (Crowley and Ubbink, 2003; Prudêncio and Ubbink, 2004; Kastiris and Bonvin, 2013).

The binding site for a biomolecule-biomolecule interaction can be determined by comparison of the spectra of the biomolecule for its free and bound states when the resonance assignments are known. The position and intensities of the mentioned cross-peaks can change upon interaction with one or more partners. CSP occurs as a result of changes in the chemical environment of the observed nucleus.

CSP analyses are commonly performed on [ $^{15}\text{N}$ - $^1\text{H}$ ] HSQC spectra of the  $^{15}\text{N}$  labeled molecule recorded in the absence and presence of increasing amounts of the unlabeled partner. Thus, it is possible to obtain a map of the residues involved in the interaction and visualize the binding sites. The analysis of NMR spectra can be performed using the proper NMR analysis software, such as Sparky (Goddard and Kneller, University of California). The chemical-shift differences between free and bound spectra can be easily followed and calculated. With  $^{15}\text{N}$ - $^1\text{H}$  correlation spectra, average CSP values ( $\Delta\delta_{\text{avg}}$ ) from nitrogen and hydrogen nuclei ( $\Delta\delta^{\text{N}}$  or  $\Delta\delta^{\text{H}}$ ) are calculated according to the following equation (Williamson, 2013):

$$\Delta\delta_{\text{avg}} = \frac{\sqrt{(\Delta\delta^{\text{N}}/5)^2 + (\Delta\delta^{\text{H}})^2}}{2} \quad (1)$$

Further, the CSP mapping and analysis can also provide information about the time scale of association and dissociation events, the stoichiometry of the binding reaction and the affinity constant of the binding (Crowley and Ubbink, 2003; Prudêncio and Ubbink, 2004; Kastiris and Bonvin, 2013).

In comprehensive terms, the average size of the CSP of backbone amide resonances provides information on the degree of dynamics of the



complex, and thus the population of the encounter complex. Large CSP indicate well-defined, short-range interactions, whereas small CSP denote high dynamics and weaker interactions. Mainly hydrophobic, short-range interactions are involved in the formation of the final complex, which is stabilized in a single orientation through a network of hydrogen bonds, salt bridges and van der Waals interactions. Water exclusion also takes place. Average CSP values can reflect the population of the encounter state and, therefore, can also be used as a reliable diagnostic tool for the dynamics within transient inter-protein complexes (Worrall *et al.*, 2001; Worrall *et al.*, 2002; Worrall *et al.*, 2003; Hulsker *et al.*, 2008; Xu *et al.*, 2008; Bashir *et al.*, 2011; Kastiris and Bonvin, 2013; Schilder and Ubbink, 2013).

Moreover, in inter-protein interactions, the increase of molecular weight due to the complex formation leads to significant changes in the line widths of resonances, which are associated with increased transverse relaxation rates. If the binding kinetics of a complex are slow-to-intermediate in the NMR timescale, line broadening can also be observed. By analyzing the line-width differences between the free and bound states in the [ $^{15}\text{N}$ - $^1\text{H}$ ] correlation spectra mentioned before, the binding interface can also be mapped (Madl and Sattler, 2012).

## **V.4.2 PARAMAGNETIC RELAXATION ENHANCEMENT**

The information obtained from CSP analyses is not enough to study lowly populated and dynamic states like the encounter ensembles. For this reason, other NMR methods, such as paramagnetic NMR, are

required for detailed structure determination, providing valuable information about the dynamics in biomolecule complexes (Bashir *et al.*, 2011; Schilder and Ubbink, 2013).

The presence of a paramagnetic center causes distance-dependent effects on the NMR signals of observed nuclei, which can provide very precise structural information. The paramagnetic source, which contains an unpaired electron, can be intrinsic to the molecule, for example, a metal of the protein, or can be inserted into it via site-directed spin labeling (Figure 11). In the latter case, a paramagnetic probe is linked to a cysteine residue that, in many cases, is introduced by site-directed mutagenesis. Paramagnetic tags are attached at different places on the target surface to facilitate a proper evaluation of complex orientations (Bashir *et al.*, 2011; Kastiris and Bonvin, 2013; Hass and Ubbink, 2014; Schilder and Ubbink, 2013; Camacho-Zarco *et al.*, 2015).

In general, when a complex is studied by NMR PRE, one of the interaction partners contains the paramagnetic center, whereas the other one is isotopically labeled, so as to monitor its signals in NMR spectra. The properties of the paramagnetic center determine the nature of the effects on the NMR spectrum. In the case of PRE, the unpaired electron causes signal line broadening of the proximal nuclei. This PRE effect is proportional to  $r^{-6}$  ( $r$  is the distance between the paramagnetic center and the observed nucleus), which is analogous to NOE. The peaks corresponding to residues close to the paramagnetic center show a decrease in peak height or disappear entirely from the spectrum. In fact, PREs can be very strong and can affect nuclei located up to 10-40 Å from the paramagnetic center. This distance dependence makes PRE particularly sensitive to lowly populated states of proteins orientations

(Iwahara *et al.*, 2004; Tang *et al.*, 2006; Volkov *et al.*, 2006; Tang *et al.*, 2008; Bashir *et al.*, 2011; Kastritis and Bonvin, 2013; Schilder and Ubbink, 2013).

For each observed amide proton of a  $^{15}\text{N}$ -labeled protein, a paramagnetic center-induced PRE can be calculated according to equation 2 (Volkov *et al.*, 2006; Bashir *et al.*, 2011):

$$\frac{I_{\text{para}}}{I_{\text{dia}}} = \frac{R_{2,\text{dia}} \exp(-tR_{2,\text{para}})}{R_{2,\text{dia}} + R_{2,\text{para}}} \quad (2)$$

Where  $I_{\text{para}}$  and  $I_{\text{dia}}$  are measured intensities of HSQC peaks for the  $^{15}\text{N}$ -labeled protein probe in the complex with a particular protein target in the presence of a paramagnetic or diamagnetic (control) spin label;  $R_{2,\text{dia}}$  is the transverse relaxation rate of amide protons of the protein probe in the complex with the diamagnetic spin label;  $R_{2,\text{para}}$  is the paramagnetic contribution to the relaxation rate (PRE); and  $t$  is the total polarization transfer time of the HSQC. For the residues whose resonances disappear in the paramagnetic spectrum,  $I_{\text{para}}$  was estimated from the noise level of the spectrum.

Calculated PRE rates can be converted into distances as follows (Volkov *et al.*, 2006; Bashir *et al.*, 2011):

$$r = \sqrt[6]{\frac{\gamma^2 g^2 \beta^2 \tau_c}{20R_{2,\text{para}}} \left( 4 + \frac{3}{1 + \omega_h^2 \tau_c^2} \right)} \quad (3)$$

Where  $r$  is the distance between the unpaired electron of the paramagnetic spin label and a given amide proton of the protein probe;  $\tau_c$  is the rotational correlation time of the electron-nucleus vector;  $\omega_h$  and  $\gamma$

are the proton Larmor frequency and the gyromagnetic ratio, respectively;  $g$  is the electronic  $g$  factor; and  $\beta$  is the Bohr magneton.

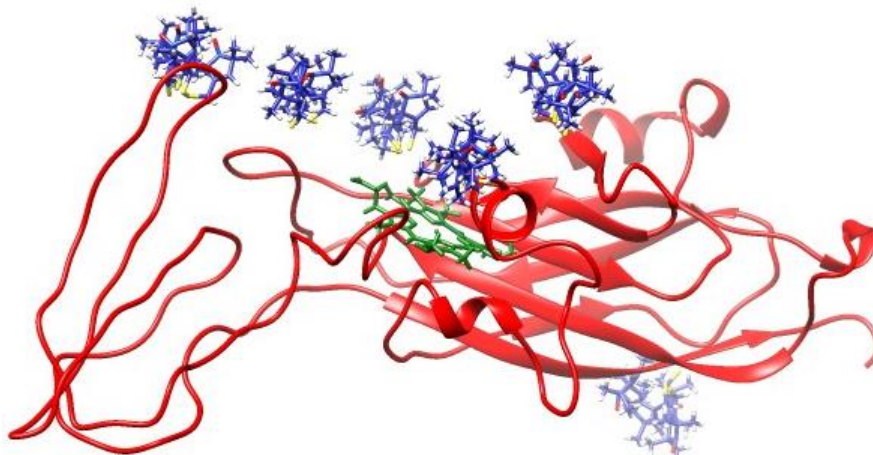


**Figure 11. Site-directed spin labeling of Cf.** Several spin labels are colored in blue at distinct positions on Cf, colored in red. The heme group of Cf is colored in green. PDB coordinates were taken from the crystal structure of *Nostoc Cf* (PDB entry 2ZT9). The structure was modified to introduce Cys residues and spin labels at the following positions: Gln7, Ala63, Asn71, Gln104 and Ser192. This figure was generated with Chimera (Pettersen *et al.*, 2004).

To study encounter ensembles, other paramagnetic effects can be measured, such as Pseudo-Contact Shifts (PCS). PCS provide long-range restraints optimal for structure determination. Most lanthanoids have an anisotropic magnetic susceptibility that gives rise to PCS. The PCS is usually measured as the difference in the observed NMR shift between a paramagnetic sample and a diamagnetic analog. Ideally, the diamagnetic analog should be identical to the paramagnetic sample except for the absence of paramagnetism. Due to novel advances in developed tags,

PCS can be observed over very large distances (1-15 nm) and measured with great accuracy (Hass and Ubbink, 2014).

### **V.4.3 NUCLEAR MAGNETIC RESONANCE RESTRAINED-DRIVEN DOCKING COMPUTATIONS**

Several methods based on docking computations have been developed to study protein-protein complexes over the last few decades. Most of these approaches are, however, not driven by experimental data but based on combination of energetics and shape complementarity using distinct algorithms. These traditional algorithms generally carry out *ab initio* docking simulations followed by *a posteriori* scoring based on the experimental information. However, the use of *a priori* restrained driving docking computations, such as High Ambiguity Driven biomolecular DOCKing (HADDOCK) or in-home, XPLOR-NIH scripts-based docking computations, has significantly improved the reliability and accuracy of such docking models (van Dijk *et al.*, 2005; Kastiris and Bonvin, 2013).

HADDOCK is a docking approach that makes use of biophysical data, such as CSP resulting from NMR titration experiments. This information is introduced as Ambiguous Interaction Restraints (AIRs) to drive the docking process. An AIR is defined as an ambiguous distance between all residues shown to be involved in the interaction. HADDOCK protocol includes several essential steps for the proper performance of docking simulations: generation of topologies for cofactors, rigid body energy minimization, semi-flexible simulated annealing and flexible refinement in water. In addition, the specifications of several parameters are critical,

such as the number of structures to generate and refine, the histidine protonation states, the definition of flexible segments, electrostatic treatment, scoring scheme or solvated docking options. The accuracy of the HADDOCK approach has been tested with many transient complexes, being applied to a large variety of them (Díaz-Moreno *et al.*, 2005a; Domínguez *et al.*, 2003; van Dijk *et al.*, 2005; van Dijk and Bonvin, 2006; de Vries *et al.*, 2007; Kastritis and Bonvin, 2013; Díaz-Moreno *et al.*, 2014; Moreno-Beltrán *et al.*, 2014).

NMR-restrained docking calculations can be also run by XPLOR-NIH rigid body docking scripts, which allow introducing manually those docking steps that can be critical for the correct modeling of particular interactions, as happens for ensemble dockings. For ensemble determination, XPLOR-NIH docking scripts based on PRE restraints constitute an excellent and better alternative to standard methods for structural elucidation of transient complexes. The PRE restraints are transformed into distances, being classified in several categories according to the PRE values. In some cases, a first docking protocol is launched before the ensemble docking. Those distance restraints satisfied by the single docking are then subtracted from all available PRE constraints. These differences serve as input data for the ensemble docking. In other cases, the all available PRE constraints are used to calculate the ensemble docking (Clare and Schwieters, 2003; Scanu *et al.*, 2013; Kastritis and Bonvin, 2013; Díaz-Moreno *et al.*, 2014).

## V.4.4 NUCLEAR MAGNETIC RESONANCE STRUCTURE CALCULATION

NMR spectroscopy is a fundamental technique for understanding the behavior of proteins, especially highly dynamic and small proteins that adopt several conformations in solution. Sophisticated 2D, 3D and even 4D NMR experiments and the development of molecular biology tools for the production of sufficient quantities of the appropriately labeled samples have all played important roles in establishing NMR at the vanguard of modern structural biology. However, protein structures determined from NMR spectroscopy data only constitute about 10% of the PDB collection (Bonvin and Brünger, 1995; Kay, 2005; Berman *et al.*, 2000; Kleckner and Foster, 2011).

In particular, NMR has emerged as a powerful probe for the study of protein structure and dynamics. The goal is to relate function to dynamics and to study structures of weakly populated protein states that are thought to play an important role in biology (Güntert, 1997; Kleckner and Foster, 2011).

The backbone chemical-shift assignments serve as a starting point for studies of structure and dynamics of proteins. In fact, triple resonance experiments with  $^{15}\text{N}$  and  $^{13}\text{C}$ -labeled proteins are usually carried out for this purpose. In addition, the side chain chemical-shift assignments are necessary for structural determination. However, to extract distance constraints for further structure determination calculations, the conformation data are mainly derived from 2D and 3D NOE spectroscopy (NOESY) spectra. Most of NOESY cross-peaks have to be

assigned, by hand or automated modes, using the assigned chemical-shifts lists. In addition to the problem of peak overlap, some difficulties arise from spectral artifacts, noise, fast relaxation or conformational exchange. Once NOE assignments are carried out, peak volumes are integrated and introduced as input data for structure calculations. The evaluation of NOESY spectra is generally the time-limiting step in protein structure determination by NMR (Wüthrich, 1986; Güntert, 1997; Güntert *et al.*, 1997; Kleckner and Foster, 2011; Maslennikov and Choe, 2013; Oxenoid and Chou, 2013; Gautier, 2014). Dihedral-angle constraints are also used as input data in these computations. TALOS software is habitually used to predict protein backbone torsion angles from NMR chemical-shifts (Shen *et al.*, 2009). Other restraints derived from NMR data, such as pseudo-contact shifts (PCS) and residual dipolar couplings (RDC), can be included during a structure calculation to better restrict molecular conformations to those which are consistent with the observed data.

In the program CYANA, iterative cycles of calculation and refinement are required to perform the structure calculation, in which NMR-derived structural data is transformed into PDB coordinates. Some of the critical steps in this process are: calibration of distance constraints, elimination of spurious NOESY cross-peaks and re-assignment of incorrect NOE cross-peaks (Güntert *et al.*, 1997). In addition, NMR-restrained molecular dynamics (RMD) simulations are performed to minimize the structure (Berndt *et al.*, 1996; Marion, 2013). Finally, NMR data and structures have to be deposited in the Protein Data Bank (PDB, <http://www.rcsb.org/pdb/>) and the Biological Magnetic Resonance Data Bank (BMRB, <http://www.bmrb.wisc.edu/>).



## V.5 ISOTHERMAL TITRATION CALORIMETRY EXPERIMENTS

Isothermal Titration Calorimetry (ITC) is the most quantitative technique available for measuring the stoichiometry and thermodynamic properties of a biomolecule-biomolecule interaction. ITC measures the heat uptake or release during an inter-molecule interaction in solution. An ITC titration experiment consists of successive additions of a biomolecule target to a solution of a protein contained in a reaction cell. Each addition leads to a specific amount of complex formation and can be monitored as the heat released or absorbed. ITC can precisely determine the equilibrium dissociation constant ( $K_D$ ), the binding enthalpy ( $\Delta H$ ) and the stoichiometry of the reaction ( $n$ ). In addition, the Gibbs energy ( $\Delta G$ ) and binding entropy ( $\Delta S$ ) parameters can be determined from the  $K_D$  values. Notably, ITC is extensively used for transient interactions (Velázquez-Campoy *et al.*, 2015). Analysis of the ITC data can be performed using distinct binding models that consider independent binding sites or cooperative effects, among other binding parameters (Velázquez-Campoy *et al.*, 2004; Freire *et al.*, 2009).



## **VI. OBJECTIVES**



---

## VI. OBJECTIVES

---

The main objectives of this PhD thesis are as follows:

1. To determine the biophysical and structural features of the transient complex between plant cytochrome *c* and the globular domain of plant cytochrome *c*<sub>1</sub>, by means of Nuclear Magnetic Resonance in solution and restrained-docking methodologies.
2. To understand the structural aspects of the transient interaction of respiratory cytochrome *c* with complexes III and IV in solution by using heterologous proteins, namely human cytochrome *c*, the globular domain of plant cytochrome *c*<sub>1</sub> and bovine cytochrome *c* oxidase.
3. To search for the structural basis for the role of cytochrome *c* transferring electrons into the mitochondrial electron transport chain in plants and animals.
4. To solve the Nuclear Magnetic Resonance Structure and Dynamics of a phosphomimetic variant of cytochrome *c*, built using transfer RNA-based technologies.

In addition, secondary objectives are listed below:

1. To model the transient encounter complex between cyanobacterial cytochrome *c*<sub>6</sub> and the soluble domain of cyanobacterial cytochrome *f* by means of ensemble restrained-docking calculations.
2. To provide further insight into the biophysical characterization of the transient communication between plant cytochrome *c* and

## VI. Objectives

---

plant L-galactono-1,4-lactone dehydrogenase, by Nuclear Magnetic Resonance in solution.

## **VII. RESULTS AND DISCUSSION**





---

## VII. RESULTS AND DISCUSSION

---

In this section, a quick overview at the Results and Discussion of published works is presented. Several subsections have been included to address the following topics: short-lived complexes, promiscuity and binding surfaces, binding affinity and stoichiometry, transient complex formation, electron transfer pathways within supercomplexes, variability in binding mode and post-translational modifications. Please, refer to the journal publications in Appendix I for further details.

### VII.1. ELECTRON TRANSFER COMPLEXES AS EXAMPLES OF SHORT-LIVED COMPLEXES

Inter-protein complexes analyzed in this PhD thesis involve ET reactions that take place during cellular respiration (*e.g.*, Cc-Cc<sub>1</sub> or Cc-CcO), photosynthesis (*e.g.*, Cc<sub>6</sub>-Cf or Pc-Cf) and vitamin C synthesis (*e.g.*, Cc-GALDH). All these complexes are excellent examples of short-lived interactions, in which soluble proteins exchange electrons with membrane-proteins via transient contacts (Lenaz and Genova, 2010; Díaz-Quintana *et al.*, 2015; Moreno-Beltrán *et al.*, 2015a). The molecular interactions within any short-lived complex must be able to balance high dissociation rates with binding specificity (Bashir *et al.*, 2011).

The binding affinities of the above mentioned redox complexes are weak, with  $K_D$  values within the micromolar-minimolar range (Hervás *et al.*, 2013; Díaz-Moreno *et al.*, 2014; Moreno-Beltrán *et al.*, 2014; Moreno-Beltrán *et al.*, 2015b), with the exception of the Cc-CcO complex (Moreno-Beltrán *et al.*, 2015b). The higher binding affinity of

the latter complex could be ascribed to the use of the entire membrane-bound CcO in contrast to the use of soluble domains, as previously suggested for cyanobacterial respiratory complexes (Navarro *et al.*, 2005).

The intermediate/fast exchange regimes observed by NMR for Cc-Cc<sub>1</sub>, Cc-CcO, Cc-GALDH and Cc<sub>6</sub>-Cf complexes are consistent with  $k_{\text{off}}$  values greater than or equal to  $10^3 \text{ s}^{-1}$  and lifetimes in the microsecond-millisecond range. This guarantees the balance between specificity and turnover, which is critical for ET (Sakamoto *et al.*, 2011; Hervás *et al.*, 2013; Scanu *et al.*, 2013; Díaz-Moreno *et al.*, 2014; Moreno-Beltrán *et al.*, 2014; Moreno-Beltrán *et al.*, 2015b).

## VII.2. PROMISCUITY AND BINDING SURFACES

In addition to a high turnover, a certain amount of promiscuity in the electron carriers Cc, Cc<sub>6</sub> and Pc is needed, since their surfaces are often optimized to recognize and interact with multiple redox partners (Schreiber and Keating, 2011; Hervás *et al.*, 2013; Díaz-Moreno *et al.*, 2014; Moreno-Beltrán *et al.*, 2014; Moreno-Beltrán *et al.*, 2015a; Moreno-Beltrán *et al.*, 2015b). In general, redox centers of the electron carriers are usually surrounded by a hydrophobic patch and a charged rim where the interacting partners bind (Williams *et al.*, 1995).

NMR CSP analyses have been performed for the identification of the inter-protein binding surfaces of the Cc-Cc<sub>1</sub>, Cc-CcO, Cc-GALDH, Cc<sub>6</sub>-Cf and Pc-Cf complexes in solution (Sakamoto *et al.*, 2011; Hervás *et al.*, 2013; Scanu *et al.*, 2013; Díaz-Moreno *et al.*, 2014; Moreno-Beltrán *et al.*

*al.*, 2014; Moreno-Beltrán *et al.*, 2015b). Such CSP maps provide valuable data about key residues involved in ET.

For the case of Cc-involving complexes, the participation of the surface surrounding the heme crevice of Cc was found not only to be involved in its binding with the mitochondrial redox targets, such as Cc<sub>1</sub> and CcO (Moreno-Beltrán *et al.*, 2014; Moreno-Beltrán *et al.*, 2015b), but also with their pro-apoptotic targets in the cytosol and even in the nuclei (Martínez-Fábregas *et al.*, 2013; Martínez-Fábregas *et al.*, 2014a; Moreno-Beltrán *et al.*, 2015a). However, in contrast to the high turnover rate of the mitochondrial Cc redox adducts, those occurring under apoptosis lead to the formation of stable complexes, as inferred mainly from Surface Plasmon Resonance (SPR) measurements (Martínez-Fábregas *et al.*, 2013; Martínez-Fábregas *et al.*, 2014a). Such diversity in the binding mode can be understood due to the distinct contexts of the various interactions of Cc-involving complexes. Whereas respiration is governed by highly transient interactions of Cc required for an efficient ET within the mitochondria, the amazingly stable nucleocytoplasmic adducts of Cc could both block survival pathways and unlock pro-apoptotic signals (Martínez-Fábregas *et al.*, 2013; Martínez-Fábregas *et al.*, 2014a; Martínez-Fábregas *et al.*, 2014b; Moreno-Beltrán *et al.*, 2015a).

The variability of binding modes in complexes involving heterologous transient partners can be determined by CSP analysis (Díaz-Moreno *et al.*, 2005b; Hervás *et al.*, 2013; Moreno-Beltrán *et al.*, 2015b). Indeed, such chemical-shift maps can be indicative of how dynamic or unspecific a complex is, as has been observed in the case of Cc-GALDH and Cc-Cc<sub>1</sub> heterologous complexes (Hervás *et al.*, 2013; Moreno-Beltrán *et al.*,

2015b). The diffusion properties of orthologous proteins may not differ substantially, due to their nearly identical sizes and shapes. However, the binding and ET rates of heterologous complexes usually differ from physiological ones, insofar as the ET may be optimum within the physiological complexes (Moreno-Beltrán *et al.*, 2015b). Such differences can be rationalized not only in terms of the total net charge of the proteins, but also in subtle changes arising from specific charge localizations on the surfaces of the two molecules, as was described for the heterologous complexes Cc-GALDH and Cc-Cc<sub>1</sub> (Hervás *et al.*, 2013; Moreno-Beltrán *et al.*, 2015b).

### **VII.3. STOICHIOMETRY AND BINDING AFFINITY**

To transport an electron from a donor protein to a remote acceptor one, the carrier must specifically recognize the two partners, along with being dissociated quickly from them (Bashir *et al.*, 2011; Díaz-Quintana *et al.*, 2015; Moreno-Beltrán *et al.*, 2015a). The binding affinity, as well as the stoichiometry of the interaction, is essential to properly understand the biological system (Moreno-Beltrán *et al.*, 2015a). Both reaction parameters can be determined by CSP using distinct mathematical binding models, as is done for Cc-Cc<sub>1</sub> complexes (Moreno-Beltrán *et al.*, 2014; Moreno-Beltrán *et al.*, 2015b).

In addition, binding parameters are strongly modulated by the ionic strength since the short-lived ET complexes are electrostatically driven (Hervás *et al.*, 2013; Moreno-Beltrán *et al.*, 2014; Moreno-Beltrán *et al.*, 2015b). Indeed, the two principal interaction forces leading to the

formation of such adducts are mainly electrostatics and hydrophobics, as concluded from theoretical and experimental data for many transient complexes (Moreno-Beltrán *et al.*, 2014; Moreno-Beltrán *et al.*, 2015a).

As a complement to solution NMR, ITC binding experiments have been used to accurately determine the binding affinity and stoichiometry of such transient complexes in solution (Hervás *et al.*, 2013; Moreno-Beltrán *et al.*, 2014; Moreno-Beltrán *et al.*, 2015b). The differences in dissociation constants obtained in some cases by ITC and NMR can be explained by the distinct physical phenomena measured and by differences in the experimental conditions. However, there are no significant discrepancies in the results obtained from the biological systems that we have analyzed in this PhD thesis.

It is important to note here that most NMR or ITC analyses are performed at low ionic strength. Under such conditions, the non-specific long-range interactions are favored (Díaz-Quintana *et al.*, 2015; Moreno-Beltrán *et al.*, 2015b). A full comprehension of the reaction mechanism for ET complexes demands the consideration of the diverse available data, including the cross-linking approaches, direct binding or kinetics experiments (Díaz-Quintana *et al.*, 2015; Moreno-Beltrán *et al.*, 2015a). For instance, in addition to the NMR and ITC assays, laser-flash measurements were carried out to monitor the oxidation of GALDH by Cc. These experiments showed a nonlinear dependence on Cc concentration at low ionic strength, suggesting the formation of a transient complex prior to the ET step. Notably, in contrast to what happens at low ionic strength, the ET rate of this interaction increases at high ionic strength and is consistent with a second-order collision process (Hervás *et al.*, 2013).

## VII.4. FROM THE ENCOUNTER ENSEMBLE TO THE WELL-DEFINED COMPLEX

The formation of protein-protein complexes is thought to be a two-step process in which the final complex is preceded by an intermediate state, or a so-called encounter complex (Bashir *et al.*, 2011; Schilder and Ubbink, 2013; Hass and Ubbink, 2014). The binding event is first described by a coupled diffusion model where a protein binds nonspecifically to its partner's surface – forming the so-called encounter complex – and then diffuses along the partner's surface (*i.e.*, slides on it) until it either finds an active conformation or dissociates from its partner. At this stage, it is worth noting that the population of complexes capable of ET reactions may correspond to either a single conformation or a subset of an ensemble of conformers.

On the one hand, paramagnetic NMR experiments have shown that cyanobacterial  $Cc_6$  slides along a particular region on the surface of  $Cf$ , generating an encounter complex in which the achievement of the productive conformation is practically guaranteed during the lifetime of the complex (Díaz-Moreno *et al.*, 2014). Although previous docking models have pointed to a well-defined  $Cc_6$ - $Cf$  complex (Díaz-Moreno *et al.*, 2005a), PRE NMR data are not compatible with this (Díaz-Moreno *et al.*, 2014). The complex is best described by a highly dynamic ensemble, first formed by electrostatic pre-orientation and then stabilized mainly by hydrophobic contacts.

The binding affinity in this complex is lower in comparison with those calculated for  $Cc$ -involving complexes at low ionic strength (Díaz-

Moreno *et al.*, 2014; Moreno-Beltrán *et al.*, 2014; Martínez-Fábregas *et al.*, 2014a), but comparable with those performed at a moderate or high ionic strength (Hervás *et al.*, 2013; Moreno-Beltrán *et al.*, 2015b). It is relevant to mention that the high off-rate is as significant as the binding affinity for the success of the transient complexes (Díaz-Quintana *et al.*, 2015). In fact, given the high local concentration of  $Cc_6$  and  $Cf$  in the lumen, the low affinity does not imply a strict requirement for this complex formation.

PRE NMR profiles indicate a major encounter population in which electrostatic forces promote the establishment of hydrophobic forces, but do not take part in the activation barrier. This activation barrier might be low due to the gradual resolution proposed for this interaction (Díaz-Moreno *et al.*, 2014). This coincides with the finding that complexes involving *Nostoc Cc<sub>6</sub>* do not show the enthalpy-entropy compensation in activation energy characteristic of other ones and exhibits a rate constant for electron donation to PSI that is independent of temperature (Hervás *et al.*, 1996).

The idea that multiple orientations of an encounter ensemble are suitable for ET was also described for the myoglobin-cytochrome  $b_5$  complex, although the latter complex appears to be dominated by charge-charge interactions (Liang *et al.*, 2002; Worrall *et al.*, 2002). Notably, the encounter complexes cannot be fully analyzed by X-ray diffraction or standard NMR methodologies like diamagnetic CSP, as they are not sensitive to populations of less than 10% of the molecules in question. They can be studied, however, using paramagnetic NMR methodologies.

On the other hand, the X-ray diffraction structure of yeast *Cc* bound to the *Cbc*<sub>1</sub> complex can serve as an example of a transient complex that adopts a single, well-defined ET conformation resulting from multiple encounters of *Cc* on the *Cbc*<sub>1</sub> surface (Lange and Hunte, 2002; Heinemeyer *et al.*, 2007). This productive conformation of *Cc* with respect to the surface of plant *Cc*<sub>1</sub> has also been detected in solution by NMR and ITC. Notably, a second non-ET conformation of *Cc* was also identified by combining NMR and ITC with computational methods (Moreno-Beltrán *et al.*, 2014). The docking of *Cc* at a negatively-charged pocket of plant *Cc*<sub>1</sub>, named as the *distal* binding site, is fully compatible with the complex III structure (Moreno-Beltrán *et al.*, 2014). The finding of this *distal* site matches previous cross-linking and functional assays (Speck and Margoliash, 1984; Stonehuerner *et al.*, 1985; Devanathan *et al.*, 2007; Genova and Lenaz, 2013). Both the *distal* and the productive site, named as the *proximal* site, differ in the heme-to-heme distance according to the *ab-initio* and NMR-restrained docking calculations (Moreno-Beltrán *et al.*, 2014). The visualization of the *proximal*, but not the *distal* site in X-ray coordinates, could be explained by assuming a weaker nature of the *distal* binding site, which could be, on the contrary, stable enough to be detected by NMR. Indeed, *Cc* interacts with both the *proximal* and *distal* sites of *Cc*<sub>1</sub> with different dissociation constants. The differences in affinity between both binding sites are moderate. This latter finding is compatible with the linear behavior of the CSP observed for *Cc* amide groups and with a similar chemical environment on the surface of plant *Cc*<sub>1</sub>, which is negatively charged (Moreno-Beltrán *et al.*, 2014; Moreno-Beltrán *et al.*, 2015b).



## VII.5. ELECTRON TRANSFER PATHWAYS WITHIN RESPIRATORY SUPERCOMPLEXES

The concept of substrate channeling has been applied in enzymology to explain how small molecules undergo sequential transformations without diffusing to the bulk phase (Kholodenko and Westerhoff, 1993; Brown *et al.*, 1996). Recently, a channeling of plant Cc molecules was proposed to account for the ET between the Cbc<sub>1</sub> and CcO complexes (Genova and Lenaz, 2013; Moreno-Beltrán *et al.*, 2014). According to our results, a novel, extra *distal* site of plant Cc<sub>1</sub> detected in solution may provide a path for diffusion of the Cc molecules towards CcO, facilitating the functional shuttle of electrons (Moreno-Beltrán *et al.*, 2014).

The presence of additional binding sites for Cc has also been detected in bovine CcO in equilibrium conditions (Moreno-Beltrán *et al.*, 2015b) and in gel filtration studies (Osheroff, *et al.*, 1983). These new sites of Cc on Cc<sub>1</sub> and CcO open up new scenarios within the mitochondrial electron chain, which could explain the “sliding” dissociation pathway hypothesis in mammals (De March *et al.*, 2014; Moreno-Beltrán *et al.*, 2015b). This model suggests that the Cc glides along the surface of Cc<sub>1</sub> during their functional binding instead of a direct dissociation from the Cc<sub>1</sub> surface.

## VII.6. POST-TRANSLATIONAL REGULATION

Cc is a target of several post-translational modifications such as nitration (Rodríguez-Roldán *et al.*, 2008; García-Heredia *et al.*, 2010; Díaz-Moreno *et al.*, 2011b; García-Heredia *et al.*, 2012) and phosphorylation (García-Heredia *et al.*, 2011), which have an effect on

the conformation of the heme moiety and its functionality as an electron carrier and apoptotic protein (Lee *et al.*, 2006; Yu *et al.*, 2008; Pecina *et al.*, 2010; Hüttemann *et al.*, 2011; Díaz-Moreno *et al.*, 2011; García-Heredia *et al.*, 2011; García-Heredia *et al.*, 2012; Ly *et al.*, 2012).

However, many functional and structural aspects of the biointeractomics of *Cc* inside the mitochondria upon these modifications still remain obscure. Further research is now in progress to unveil the role of phosphorylated human *Cc* at Tyr48 in cellular respiration and PCD. Unfortunately, the specific *Cc*-phosphorylating kinase remains unknown and due to the technical difficulties of obtaining enough phosphorylated *Cc* from cell extracts, it is usually mimicked by using Tyr-by-Glu mutations (García-Heredia *et al.*, 2011). To improve the traditional mimicking of Tyr48 phosphorylation, Tyr48 residue can be replaced by the non-canonical amino acid *p*-carboxymethyl-L-phenylalanine (*p*CMF). *p*CMF better emulates the volume of a phosphorylated tyrosine residue than a glutamic residue (Xie *et al.*, 2007). Thus, the Tyr48-encoding triplet of the human *Cc* gene was substituted by an amber stop codon to replace the original residue with the non-canonical amino acid by the evolved tRNA technique. This innovative approach allows for the efficient incorporation of *p*CMF at a site-specific position as a result of the action of an orthogonal tRNA that recognizes the amber codon.

The structure and dynamics of this novel phosphomimetic *Cc* at position 48 have been solved by using NMR in solution. Notably, the structure of phosphomimetic *Cc* reveals significant changes at the loop containing the *p*CMF and its 3D proximal environment, especially the 50's helix and the omega-loop including the methionine ligand of the iron. In addition, the NMR relaxation measurements point to a highly

dynamic behavior of the loop containing the mutation, which displays a high flexibility in the  $\mu\text{s}$ -ns timescale as can be inferred from heteronuclear NOE (HetNOE) and longitudinal relaxation rate ( $R_1$ ) measurements. In addition, conformational exchanges in the ms timescale are also detected, as determined by transverse relaxation rate ( $R_2$ ) parameters and a careful evaluation of NOESY spectra. These structural data strongly support its biological functionality, in which this post-translationally modified Cc impairs both mitochondrial respiration and programmed cell death events (Moreno-Beltrán *et al.*, unpublished data).



## **VIII. CONCLUSIONS**



---

## VIII. CONCLUSIONS

---

The main conclusions of this PhD thesis inferred from the distinct redox systems are:

1. Additional binding sites in equilibrium conditions for respiratory cytochrome *c* in both mitochondrial complexes III and IV have been elucidated *in vitro*. These extra sites could facilitate the turnover and sliding mechanisms of cytochrome *c* molecules between complexes III and IV within plant and mammalian supercomplexes. In this context, the traditional and simple view of cytochrome *c* as a long-distance carrier in the membrane would be replaced by a new and innovative one, in which cytochrome *c* molecules would glide on respiratory complexes III and IV surfaces without entering into the mitochondrial bulk phase. Such diffusion paths might have physiological significance in the electron flow within supercomplexes so as to optimize the use of available substrates.
2. The Nuclear Magnetic Resonance structure of phosphomimetic cytochrome *c* shows significant changes at the region containing the analogue of the phosphorylated tyrosine and its environment, affecting proximal areas of cytochrome *c*, such as the 50's helix and the omega-loop containing the methionine axial ligand. The Nuclear Magnetic Resonance relaxation measurements point to a

highly dynamic behavior of the phosphomimetic protein. These structural data can support its functional behavior, in which this post-translationally modified cytochrome *c* impairs both mitochondrial respiration and programmed cell death events.

3. The structure of the cyanobacterial complex between cytochrome *f* and cytochrome *c*<sub>6</sub> reveals that the encounter ensemble is essential to molecular recognition events among photosynthetic electron transfer proteins. Experimental evidence for the role of hydrophobic interactions in the encounter complex is cumulative, blurring the distinction between encounter complex and stereospecific complex. This finding becomes more evident in electron transfer complexes, where a short distance between the metal ions is all that is required for their electron transfer activity. Then, there is no reason for the assembly of a single, active orientation within the complex.
4. Plant L-galactono-1,4-lactone dehydrogenase forms a transient low affinity complex with plant and yeast cytochrome *c*. This relatively non-specific interaction involves protein–protein dynamic motions and does not preclude rapid electron transfer within the complex, since sufficient electron transfer permissible conformations are apparently sampled in this dynamic complex.



## **IX. GENERAL REFERENCES**



---

## IX. GENERAL REFERENCES

---

- Acín-Pérez R, Fernández-Silva P, Peleato ML, Pérez-Martos A & Enriquez JA (2008) Respiratory active mitochondrial supercomplexes. *Mol Cell* 32, 529-539.
- Acín-Pérez R & Enriquez JA (2014) The function of the respiratory supercomplexes: The plasticity model. *Biochim Biophys Acta - Bioenergetics* 1837, 444-450.
- Althoff T, Mills DJ, Popot J-L & Kühlbrandt W (2011) Arrangement of electron transport chain components in bovine mitochondrial supercomplex I<sub>1</sub>III<sub>2</sub>IV<sub>1</sub>. *EMBO J* 30, 4652-4664.
- Amunts A, Drory O & Nelson N (2007) The structure of a plant photosystem I supercomplex at 3.4 Å resolution. *Nature* 447, 58-63.
- Amunts A, Toporik H, Borovikova A & Nelson N (2010) Structure determination and improved model of plant photosystem I. *J Biol Chem* 285, 3478-3486.
- Bailey S, Melis A, Mackey KRM, Cardol P, Finazzi G, van Dijken G, Berg GM, Arrigo K, Shrager J & Grossman A (2008) Alternative photosynthetic electron flow to oxygen in marine *Synechococcus*. *Biochim Biophys Acta - Bioenergetics* 1777, 269-276.
- Baistrocchi P, Banci L, Bertini I & Turano P (1996) Three-dimensional solution structure of *Saccharomyces cerevisiae* reduced iso-1-cytochrome *c*. *Biochemistry* 35, 13788-13796.
- Banci L, Bertini I, Bren KL, Gray HB, Sompornpisut P & Turano P (1997) Solution structure of oxidized *Saccharomyces cerevisiae* iso-1-cytochrome *c*. *Biochemistry* 36, 8992-9001.
- Baniulis D, Yamashita E, Zhang H, Hasan SS & Cramer WA (2008) Structure–function of the cytochrome *b<sub>f</sub>* complex. *Photochem Photobiol* 84, 1349-1358.

- Bashir Q, Scanu S & Ubbink M (2011) Dynamics in electron transfer protein complexes. *FEBS J* 278, 1391-1400.
- Berndt KD, Güntert P & Wüthrich K (1996) Conformational sampling by NMR solution structures calculated with the program DIANA evaluated by comparison with long-time molecular dynamics calculations in explicit water. *Proteins* 24, 304-313.
- Berman HM, Battistuz T, Bhat TN, Bluhm WF, Bourne PE, Burkhardt K, Feng Z, Gilliland GL, Iype L, Jain S, *et al.* (2002) The Protein Data Bank. *Acta Crystallogr Sect D* 58, 899-907.
- Bialek W, Krzywda S, Jaskolski M & Szczepaniak A (2009) Atomic-resolution structure of reduced cyanobacterial cytochrome  $c_6$  with an unusual sequence insertion. *FEBS J* 276, 4426-4436.
- Bianchi C, Genova ML, Parenti Castelli G & Lenaz G (2004) The mitochondrial respiratory chain is partially organized in a supercomplex assembly: kinetic evidence using flux control analysis. *J Biol Chem* 279, 36562-36569.
- Bonvin AMJJ & Brünger AT (1995) Conformational variability of solution nuclear magnetic resonance structures. *J Mol Biol* 250, 80-93.
- Breyton C (2000) The cytochrome  $b_6f$  complex: structural studies and comparison with the  $bc_1$  complex. *Biochim Biophys Acta - Bioenergetics* 1459, 467-474.
- Brown GC, Westerhoff HV & Kholodenko BN (1996) Molecular control analysis: control within proteins and molecular processes. *J Theor Biol* 182, 389-396.
- Bultema JB, Braun H-P, Boekema EJ & Kouřil R (2009) Megacomplex organization of the oxidative phosphorylation system by structural analysis of respiratory supercomplexes from potato. *Biochim Biophys Acta - Bioenergetics* 1787, 60-67.

## IX. General References

---

- Busch A & Hippler M (2011) The structure and function of eukaryotic photosystem I. *Biochim Biophys Acta - Bioenergetics* 1807, 864-877.
- Caffarri S, Kouřil R, Kerešič S, Boekema EJ & Croce R (2009) Functional architecture of higher plant photosystem II supercomplexes. *EMBO J* 28, 3052-3063.
- Camacho-Zarco AR, Munari F, Wegstroth M, Liu W.M, Ubbink M, Becker S & Zweckstetter M (2015) Multiple paramagnetic effects through a tagged reporter protein. *Angew Chem Int Ed Engl* 54, 336-339.
- Canters GW & Gilardi G (1993) Engineering type 1 copper sites in proteins. *FEBS Lett* 325, 39-48.
- Chance B & Williams GR (1955) Respiratory enzymes in oxidative phosphorylation: IV. The respiratory chain. *J Biol Chem* 217, 429-438.
- Chen Y.C, Taylor Eric B, Dephoure N, Heo J.M, Tonhato A, Papandreou I, Nath N, Denko Nicolas C, Gygi Steven P & Rutter J (2012) Identification of a protein mediating respiratory supercomplex stability. *Cell Metab* 15, 348-360.
- Clore GM & Schwieters CD (2003) Docking of protein-protein complexes on the basis of highly ambiguous intermolecular distance restraints derived from  $^1\text{HN}/^{15}\text{N}$  chemical shift mapping and backbone  $^{15}\text{N}-^1\text{H}$  residual dipolar couplings using conjoined rigid body/torsion angle dynamics. *J Am Chem Soc* 125, 2902-2912.
- Croce R & van Amerongen H (2014) Natural strategies for photosynthetic light harvesting. *Nat Chem Biol* 10, 492-501.
- Crowley PB & Ubbink M (2003) Close encounters of the transient kind: proteins interactions in the photosynthetic redox chain investigated by NMR spectroscopy. *Acc Chem Res* 36, 723-730.
- De March M, Demitri N, De Zorzi R, Casini A, Gabbiani C, Guerri A, Messori L & Geremia S (2014) Nitrate as a probe of cytochrome c

surface: Crystallographic identification of crucial “hot spots” for protein–protein recognition. *J Inorg Biochem* 135, 58-67.

- de Vries SJ, van Dijk ADJ, Krzeminski M, van Dijk M, Thureau A, Hsu V, Wassenaar T & Bonvin AMJJ (2007) HADDOCK versus HADDOCK: New features and performance of HADDOCK 2.0 on the CAPRI targets. *Proteins* 69, 726-733.
- Dekker JP & Boekema EJ (2005) Supramolecular organization of thylakoid membrane proteins in green plants. *Biochim Biophys Acta - Bioenergetics* 1706, 12-39.
- Desmurs M, Foti M, Raemy E, Vaz FM, Martinou J-C, Bairoch A & Lane L (2015) C11orf83, a mitochondrial cardiolipin-binding protein involved in *bc*<sub>1</sub> complex assembly and supercomplex stabilization. *Mol Cell Biol* 35, 1139-1156.
- Devanathan S, Salamon Z, Tollin G, Fitch JC, Meyer TE, Berry EA & Cusanovich MA (2007) Plasmon waveguide resonance spectroscopic evidence for differential binding of oxidized and reduced *Rhodobacter capsulatus* cytochrome *c*<sub>2</sub> to the cytochrome *bc*<sub>1</sub> complex mediated by the conformation of the Rieske iron–sulfur protein. *Biochemistry* 46, 7138-7145.
- Díaz-Moreno I, Díaz-Quintana A, Ubbink M & De la Rosa MA (2005a) An NMR-based docking model for the physiological transient complex between cytochrome *f* and cytochrome *c*<sub>6</sub>. *FEBS Lett* 579, 2891-2896.
- Díaz-Moreno I, Díaz-Quintana A, De la Rosa MA, Crowley PB & Ubbink M (2005b) Different modes of interaction in cyanobacterial complexes of plastocyanin and cytochrome *f*. *Biochemistry* 44, 3176-3183.
- Díaz-Moreno I & De la Rosa MA (2011) Transient interactions between biomolecules. *Eur Biophys J* 40, 1273-1274.

## IX. General References

---

- Díaz-Moreno I, García-Heredia JM, Díaz-Quintana A & De la Rosa MA (2011) Cytochrome *c* signalosome in mitochondria. *Eur Biophys J* 40, 1301-1315.
- Díaz-Moreno I, Hulsker R, Skubak P, Foerster JM, Cavazzini D, Finiguerra MG, Díaz-Quintana A, Moreno-Beltrán B, Rossi G-L, Ullmann GM, *et al.* (2014) The dynamic complex of cytochrome *c*<sub>6</sub> and cytochrome *f* studied with paramagnetic NMR spectroscopy. *Biochim Biophys Acta - Bioenergetics* 1837, 1305-1315.
- Díaz-Quintana A, Cruz-Gallardo I, De la Rosa MA & Díaz-Moreno I (2015) Diversity of interactions of redox systems: from short-lived to long-lived complexes. In *Redox proteins in supercomplexes and signalosomes*. Taylor and Francis Editorial Group.
- DiMauro S (2004) Mitochondrial diseases. *Biochim Biophys Acta - Molecular Basis of Disease* 1658, 80-88.
- Dominguez C, Boelens R & Bonvin AMJJ (2003) HADDOCK: A protein-protein docking approach based on biochemical or biophysical information. *J Am Chem Soc* 125, 1731-1737.
- Drop B, Webber-Birungi M, Fusetti F, Kouřil R, Redding KE, Boekema EJ & Croce R (2011) Photosystem I of *Chlamydomonas reinhardtii* contains nine light-harvesting complexes (Lhca) located on one side of the core. *J Biol Chem* 286, 44878-44887.
- Dudkina NV, Kudryashev M, Stahlberg H & Boekema EJ (2011) Interaction of complexes I, III, and IV within the bovine respirasome by single particle cryoelectron tomography. *Proc Natl Acad Sci USA* 108, 15196-15200.
- Eubel H (2003) New insights into the respiratory chain of plant mitochondria. Supercomplexes and a unique composition of complex II. *Plant Physiol* 133, 274-286.

- Eubel H, Heinemeyer J, Sunderhaus S & Braun HP (2004) Respiratory chain supercomplexes in plant mitochondria. *Plant Physiol Biochem* 42, 937-942.
- Freire E, Schön A & Velazquez-Campoy A (2009) Isothermal titration calorimetry: general formalism using binding polynomials. *Methods Enzymol* 455, 127-155.
- García-Heredia JM, Díaz-Moreno I, Nieto PM, Orzáez M, Kocanis S, Teixeira M, Pérez-Payá E, Díaz-Quintana A & De la Rosa MA (2010) Nitration of tyrosine 74 prevents human cytochrome *c* to play a key role in apoptosis signaling by blocking caspase-9 activation. *Biochim Biophys Acta - Bioenergetics* 1797, 981-993.
- García-Heredia JM, Díaz-Quintana A, Salzano M, Orzáez M, Pérez-Payá E, Teixeira M, De la Rosa MA & Díaz-Moreno I (2011) Tyrosine phosphorylation turns alkaline transition into a biologically relevant process and makes human cytochrome *c* behave as an anti-apoptotic switch. *J Biol Inorg Chem* 16, 1155-1168.
- García-Heredia JM, Díaz-Moreno I, Díaz-Quintana A, Orzáez M, Navarro JA, Hervás M & De la Rosa MA (2012) Specific nitration of tyrosines 46 and 48 makes cytochrome *c* assemble a non-functional apoptosome. *FEBS Lett* 586, 154-158.
- Gautier A (2014) Structure determination of  $\alpha$ -helical membrane proteins by solution-state NMR: Emphasis on retinal proteins. *Biochim Biophys Acta - Bioenergetics* 1837, 578-588.
- Genova ML & Lenaz G (2013) A critical appraisal of the role of respiratory supercomplexes in mitochondria. *Biol Chem* 394, 631-639.
- Genova ML & Lenaz G (2014) Functional role of mitochondrial respiratory supercomplexes. *Biochim Biophys Acta - Bioenergetics* 1837, 427-443.



## IX. General References

---

- Gong XS, Wen JQ & Gray JC (2000) The role of amino-acid residues in the hydrophobic patch surrounding the haem group of cytochrome *f* in the interaction with plastocyanin. *Eur J Biochem* 267, 1732-1742.
- Güntert P (1997) Calculating Protein Structures from NMR Data. In *Protein NMR Techniques*. Humana Press.
- Güntert P, Mumenthaler C & Wüthrich K (1997) Torsion angle dynamics for NMR structure calculation with the new program Dyana. *J Mol Biol* 273, 283-298.
- Gupte SS, Wu ES, Hoehli L, Hoehli M, Jacobson K, Sowers AE & Hackenbrock CR (1984) Relationship between lateral diffusion, collision frequency, and electron transfer of mitochondrial inner membrane oxidation-reduction components. *Proc Natl Acad Sci USA* 81, 2606-2610.
- Hackenbrock CR, Chazotte B & Gupte SS (1986) The random collision model and a critical assessment of diffusion and collision in mitochondrial electron transport. *J Bioenerg Biomembr* 18, 331-368.
- Hasan SS & Cramer WA (2012) On rate limitations of electron transfer in the photosynthetic cytochrome *b<sub>6</sub>f* complex. *Phys Chem Chem Phys* 14, 13853-13860.
- Hass MAS & Ubbink M (2014) Structure determination of protein–protein complexes with long-range anisotropic paramagnetic NMR restraints. *Curr Opin Struct Biol* 24, 45-53.
- Hayashi T, Asano Y, Shintani Y, Aoyama H, Kioka H, Tsukamoto O, Hikita M, Shinzawa-Itoh K, Takafuji K, Higo S, *et al.* (2015) Higd1a is a positive regulator of cytochrome *c* oxidase. *Proc Natl Acad Sci USA* 112, 1553-1558.
- Heinemeyer J, Braun H-P, Boekema EJ & Kouřil R (2007) A structural model of the cytochrome *c* reductase/oxidase supercomplex from yeast mitochondria. *J Biol Chem* 282, 12240-12248.

- Hervás M, Navarro JA, Díaz A, Bottin H & De la Rosa MA (1995) Laser-flash kinetic analysis of the fast electron transfer from plastocyanin and cytochrome  $c_6$  to photosystem I. Experimental evidence on the evolution of the reaction mechanism. *Biochemistry* 34, 11321-11326.
- Hervás M, Navarro JA, Díaz A & De la Rosa MA (1996) A comparative thermodynamic analysis by laser-flash absorption spectroscopy of photosystem I reduction by plastocyanin and cytochrome  $c_6$  in *Anabaena* PCC 7119, *Synechocystis* PCC 6803, and spinach. *Biochemistry* 35, 2693-2698.
- Hervás M, Navarro JA & De la Rosa MA (2003) Electron transfer between membrane complexes and soluble proteins in photosynthesis. *Acc Chem Res* 36, 798-805.
- Hervás M, Bashir Q, Leferink NGH, Ferreira P, Moreno-Beltrán B, Westphal AH, Díaz-Moreno I, Medina M, de la Rosa MA, Ubbink M, *et al.* (2013) Communication between L-galactono-1,4-lactone dehydrogenase and cytochrome  $c$ . *FEBS J* 280, 1830-1840.
- Horton P, Ruban AV & Walters RG (1996) Regulation of light harvesting in green plants. *Annu Rev of Plant Physiol Plant Mol Biol* 47, 655-684.
- Howe CJ, Schlarb-Ridley BG, Wastl J, Purton S & Bendall DS (2006) The novel cytochrome  $c_6$  of chloroplasts: a case of evolutionary bricolage? *J Exp Bot* 57, 13-22.
- Hulsker R, Baranova MV, Bullerjahn GS & Ubbink M (2008) Dynamics in the transient complex of plastocyanin-cytochrome  $f$  from *Prochlorothrix hollandica*. *J Am Chem Soc* 130, 1985-1991.
- Hüttemann M, Pecina P, Rainbolt M, Sanderson TH, Kagan VE, Samavati L, Doan JW & Lee I (2011) The multiple functions of cytochrome  $c$  and their regulation in life and death decisions of the

- mammalian cell: From respiration to apoptosis. *Mitochondrion* 11, 369-381.
- Hüttemann M, Helling S, Sanderson TH, Sinkler C, Samavati L, Mahapatra G, Varughese A, Lu G, Liu J, Ramzan R, *et al.* (2012a) Regulation of mitochondrial respiration and apoptosis through cell signaling: Cytochrome *c* oxidase and cytochrome *c* in ischemia/reperfusion injury and inflammation. *Biochim Biophys Acta - Bioenergetics* 1817, 598-609.
  - Hüttemann M, Lee I, Grossman LI, Doan JW & Sanderson TH (2012b) Phosphorylation of mammalian cytochrome *c* and cytochrome *c* oxidase in the regulation of cell destiny: Respiration, apoptosis, and human disease. In *Mitochondrial Oxidative Phosphorylation*. Springer New York.
  - Ifuku K, Ido K & Sato F (2011) Molecular functions of PsbP and PsbQ proteins in the photosystem II supercomplex. *J Photochem Photobiol B* 104, 158-164.
  - Iwai M, Takizawa K, Tokutsu R, Okamuro A, Takahashi Y & Minagawa J (2010) Isolation of the elusive supercomplex that drives cyclic electron flow in photosynthesis. *Nature* 464, 1210-1213.
  - Iwahara J, Schwieters CD & Clore GM (2004) Ensemble approach for NMR structure refinement against  $^1\text{H}$  paramagnetic relaxation enhancement data arising from a flexible paramagnetic group attached to a macromolecule. *J Am Chem Soc* 126, 5879-5896.
  - Kastiris PL & Bonvin AMJJ (2013) Molecular origins of binding affinity: seeking the Archimedean point. *Curr Opin Struct Biol* 23, 868-877.
  - Kay LE (2011) NMR studies of protein structure and dynamics – A look backwards and forwards. *J Magn Reson* 213, 492-494.

- Keilin D & Hartree EF (1955) Relationship between certain components of the cytochrome system. *Nature* 176, 200-206.
- Kholodenko BN & Westerhoff HV (1993) Metabolic channelling and control of the flux. *FEBS Lett* 320, 71-74.
- Klammt C, Maslennikov I, Bayrhuber M, Eichmann C, Vajpai N, Chiu EJC, Blain KY, Esquivies L, Kwon JHJ, Balana B, *et al.* (2012) Facile backbone structure determination of human membrane proteins by NMR spectroscopy. *Nat Meth* 9, 834-839.
- Kleckner IR & Foster MP (2011) An introduction to NMR-based approaches for measuring protein dynamics. *Biochim Biophys Acta - Proteins and Proteomics* 1814, 942-968.
- Koopman WJH, Distelmaier F, Smeitink JAM & Willems PHGM (2012) OXPHOS mutations and neurodegeneration. *EMBO J* 32, 9-29.
- Kouřil R, Strouhal O, Nosek L, Lenobel R, Chamrád I, Boekema EJ, Šebela M & Ilík P (2014) Structural characterization of a plant photosystem I and NAD(P)H dehydrogenase supercomplex. *Plant J* 77, 568-576.
- Krause F, Reifschneider NH, Vocke D, Seelert H, Rexroth S & Dencher NA (2004) “Respirasome”-like supercomplexes in green leaf mitochondria of spinach. *J Biol Chem* 279, 48369-48375.
- Lange C & Hunte C (2002) Crystal structure of the yeast cytochrome *bc*<sub>1</sub> complex with its bound substrate cytochrome *c*. *Proc Natl Acad Sci USA* 99, 2800-2805.
- Lapuente-Brun E, Moreno-Loshuertos R, Acín-Pérez R, Latorre-Pellicer A, Colás C, Balsa E, Perales-Clemente E, Quirós PM, Calvo E, Rodríguez-Hernández MA, *et al.* (2013) Supercomplex assembly determines electron flux in the mitochondrial electron transport chain. *Science* 340, 1567-1570.

## IX. General References

---

- Lea-Smith DJ, Ross N, Zori M, Bendall DS, Dennis JS, Scott SA, Smith AG & Howe CJ (2013) Thylakoid terminal oxidases are essential for the cyanobacterium *Synechocystis* sp. PCC 6803 to survive rapidly changing light intensities. *Plant Physiol* 162, 484-495.
- Lee I, Salomon AR, Yu K, Doan JW, Grossman LI & Hüttemann M (2006) New Prospects for an Old Enzyme: Mammalian cytochrome *c* is tyrosine-phosphorylated in vivo. *Biochemistry* 45, 9121-9128.
- Leferink NGH, van den Berg WAM & van Berkel WJH (2008) 1-Galactono- $\gamma$ -lactone dehydrogenase from *Arabidopsis thaliana*, a flavoprotein involved in vitamin C biosynthesis. *FEBS J* 275, 713-726.
- Lenaz G & Genova ML (2010) Structure and organization of mitochondrial respiratory complexes: A new understanding of an old subject. *Antioxid Redox Signal* 12, 961-1008.
- Lenaz G, Baracca A, Barbero G, Bergamini C, Dalmonte ME, Del Sole M, Faccioli M, Falasca A, Fato R, Genova ML, *et al.* (2010) Mitochondrial respiratory chain super-complex I-III in physiology and pathology. *Biochim Biophys Acta - Bioenergetics* 1797, 633-640.
- Liang Z-X, Nocek JM, Huang K, Hayes RT, Kurnikov IV, Beratan DN & Hoffman BM (2002) Dynamic docking and electron transfer between Zn-myoglobin and Cytochrome *b<sub>5</sub>*. *J Am Chem Soc* 124, 6849-6859.
- Ly HK, Utesch T, Díaz-Moreno I, García-Heredia JM, De La Rosa MÁ & Hildebrandt P (2012) Perturbation of the redox site structure of cytochrome *c* variants upon tyrosine nitration. *J Phys Chem B* 116, 5694-5702.
- Madl T & Sattler M (2012) NMR methodologies for the analysis of protein-protein interactions. In *NMR of Biomolecules: towards mechanistic systems biology*. Wiley-VCH Verlag GmbH & Co.
- Maranzana E, Barbero G, Falasca AI, Lenaz G & Genova ML (2013) Mitochondrial respiratory supercomplex association limits production

- of reactive oxygen species from complex I. *Antioxid Redox Signal* 19, 1469-1480.
- Marion D (2013) An introduction to biological NMR spectroscopy. *Mol Cell Proteomics* 12, 3006-3025.
  - Martínez-Fábregas J, Díaz-Moreno I, González-Arzola K, Janocha S, Navarro JA, Hervás M, Bernhardt R, Díaz-Quintana A & De la Rosa MÁ (2013) New *Arabidopsis thaliana* cytochrome *c* partners: A look into the elusive role of cytochrome *c* in programmed cell death in plants. *Mol Cell Proteomics* 12, 3666-3676.
  - Martínez-Fábregas J, Díaz-Moreno I, González-Arzola K, Janocha S, Navarro JA, Hervás M, Bernhardt R, Velázquez-Campoy A, Díaz-Quintana A & De la Rosa MA (2014a) Structural and functional analysis of novel human cytochrome *c* targets in apoptosis. *Mol Cell Proteomics* 13, 1439-1456.
  - Martínez-Fábregas J, Díaz-Moreno I, González-Arzola K, Díaz-Quintana A & De la Rosa MA (2014b) A common signalosome for programmed cell death in humans and plants. *Cell Death & Disease* 5, e1314.
  - Maslennikov I & Choe S (2013) Advances in NMR structures of integral membrane proteins. *Curr Opin Struct Biol* 23, 555-562.
  - Mason JM, Bendall DS, Howe CJ & Worrall JAR (2012) The role of a disulfide bridge in the stability and folding kinetics of *Arabidopsis thaliana* cytochrome *c*<sub>6A</sub>. *Biochim Biophys Acta - Proteins and Proteomics* 1824, 311-318.
  - Moreno-Beltrán B, Díaz-Quintana A, González-Arzola K, Velázquez-Campoy A, De la Rosa MA & Díaz-Moreno I (2014) Cytochrome *c*<sub>1</sub> exhibits two binding sites for cytochrome *c* in plants. *Biochim Biophys Acta - Bioenergetics* 1837, 1717-1729.

## IX. General References

---

- Moreno-Beltrán B, González-Arzola K, Martínez-Fábregas J, Díaz-Moreno I & De la Rosa MA (2015a) Cytochrome *c*-based signalosome. In *Redox proteins in supercomplexes and signalosomes*. Taylor and Francis Editorial Group.
- Moreno-Beltrán B, Díaz-Moreno I, González-Arzola K, Guerra-Castellano A, Velázquez-Campoy A, De la Rosa MA & Díaz-Quintana A (2015b) Respiratory complexes III and IV can each bind two molecules of cytochrome *c* at low ionic strength. *FEBS Lett* 589, 476-483.
- Murata N, Takahashi S, Nishiyama Y & Allakhverdiev SI (2007) Photoinhibition of photosystem II under environmental stress. *Biochim Biophys Acta - Bioenergetics* 1767, 414-421.
- Navarro JA, Durán RV, De la Rosa MA & Hervás M (2005) Respiratory cytochrome *c* oxidase can be efficiently reduced by the photosynthetic redox proteins cytochrome *c<sub>6</sub>* and plastocyanin in cyanobacteria. *FEBS Lett* 579, 3565-3568.
- Osheroff N, Speck SH, Margoliash E, Veerman EC, Wilms J, König BW & Muijsers AO (1983) The reaction of primate cytochromes *c* with cytochrome *c* oxidase. Analysis of the polarographic assay. *J Biol Chem* 258, 5731-5738.
- Oxenoid K & Chou JJ (2013) The present and future of solution NMR in investigating the structure and dynamics of channels and transporters. *Curr Opin Struct Biol* 23, 547-554.
- Pagliano C, Nield J, Marsano F, Pape T, Barera S, Saracco G & Barber J (2014) Proteomic characterization and three-dimensional electron microscopy study of PSII-LHCII supercomplexes from higher plants. *Biochim Biophys Acta - Bioenergetics* 1837, 1454-1462.
- Panov A, Dikalov S, Shalbuyeva N, Hemendinger R, Greenamyre JT & Rosenfeld J (2007) Species- and tissue-specific relationships between

mitochondrial permeability transition and generation of ROS in brain and liver mitochondria of rats and mice. *Am J Physiol Cell Physiol* 292, 708-718.

- Pecina P, Borisenko GG, Belikova NA, Tyurina YY, Pecinova A, Lee I, Samhan-Arias AK, Przyklenk K, Kagan VE & Hüttemann M (2010) Phosphomimetic substitution of cytochrome *c* tyrosine 48 decreases respiration and binding to cardiolipin and abolishes ability to trigger downstream caspase activation. *Biochemistry* 49, 6705-6714.
- Pettersen EF, Goddard TD, Huang CC, Couch GS, Greenblatt DM, Meng EC & Ferrin TE (2004) UCSF Chimera—A visualization system for exploratory research and analysis. *J Comput Chem* 25, 1605-1612.
- Pinto M & Moraes CT (2014) Mitochondrial genome changes and neurodegenerative diseases. *Biochim Biophys Acta - Molecular Basis of Disease* 1842, 1198-1207.
- Prudêncio M & Ubbink M (2004) Transient complexes of redox proteins: structural and dynamic details from NMR studies. *J Mol Recognit* 17, 524-539.
- Ramírez-Aguilar SJ, Keuthe M, Rocha M, Fedyaev VV, Kramp K, Gupta KJ, Rasmusson AG, Schulze WX & van Dongen JT (2011) The composition of plant mitochondrial supercomplexes changes with oxygen availability. *J Biol Chem* 286, 43045-43053.
- Rodríguez-Roldán V, García-Heredia JM, Navarro JA, De la Rosa MA & Hervás M (2008) Effect of nitration on the physicochemical and kinetic features of wild-type and monotyrosine mutants of human respiratory cytochrome *c*. *Biochemistry* 47, 12371-12379.
- Sakamoto K, Kamiya M, Imai M, Shinzawa-Itoh K, Uchida T, Kawano K, Yoshikawa S & Ishimori K (2011) NMR basis for interprotein electron transfer gating between cytochrome *c* and cytochrome *c* oxidase. *Proc Natl Acad Sci USA* 108, 12271-12276.



## IX. General References

---

- Sanderson TH, Mahapatra G, Pecina P, Ji Q, Yu K, Sinkler C, Varughese A, Kumar R, Bukowski MJ, Tousignant RN, *et al.* (2013) Cytochrome *c* is tyrosine 97 phosphorylated by neuroprotective insulin treatment. *PLoS ONE* 8, e78627.
- Scanu S, Foerster JM, Ullmann GM & Ubbink M (2013) Role of Hydrophobic interactions in the encounter complex formation of the plastocyanin and cytochrome *f* complex revealed by paramagnetic NMR spectroscopy. *J Am Chem Soc* 135, 7681-7692.
- Schäfer E, Dencher NA, Vonck J & Parcej DN (2007) Three-dimensional structure of the respiratory chain supercomplex I<sub>1</sub>III<sub>2</sub>IV<sub>1</sub> from bovine heart mitochondria. *Biochemistry* 46, 12579-12585.
- Schägger H & Pfeiffer K (2000) Supercomplexes in the respiratory chains of yeast and mammalian mitochondria. *EMBO J* 19, 1777-1783.
- Schägger H & Pfeiffer K (2001) The ratio of oxidative phosphorylation complexes I-V in bovine heart mitochondria and the composition of respiratory chain supercomplexes. *J Biol Chem* 276, 37861-37867.
- Schilder J & Ubbink M (2013) Formation of transient protein complexes. *Curr Opin Struct Biol* 23, 911-918.
- Schreiber G & Keating AE (2011) Protein binding specificity versus promiscuity. *Curr Opin Struct Biol* 21, 50-61.
- Shen Y, Delaglio F, Cornilescu G & Bax A (2009) TALOS+: a hybrid method for predicting protein backbone torsion angles from NMR chemical shifts. *J Biomol NMR* 44, 213-223.
- Shikanai T (2007) Cyclic electron transport around photosystem I: genetic approaches. *Annu Rev Plant Biol* 58, 199-217.
- Shikanai T (2014) Central role of cyclic electron transport around photosystem I in the regulation of photosynthesis. *Curr Opin Biotechnol* 26, 25-30.

- Sowers AE & Hackenbrock CR (1981) Rate of lateral diffusion of intramembrane particles: measurement by electrophoretic displacement and rerandomization. *Proc Natl Acad Sci USA* 78, 6246-6250.
- Speck SH & Margoliash E (1984) Characterization of the interaction of cytochrome *c* and mitochondrial ubiquinol-cytochrome *c* reductase. *J Biol Chem* 259, 1064-1072.
- Stonehuerner J, O'Brien P, Geren L, Millett F, Steidl J, Yu L & Yu CA (1985) Identification of the binding site on cytochrome *c*<sub>1</sub> for cytochrome *c*. *J Biol Chem* 260, 5392-5398.
- Strogolova V, Furness A, Robb-McGrath M, Garlich J & Stuart RA (2012) Rcf1 and Rcf2, members of the hypoxia-induced gene 1 protein family, are critical components of the mitochondrial cytochrome *bc*<sub>1</sub>-cytochrome *c* oxidase supercomplex. *Mol Cell Biol* 32, 1363-1373.
- Tang C, Iwahara J & Clore GM (2006) Visualization of transient encounter complexes in protein-protein association. *Nature* 444, 383-386.
- Tang C, Louis JM, Aniana A, Suh J-Y & Clore GM (2008) Visualizing transient events in amino-terminal autoprocessing of HIV-1 protease. *Nature* 455, 693-696.
- Tikkanen M & Aro EM (2014) Integrative regulatory network of plant thylakoid energy transduction. *Trends Plant Sci* 19, 10-17.
- Trouillard M, Meunier B & Rappaport F (2011) Questioning the functional relevance of mitochondrial supercomplexes by time-resolved analysis of the respiratory chain. *Proc Natl Acad Sci USA* 108, E1027-1034.
- Umena Y, Kawakami K, Shen J & Kamiya N (2011) Crystal structure of oxygen-evolving photosystem II at a resolution of 1.9 Å. *Nature* 473, 55-60.

## IX. General References

---

- van Dijk ADJ & Bonvin AMJJ (2006) Solvated docking: introducing water into the modelling of biomolecular complexes. *Bioinformatics* 22, 2340-2347.
- van Dijk ADJ, Boelens R & Bonvin AMJJ (2005) Data-driven docking for the study of biomolecular complexes. *FEBS J* 272, 293-312.
- Velázquez-Campoy A, Ohtaka H, Nezami A, Muzammil S & Freire E (2004) Isothermal titration calorimetry. In *Current Protocols in Cell Biology*. John Wiley & Sons, Inc.
- Velázquez-Campoy A, Leavitt S.A. & Freire E (2015) Characterization of protein-protein interactions by isothermal titration calorimetry. In *Methods in Molecular Biology*. Humana Press.
- Volkov AN, Worrall JAR, Holtzmann E & Ubbink M (2006) Solution structure and dynamics of the complex between cytochrome *c* and cytochrome *c* peroxidase determined by paramagnetic NMR. *Proc Natl Acad Sci USA* 103, 18945-18950.
- Vukotic M, Oeljeklaus S, Wiese S, Vögtle FN, Meisinger C, Meyer Helmut E, Ziesenis A, Katschinski Doerthe M, Jans Daniel C, Jakobs S, *et al.* (2012) Rcf1 mediates cytochrome oxidase assembly and respirasome formation, revealing heterogeneity of the enzyme complex. *Cell Metab* 15, 336-347.
- Wientjes E, Oostergetel GT, Jansson S, Boekema EJ & Croce R (2009) The role of Lhca complexes in the supramolecular organization of higher plant photosystem I. *J Biol Chem* 284, 7803-7810.
- Williams PA, Fülöp V, Leung YC, Chan C, Moir JW, Howlett G, Ferguson SJ, Radford SE & Hajdu J (1995) Pseudospecific docking surfaces on electron transfer proteins as illustrated by pseudoazurin, cytochrome *c*<sub>550</sub> and cytochrome *cd*<sub>1</sub> nitrite reductase. *Nat Struct Biol* 2, 975-982.

- Worrall JAR, Kolczak U, Canters GW & Ubbink M (2001) Interaction of yeast iso-1-cytochrome *c* with cytochrome *c* peroxidase investigated by [<sup>15</sup>N,<sup>1</sup>H] heteronuclear NMR spectroscopy. *Biochemistry* 40, 7069-7076.
- Worrall JAR, Liu Y, Crowley PB, Nocek JM, Hoffman BM & Ubbink M (2002) Myoglobin and cytochrome *b*<sub>5</sub>: A nuclear magnetic resonance study of a highly dynamic protein complex. *Biochemistry* 41, 11721-11730.
- Worrall JAR, Reinle W, Bernhardt R & Ubbink M (2003) Transient protein interactions studied by NMR spectroscopy: The case of cytochrome *c* and adrenodoxin. *Biochemistry* 42, 7068-7076.
- Worrall JAR, Schlarb-Ridley BG, Reda T, Marcaida MJ, Moorlen RJ, Wastl J, Hirst J, Bendall DS, Luisi BF & Howe CJ (2007) Modulation of heme redox potential in the cytochrome *c*<sub>6</sub> family. *J Am Chem Soc* 129, 9468-9475.
- Worrall JAR, Luisi BF, Schlarb-Ridley BG, Bendall DS & Howe CJ (2008) Cytochrome *c*<sub>6A</sub>: discovery, structure and properties responsible for its low haem redox potential. *Biochem Soc Trans* 36, 1175–1179.
- Wüthrich K (1986) NMR of proteins and nucleic Acids. Wiley, New York.
- Xie J, Supekova L & Schultz PG (2007) A genetically encoded metabolically stable analogue of phosphotyrosine in *Escherichia coli*. *ACS Chem Biol* 2, 474-478.
- Yu H, Lee I, Salomon AR, Yu K & Hüttemann M (2008) Mammalian liver cytochrome *c* is tyrosine-48 phosphorylated in vivo, inhibiting mitochondrial respiration. *Biochim Biophys Acta - Bioenergetics* 1777, 1066-1071.

## **X. APPENDIX I**



---

## X. APPENDIX I

---

### JOURNAL PAPERS:

1. **Moreno-Beltrán, B**, Díaz-Quintana, A, González-Arzola, K, Velázquez-Campoy, A, De la Rosa, MA and Díaz-Moreno, I. (2014) Cytochrome  $c_1$  exhibits two binding sites for cytochrome  $c$  in plants. *Biochim. Biophys. Acta – Bioenergetics* 1837, 1717-1729.
2. **Moreno-Beltrán, B**, Díaz-Moreno, I, González-Arzola, K, Guerra-Castellano, A, Velázquez-Campoy, A, De la Rosa, MA and Díaz-Quintana, A. (2015) Respiratory complexes III and IV can each bind two molecules of cytochrome  $c$  at low ionic strength. *FEBS Lett.* 589, 476-483.
3. Díaz-Moreno, I, Hulsker, R, Skubak, P, Foerster, JM, Cavazzini, D, Finiguerra, MG, Díaz-Quintana, A, **Moreno-Beltrán, B**, Rossi, G, Ullmann, GM, Pannu, NS, De la Rosa, MA and Ubbink, M. (2014) The dynamic complex of cytochrome  $c_6$  and cytochrome  $f$  studied with paramagnetic NMR spectroscopy. *Biochim. Biophys. Acta – Bioenergetics* 1837, 1305-1315.
4. Hervás, M, Bashir, Q, Leferink, NG, Ferreira, P, **Moreno-Beltrán, B**, Westphal, AH, Díaz-Moreno, I, Medina, M, De la Rosa, MA, Ubbink, M, Navarro, JA and van Berkel, WJ. (2013) Communication between (L)-galactono-1,4-lactone dehydrogenase and cytochrome  $c$ . *FEBS J.* 280, 1830-1840.

**BOOK CHAPTER:**

1. **Moreno-Beltrán, B\***, González-Arzola, K\*, Martínez-Fábregas, J, Díaz-Moreno, I and De la Rosa, MA (2015). Cytochrome *c*-based signalosome. In *Redox proteins in supercomplexes and signalosomes*, Editors: R.O. Louro and I. Díaz-Moreno. Taylor and Francis Editorial Group. ISBN: 978-1-4822-5110-4.

\* These authors have equally contributed.



## Journal Paper

1. **Moreno-Beltrán, B**, Díaz-Quintana, A, González-Arzola, K, Velázquez-Campoy, A, De la Rosa, MA and Díaz-Moreno, I. (2014) Cytochrome  $c_1$  exhibits two binding sites for cytochrome  $c$  in plants. *Biochim. Biophys. Acta – Bioenergetics* 1837, 1717-1729.



## Journal Paper

2. **Moreno-Beltrán, B**, Díaz-Moreno, I, González-Arzola, K, Guerra-Castellano, A, Velázquez-Campoy, A, De la Rosa, MA and Díaz-Quintana, A. (2015) Respiratory complexes III and IV can each bind two molecules of cytochrome *c* at low ionic strength. *FEBS Lett.* 589, 476-483.



## Journal Paper

3. Díaz-Moreno, I, Hulsker, R, Skubak, P, Foerster, JM, Cavazzini, D, Finiguerra, MG, Díaz-Quintana, A, **Moreno-Beltrán, B**, Rossi, G, Ullmann, GM, Pannu, NS, De la Rosa, MA and Ubbink, M. (2014) The dynamic complex of cytochrome  $c_6$  and cytochrome  $f$  studied with paramagnetic NMR spectroscopy. *Biochim. Biophys. Acta – Bioenergetics* 1837, 1305-1315.

PhD candidate contribution:

Ensemble docking computations and validation of PRE NMR data were performed by Blas Moreno-Beltrán in the laboratory of Prof. Dr. Marcellus Ubbink (Leiden University, Leiden, The Netherlands).

## Journal Paper

4. Hervás, M, Bashir, Q, Leferink, NG, Ferreira, P, **Moreno-Beltrán, B**, Westphal, AH, Díaz-Moreno, I, Medina, M, De la Rosa, MA, Ubbink, M, Navarro, JA and van Berkel, WJ. (2013) Communication between (L)-galactono-1,4-lactone dehydrogenase and cytochrome *c*. *FEBS J.* 280, 1830-1840.

### PhD candidate contribution:

Expression and purification of the  $^{15}\text{N}$ -labeled form of reduced plant cytochrome *c* and the NMR assignment of its backbone amide resonances were performed by Blas Moreno-Beltrán in the Biointeractomics Unit (Universidad de Sevilla - CSIC, Sevilla, España). For this sequence-specific assignment, a 2D [ $^1\text{H}$ ,  $^{15}\text{N}$ ] HSQC, 3D [ $^1\text{H}$ ,  $^{15}\text{N}$ ] NOESY-HSQC and 3D [ $^1\text{H}$ ,  $^{15}\text{N}$ ] TOCSY-HSQC spectra of  $^{15}\text{N}$ -labeled form of reduced plant cytochrome *c* were recorded at CERM (University of Florence, Italy). The form of Access to the Research Infrastructure was funded by the BioNMR project.



## Book Chapter

1. **Moreno-Beltrán, B\***, González-Arzola, K\*, Martínez-Fábregas, J, Díaz-Moreno, I and De la Rosa, MA (2015). Cytochrome *c*-based signalosome. In *Redox proteins in supercomplexes and signalosomes*, Editors: R.O. Louro and I. Díaz-Moreno. Taylor and Francis Editorial Group. ISBN: 978-1-4822-5110-4.

\* These authors have equally contributed.



## **XI. APPENDIX II**



---

## **XI. APPENDIX II**

---

### **Structure and Dynamics of the Y48 $p$ CMF Variant of Human Cytochrome *c***

This work was performed in collaboration with  
Prof. Paola Turano  
(CERM, University of Florence, Italy).



## 1. Introduction

Post-translational modifications (PTMs) of proteins, such as phosphorylation, nitration, glycosylation or acetylation, regulate a large number of processes involved in cell metabolism. PTMs are common mechanisms for controlling the metabolic role of proteins, *e.g.* activating or inactivating their function. Among all PTMs, reversible phosphorylation is the most frequently reported, being detected in both, homeostatic and stress-induced conditions (Khoury *et al.*, 2011; Song *et al.*, 2014). Phosphorylation allows rapid modification of protein function, adapting the protein to cellular changes. Kinases and phosphatases form part of the machinery responsible for the modulation of the reversible phosphorylation and dephosphorylation events respectively, which in turn are regulated by multiple signals (Corcoran and Cotter, 2013).

Human cytochrome *c* (hCc) is a small, soluble and globular heme protein. Despite its small size, it comprises five well-known foldons or folding units (Krishna *et al.*, 2003; Maity *et al.*, 2005). hCc performs a double function in respiration and programmed cell death (PCD). Under homeostatic conditions, hCc shuttles electrons between respiratory complexes III and IV in the mitochondrial electron transport chain (Díaz-Moreno *et al.*, 2011; Moreno-Beltrán *et al.*, 2015a; Moreno-Beltrán *et al.*, 2015b). However, under PCD stimuli, hCc is released from the mitochondria to the cytosol and even to the nucleus, acting as a PCD inductor (Díaz-Moreno *et al.*, 2011; Martínez-Fábregas *et al.*, 2014a; Martínez-Fábregas *et al.*, 2014b). Both hCc functions are regulated by post-translational modifications, such as phosphorylation or nitration of tyrosine residues (García-Heredia *et al.*, 2010; Díaz-Moreno *et al.*, 2011; García-Heredia *et al.*, 2011; García-Heredia *et al.*, 2012; Hüttemann *et*

*al.*, 2012a; Hüttemann *et al.*, 2012b). Mammalian Cc can be phosphorylated *in vivo* in two different tyrosines located at positions 48 and 97 (Lee *et al.*, 2006; Yu *et al.*, 2008), and recently, novel phosphorylation sites have been reported at positions 28 and 47 (Zhao *et al.*, 2011).

Notably, phosphorylation of mammalian Cc at Tyr48 causes partial inhibition of the oxidative phosphorylation process. This PTM is associated with certain pathological situations, such as ischemia or reperfusion injury (Yu *et al.*, 2008; Pecina *et al.*, 2010; Hüttemann *et al.*, 2012a). At the same time, experiments with a phosphomimetic mutant of hCc at Tyr48 (Y48E mutant) have suggested the functional relevance of this PTM on PCD (Pecina *et al.*, 2010; García-Heredia *et al.*, 2011). The possibility that Tyr48-phosphorylation of hCc regulates PCD has potentially important therapeutic implications for diseases like cancer, in which PCD is inhibited (Hüttemann *et al.*, 2012b).

In general, tyrosine phosphorylation of hCc is mimicked by glutamic residues due to the technical difficulties of obtaining enough physiological phosphorylated protein from tissues and the fact that the specific Cc-phosphorylating kinase still remains unknown (Pecina *et al.*, 2010; García-Heredia *et al.*, 2011). However, the substitution of a tyrosine by glutamic results in a considerable decrease in the volume and surface of the replaced residue, whereas a tyrosine increases its volume upon phosphorylation.

To solve this problem, Tyr residues can be substituted by the noncanonical amino acid *p*-carboxymethyl-L-phenylalanine (*p*CMF), whose side-chain volume is closer to that of the phosphotyrosine residue (Xie *et al.*, 2007) and whose negative-charge resembles the phosphate



group. Hence, we have replaced the Tyr48-encoding triplet of the hCc gene with an amber stop codon (TAG) to substitute this residue with the phosphorylation mimic compound using the evolved tRNA technique. This approach allows the selective incorporation of *p*CMF assisted by an orthogonal tRNA that recognizes the amber stop codon (Figure 1; Xie *et al.*, 2007). The resulting phosphomimetic hCc at Tyr48, named Y48*p*CMF hCc, contains a non-canonical *p*CMF amino acid at position 48 that better emulates the effect of phosphorylation in comparison with the traditional Tyr-by-Glu substitution.

Notably, the overlap of the 2D [<sup>1</sup>H, <sup>15</sup>N] HSQC spectra of uniformly <sup>15</sup>N-labeled forms of wild-type and Y48*p*CMF hCc, acquired under the same experimental conditions, showed significant chemical shifts in many amide proton signals, as well as a higher number of exchangeable amide protons for the Y48*p*CMF hCc (Figure 2). The environmental changes of the amide protons evidenced a significant change in the overall structure of Y48*p*CMF hCc, whereas the larger number of exchangeable amide protons pointed to differences in its dynamism.

We report here the NMR solution structure of Y48*p*CMF hCc, as well as the NMR relaxation data-based dynamic properties of this phosphomimetic mutant with regards to the wild-type form. The ultimate aim of our research on Y48*p*CMF hCc has been to obtain evidence of structural and dynamical differences between this mutant and the wild-type form that can explain its distinct functional implications.

## 2. Materials and methods

### 2.1. Construct design

Site-directed mutagenesis was performed, using pBTR1 vector (Olteanu *et al.*, 2003) as a template and the QuikChange II method (Stratagene), to replace the TAT triplet corresponding to Tyr48 of hCc with the amber stop codon TAG. pBTR1 vector contains hCc gen (GenBank ID: M22877.1). The final stop codon of the hCc insert is the opal stop codon TGA. The primers for mutagenesis were Y48amber\_fw (5-CTACAGCTAGACGGCGGCGA-3) and Y48amber\_rv (5-TCGCCGCCGTCTAGCTGTAG-3). The resulting construct, named pCcY48AMBER, was verified by automated sequencing.

### 2.2. Protein expression and purification

Uniformly  $^{13}\text{C}$ ,  $^{15}\text{N}$ -labeled,  $^{15}\text{N}$ -labeled and unlabeled samples of Y48pCMF hCc were expressed using the evolved tRNA-based strategy (Xie *et al.*, 2007). *E.coli* BL21 (DE3) cells were co-transformed with the plasmids pBTR1-Y48AMBER and pEVOL/pCMF/tRNA. The latter vector encodes an orthogonal amber suppressor tRNA/aminoacyl-tRNA synthetase (aaRS) pair (Xie *et al.*, 2007). The cells were grown for 20 h at 150 rpm and 30 °C in minimal media M9 supplemented with ampicillin and chloramphenicol and induced at OD 0.6 with 0.02% arabinose and 1 mM IPTG.  $^{15}\text{N}$ -labeled ammonium chloride and  $^{13}\text{C}$ -glucose were added to minimal media to express the  $^{13}\text{C}$ ,  $^{15}\text{N}$ -labeled samples, whereas only  $^{15}\text{N}$ -labeled ammonium chloride was added to media for  $^{15}\text{N}$ -labeled samples. The non-canonical amino acid pCMF and

$\delta$ -aminolevulinic acid were immediately added after induction with IPTG at 1 mM and 0.1 mM final concentrations, respectively. The latter two compounds were unlabeled. Cells were collected by centrifugation, and then resuspended in 1.5 mM borate buffer pH 8.5, supplemented with 1 mM phenylmethylsulfonyl fluoride (PMSF), 0.02 mg mL<sup>-1</sup> DNase and 0.2 mg mL<sup>-1</sup> lysozyme. The cytoplasmic fraction was obtained by sonication and centrifuged at 20,000 g for 15 min. Then, the supernatant was loaded onto a cationic exchange column. The purification protocol was performed as previously reported for wild-type hCc (Moreno-Beltrán *et al.*, 2015a). Tryptic digestion and MALDI-TOF analyses confirmed the molecular mass and the tyrosine substitution by pCMF. Protein concentration was determined by Vis spectrophotometry, using extinction coefficients of 29 mM<sup>-1</sup> cm<sup>-1</sup> for reduced Y48pCMF hCc. Sodium ascorbate was used to reduce the sample. Pure fractions were dialyzed against 10 mM sodium phosphate pH 6.3. Finally, protein samples were concentrated in Millipore 3 K Nominal Molecular Weight Limit (NMWL) centricons to a final concentration of 0.7 mM.

### 2.3. Circular Dichroism experiments

Circular dichroism (CD) spectra were recorded in the UV range (190–250 nm) at 298 K in a J-815 spectropolarimeter, equipped with a Peltier temperature control system, using a 1-mm quartz cuvette. Samples contained 3  $\mu$ M protein in 5 mM sodium phosphate buffer (pH 6.3). Twenty scans were averaged out for each sample. Secondary structure analysis was performed using CDPRO software (Sreerama and Woody, 2000; Sreerama and Woody, 2004). CLSTR was used as reference database.

## 2.4. NMR experiments

NMR spectra of fresh 0.6 mM  $^{13}\text{C}$ ,  $^{15}\text{N}$ -labeled Y48pCMF hCc samples, in 90% buffer and 10%  $\text{D}_2\text{O}$ , were recorded at 298 K on Bruker Avance spectrometers operating at 950, 700 and 500 MHz  $^1\text{H}$  frequencies. A standard set of triple resonance experiments, necessary for the full assignment of backbone and side chain resonances, were acquired at 700 MHz  $^1\text{H}$  frequency, whereas 2D and 3D NOESY experiments required for structure determination were acquired at 950 MHz  $^1\text{H}$  frequency. Recorded NMR experiments for determination of backbone resonances were 2D [ $^1\text{H}$ ,  $^{15}\text{N}$ ] HSQC, 2D [ $^1\text{H}$ ,  $^{13}\text{C}$ ] HSQC, 3D HNCA, 3D HNCACB, 3D CACB(CO)NH, 3D HN(CA)CO and 3D HNCO, whereas specific experiments for determination of side-chain resonances were 3D HCCHTOCSY and 3D HBHA(CO)NH (Grzesiek and Bax, 1993; Zuiderweg and Fesik, 1988; Kay *et al.*, 1993). Additional 2D COSY and aromatic 2D [ $^1\text{H}$ ,  $^{13}\text{C}$ ] HSQC on an unlabeled sample of the Y48pCMF hCc were acquired for the assignment of aromatic residues. Therefore, the [ $^1\text{H}$ ,  $^{13}\text{C}$ ] HSQC spectrum was recorded in a natural abundance of  $^{13}\text{C}$ . Water suppression was achieved in all mentioned spectra by WATERGATE (Piotto *et al.*, 1992). 1D  $^1\text{H}$  spectra were launched before and after each spectrum to check the state of the sample, especially the redox state of the hemeprotein.

The following NOESY experiments were acquired: 2D [ $^1\text{H}$ ,  $^{15}\text{N}$ ] NOESY, 3D [ $^1\text{H}$ ,  $^{15}\text{N}$ ] NOESY-HSQC and 3D [ $^1\text{H}$ ,  $^{13}\text{C}$ ] NOESY-HSQC spectra in the aliphatic region (Zuiderweg and Fesik, 1989; Marion *et al.*, 1989a; Marion *et al.*, 1989b). Mixing times were 100 ms for all NOESY experiments, recorded on a  $^{15}\text{N}$ -labeled sample, with the exception of the 3D [ $^1\text{H}$ ,  $^{13}\text{C}$ ] NOESY-HSQC that was acquired on a  $^{13}\text{C}$ ,  $^{15}\text{N}$ -labeled

sample. An additional 2D [ $^1\text{H}$ ,  $^{15}\text{N}$ ] EXSY spectrum was launched for assignment of heme resonances, by using a partially oxidized  $^{15}\text{N}$ -labeled sample. WATERGATE suppression was used. 1D  $^1\text{H}$  spectra were again launched to check the state of the samples.

$^{15}\text{N}$  relaxation  $R_1$  ( $=1/T_1$ ),  $R_2$  ( $=1/T_2$ ) and  $\{^1\text{H}\}$ - $^{15}\text{N}$  NOE parameters were obtained from standard experiments recorded at 500 MHz  $^1\text{H}$  frequency and 298 K (Kay *et al.*, 1989) on  $^{15}\text{N}$ -labeled samples of the Y48pCMF and wild-type hCc species.  $\{^1\text{H}\}$ - $^{15}\text{N}$  NOE relaxation parameter is also known as HetNOE.

The NMR data processing was carried out using the Bruker Topspin software package. The assignments of 2D and 3D spectra were carried out manually with the help of the CARA and SPARKY software packages (Keller, 2004; Goddar and Kneller, SPARKY 3, University of California). A list of NOEs of the reduced yeast Cc was used as a reference (Baistrocchi *et al.*, 1996). Final reviews of peak assignments and integrations of peak volumes were carried out by XEASY (Bartels *et al.*, 1995).  $^{15}\text{N}$  relaxation parameters were analyzed using CARA routines (Keller, 2004).  $R_1/R_2$  ratios of residues in well-defined regions were used to estimate the rotational correlation times ( $\tau_c$ ) of the protein constructs (Dosset *et al.*, 2000).

## 2.5. Distance Geometry Calculations

The volumes of the cross-peaks between assigned resonances were obtained using the integration routines present in the program XEASY. Elliptical integration was applied. NOESY cross-peak intensities were converted into upper limits of inter-atomic distances by CYANA (Güntert *et al.*, 1997). Upper and lower distance limits were imposed to

build up the heme. Upper (1.90 Å) and lower (1.70 Å) distance limits from the  $\alpha$ -carbons of thioethers 2 and 4 of the heme moiety, to the S $_{\gamma}$  of cysteines 14 and 17, respectively, were used in the computations to covalently link the heme moiety to the cysteine residues. An upper distance limit of 2.50 Å and a lower distance limit of 2.20 Å between the S $_{\delta}$  of the Met80 and the iron of the heme were introduced, too. The orientation of Met80 and His18 side-chains was defined only by the experimental NOE constraints.

A residue containing the heme moiety was added to the standard CYANA library. In addition, the non-standard amino acid *p*CMF was built and added to the CYANA library. Several cycles of the structure calculation were carried out in order to recalibrate the NOE distance constraints. Indeed, CYANA calculations were performed following the procedure and with the parameters used for the determination of other *c*-type cytochromes (Baistrocchi *et al.*, 1996; Banci *et al.*, 1997; Assfalg *et al.*, 2002). Initially, 200 structures were calculated. In each calculation, violated constraints were analyzed for the best 20 structures with respect to the target function. After consecutive rounds of review and refinement of violated constraints, a final CYANA computation was performed in which no consistent violations were determined. The final value of the target function was equal to 0.73.

### **2.6. Molecular Dynamics Simulations**

NMR-restrained Molecular Dynamics (RMD) computations were performed by the AMBER 12.1 package and using the AMBER-2003 force field on a selection of the best 20 structures derived from the CYANA calculations (Duan *et al.*, 2003; Case *et al.*, 2006). Distance

constraints were introduced by the DIS\_RST module of Amber 12.1. Simulations were performed under periodic boundary conditions using an orthorhombic cell geometry (the minimum distance between protein and cell faces was initially set to 10 Å) and PME electrostatics with a Ewald summation cut off of 9 Å. The structures were solvated with SPC water molecules, and Cl<sup>-</sup> counterions were added to neutralize the net charge of the full systems. Afterwards, solvent and counter-ions were subjected to 2500 steps of steepest descent minimization followed by 500 ps NPT-MD computations using isotropic molecule position scaling and a pressure relaxation time of 2 ps at 298 K. Once the systems were NMR-restrained energy minimized (REM), these works were submitted to RMD computations for 5 ns at 298 K. Temperature was regulated using a Langevin thermostat with a collision frequency of 5 ps<sup>-1</sup> (Andersen, 1980). Finally, structures from RMD were energy minimized for 5000 steps. The SHAKE algorithm was used to constrain bonds involving hydrogen atoms (Ryckaert *et al.*, 1977). The PTRAJ module of AMBER was used for trajectory analyses. Force field parameters for the heme group were taken from a previous work (Autenrieth *et al.*, 2004). The Met80 residue was non-bonded to the iron and a constraint was applied instead. Molecular graphics were performed with UCSF Chimera (Pettersen *et al.*, 2004). Validation of final minimized structures was performed by PSVS software (Bhattacharya *et al.*, 2007). In addition, a final non-restrained MD computation of 20 ns was launched to check the stability of the resulting conformers.

### 3. Results and Discussion

#### 3.1. Sequence-Specific Assignment and Secondary Structure Elements

We have performed an extensive assignment of the resonances of reduced Y48*p*CMF hCc by means of triple resonance NMR experiments. Backbone amide groups and their sequential NH-NH connectivities have been observed for most residues of Y48*p*CMF hCc. However, the amide resonances of 9 residues (Gly1, Glu21, Thr28, Thr49, Ala51, Gly56, Ile57, Lys79 and Gly84) could not be located. In addition, the <sup>15</sup>NH resonance of *p*CMF48 was undetectable since the residue lacked labeling. Four prolines (Pro30, Pro44, Pro71 and Pro76) also broke the sequential NH-NH connectivities. Notably, the intensities of backbone amide groups of Asn31, Gly45 and Ser47 were significantly low in comparison with the rest of the signals. Triple resonance experiments were also critical to properly assign most side-chain protons. Additional two-dimensional experiments were carried out for the correct assignment of proton chemical-shifts from the heme group and from the side-chains of aromatic residues. Finally, a 96% completeness of the assignment of proton chemical shifts was achieved, and only 24 proton chemical-shifts remained missing.

The assignments of NOESY spectra, based on the previous proton chemical-shift assignment of backbone and side chain-resonances, allowed us to identify helical structures, which are characterized by strong NH-NH and medium range H $\alpha$ -NH(*i*,*i*+3) and H $\alpha$ -NH(*i*,*i*+4) NOEs. The stretches Val3-Lys13, Ala50-Asn54, Glu61-Asn70, Lys72-Ile75 and Lys88-Thr102 adopt helical structures. These segments, known



as  $\alpha_1$ ,  $\alpha_2$ ,  $\alpha_3$ ,  $\alpha_4$  and  $\alpha_5$ , are almost identical to those present in the NMR structure of wild-type reduced hCc (Jeng *et al.*, 2002). These data are in agreement with the Circular Dichroism (CD) spectra, in which Y48pCMF hCc displayed a similar CD pattern and almost the same percentage of secondary structure elements in comparison with the wild-type form (Figure 3a,b).

### 3.2. NMR $^{15}\text{N}$ -Relaxation Data-Based Dynamic Properties

Even though the secondary structure elements were conserved between both the wild-type and Y48pCMF hCc forms,  $R_1$ ,  $R_2$  and HetNOE relaxation measurements indicated that phosphomimetic hCc showed a highly dynamic behavior in distinct time scales, as compared to wild-type hCc. In particular, Y48pCMF hCc contained a highly flexible area that included the mutation loop, whereas several segments of the protein were involved in conformational exchanges. Both features were also in agreement with CD data of the reduced hCc species, in which the percentage of disordered regions was higher in the Y48pCMF hCc with regards to the wild-type form (Figure 3b).

First, the segment Gly41-Lys55, which contains the loop of the Tyr48 and corresponds to the foldon 5 of hCc, shows a larger mobility in the Y48pCMF hCc than in the wild-type form, according to the drastic change of HetNOE values for this region (Figure 4a). These data are in consonance with the differences in  $R_1$  values of the stretch Tyr46-Lys55, confirming that the pCMF-containing loop, along with the  $\alpha_2$  helix, exhibited a high mobility in the  $\mu\text{s}$ -ns time scale (Figure 4b). In addition, other residues, such as Lys27, Asp62, Lys72 and Ile85, showed a significant variation of the HetNOE values.

Second, the analyses of the differences between the  $R_2$  parameters among the wild-type and Y48pCMF hCc species evidenced the existence of three regions that exhibited conformational exchanges (Figure 4c). These regions were the following ones: His26-Thr28, Thr40-Trp59 and Ile75-Thr78. These data were consistent with a substantial decrease in the intensity of the signals and the existence of secondary conformations in mentioned segments. Indeed, such second species were identified in the stretches: Val20-Asn31 (foldon 2); Thr40-Trp59 (foldons 3 and 5) and Ile75-Glu90 (the omega loop of Met80, also known as foldon 4). Notably, residues His26, Pro30, Asn31, Tyr46, pCMF48, Trp59, Gly77, Thr78, Lys79 and Met80 showed multiple conformations.

Thus, the existence of new exchangeable amide protons in the phosphomimetic mutant (pCMF48, Thr49, Ala51, Ile57 and Lys79) could be ascribed to its highly dynamic behavior, mainly located in particular regions, such as the surroundings of the pCMF or the omega loop of the distal axial ligand. The overall analyses of the relaxation parameters determined that  $R_1$  and  $R_2$  parameters were also affected (Table 1). Remarkably, the rotational correlation time of the phosphomimetic mutant was higher than that of the wild-type form, evidencing not only specific local changes on the protein dynamics but also global changes in the protein motion as an entity upon phosphorylation (Table 1).

### 3.3. NMR solution structure

Experimental NOE constraints were transformed into upper distance limits to elucidate the solution structure of Y48pCMF hCc. A total of 2,167 NOEs were introduced into CYANA (Table 2). The number of

experimental NOE constraints per residue was shown in Figure 5. It corresponds to an average of 20.8 experimental NOEs per residue. The heme group, the axial ligands and the two Cys residues covalently linked to the porphyrin were treated as in previous computations (Banci *et al.*, 1995). Two hundred structures were initially calculated and twenty structures with the lowest target function were selected. The target function of the final computation was 0.73. Selected structures were then energy minimized by the AMBER software package.

The overall fold of the molecule was maintained with respect to the wild-type hCc, with the exception of the mutation-containing loop, which harbored the main differences in terms of protein folding and structure (Figure 6). The side-chain of *p*CMF48 was exposed to the solvent and displayed multiple conformations, which suggests a highly dynamic behavior. Nevertheless, other regions of the Y48*p*CMF hCc structure were also significantly altered with regard to the wild-type hCc, such as the 20's loop (part of foldon 2), the 50's helix ( $\alpha_2$ ; foldon 5) and the  $\Omega$ -loop of the Met80 (foldon 4).

Thus, the replacement of the Tyr48 by the *p*CMF non-canonical amino acid might lead to a local destabilization of the mutation-containing loop and its surroundings, which explain the differences in the dynamic behavior and the worse definition of several segments. Actually, the structure of Y48*p*CMF hCc had a relatively high accuracy when the stretch of the mutation was excluded. The RMSD of the backbone to the mean was  $0.87 \pm 0.16$  Å considering the whole primary sequence, whereas this value decreases to  $0.53 \pm 0.12$  Å if the Thr40-Ile57 segment is not considered. The RMSD values per residue were shown in Figure 7.

To the contrary, other regions of the NMR structure of Y48 $p$ CMF hCc exhibited high RMSD values. In particular the two segments Val20-Gly29 and Thr40-Ile57. The high RMSD values found in the segment Val20-Gly29 have also been described in other cytochromes (Banci *et al.*, 1995; Banci *et al.*, 1997; Banci *et al.*, 1999). This finding also correlates well with the existence of second conformations in this region, which were detected for His26 and Pro30 residues. A drastic decrease in the intensity of the amide group of Asn31 was also detected, which could be linked to the described phenomena. All mentioned residues are in direct contact with the mutation-containing loop, which is spatially close.

Residues at the Thr40-Ile57 stretch, which include the loop of  $p$ CMF48 and  $\alpha_2$ , were strongly affected by two distinct phenomena: a drastic reduction of the NOE cross-peaks and the existence of conformational exchanges. Thus, the high RMSD values of backbone and heavy atoms, which are the highest values considering the whole primary sequence (Figure 7), perfectly match these two findings. The conformational exchanges in this area were first evidenced by high R2 values and then confirmed by direct evaluation of NOESY spectra. Double conformations were observed for Tyr46,  $p$ CMF48 and Trp59 in the phosphomimetic mutant. In addition, the loss of amide proton signals or the severe decrease in their intensities were specifically detected for Ser47,  $p$ CMF48, Thr49, Ala51, Gly56 and Ile57 of  $p$ CMF48 hCc in comparison with the wild-type form (Jeng *et al.*, 2002).

Finally, the  $\Omega$ -loop also encloses some residues with high RMSD values. The high values of the segment Lys72-Met80 could be attributed to the same findings explained previously: a significant decrease in NOE cross-peaks and conformational exchanges. Notably, the high R<sub>2</sub> values

of residues placed at the beginning of the  $\Omega$ -loop (Ile75-Thr78) matched their second conformation. A second conformation was clearly identified for the Pro76-Met80 segment. Moreover, the high RMSD values of the heavy atoms at the end of this  $\Omega$ -loop have also been described in other cytochromes (Banci *et al.*, 1995; Banci *et al.*, 1997; Baistrocchi *et al.*, 1996).

#### **4. Conclusions**

In summary, the structural model of Y48*p*CMF hCc herein present is in agreement with relaxation measurements and highlights how the phosphomimetic Cc becomes more dynamic than the wild-type species, with potential consequences for protein function. In particular, relevant structural and dynamic changes in the *p*CMF-containing loop and its surroundings, along with the  $\Omega$ -loop of the distal axial ligand, may have direct implications in the two Cc functions, aerobic respiration and PCD.

#### **5. Acknowledgments**

This work was supported by grants AP2009-4092 and JaePre\_2011\_01248 awarded to B.M.B. and A.G.C. respectively, from the European Social Fund 2007-2013. The Andalusian Government (CVI-BIO198), the Ministry of Economy and Competitiveness (BFU2012-31670), the Ramón Areces Foundation, the European Bio-NMR Project (2012-2013) BIO-NMR-00130 and NMR services at the Centro di Ricerca di Risonanze Magnetiche (CERM), the Centro de Investigación Tecnología e Innovación (CITIUS) and the

## XI. Appendix II

---

Biointeractomics Platform (cicCartuja). We would like to thank Professor P.G. Schultz (Scripps Research Institute of California) for generously providing us the plasmid pEVOL/*p*CMF/tRNA.

## 6. References

- Andersen HC (1980) Molecular dynamics simulations at constant pressure and/or temperature. *J Chem Phys* 24, 1999-2012.
- Assfalg M, Bertini I, Turano P, Bruschi M, Durand MC, Giudici-Ortoni MT & Dolla A (2002) A quick solution structure determination of the fully oxidized double mutant K9-10A cytochrome  $c_7$  from *Desulfuromonas acetoxidans* and mechanistic implications. *J Biomol NMR* 22, 107-122.
- Autenrieth F, Tajkhorshid E, Baudry J & Luthey-Schulten Z (2004) Classical force field parameters for the heme prosthetic group of cytochrome *c*. *J Comput Chem* 25, 1613-1622.
- Baistrocchi P, Banci L, Bertini I & Turano P (1996) Three-dimensional solution structure of *Saccharomyces cerevisiae* reduced iso-1-cytochrome *c*. *Biochemistry* 35, 13788-13796.
- Banci L, Bertini I, Bren KL, Gray HB, Sompornpisut P & Turano P (1995) Three-dimensional solution structure of the cyanide adduct of a Met80Ala variant of *Saccharomyces cerevisiae* iso-1-cytochrome *c*. Identification of ligand-residue interactions in the distal heme cavity. *Biochemistry* 34, 11385-11398.
- Banci L, Bertini I, Bren KL, Gray HB, Sompornpisut P & Turano P (1997) Solution structure of oxidized *Saccharomyces cerevisiae* iso-1-cytochrome *c*. *Biochemistry* 36, 8992-9001.
- Banci L, Bertini I, Huber JG, Spyroulias GA & Turano P (1999) Solution structure of reduced horse heart cytochrome *c*. *J Biol Inorg Chem* 4, 21-31.
- Bartels C, Xia TH, Billeter M, Guntert P & Wuthrich K (1995) The program XEASY for computer-supported NMR spectral analysis of biological macromolecules. *J Biomol NMR* 6, 1-10.

- Bhattacharya A, Tejero R & Montelione GT (2007) Evaluating protein structures determined by structural genomics consortia. *Proteins* 66, 778-795.
- Case DA, Darden TA, Cheatham TE, Simmerling CL, Wang J, Duke RE, Luo R, Merz KM, Pearlman DA, Crowley M, *et al.* (2006) AMBER 9 University of California, San Francisco.
- Corcoran A & Cotter TG (2013) Redox regulation of protein kinases. *FEBS J* 280, 1944-1965.
- Díaz-Moreno I, García-Heredia JM, Díaz-Quintana A & De la Rosa MA (2011) Cytochrome *c* signalosome in mitochondria. *Eur Biophys J* 40, 1301-1315.
- Dosset P, Hus JC, Blackledge M & Marion D (2000) Efficient analysis of macromolecular rotational diffusion from heteronuclear relaxation data. *J Biomol NMR* 16, 23-28.
- Duan Y, Wu C, Chowdhury S, Lee MC, Xiong G, Zhang W, Yang R, Cieplak P, Luo R, Lee T, *et al.* (2003) A point-charge force field for molecular mechanics simulations of proteins based on condensed-phase quantum mechanical calculations. *J Comput Chem* 24, 1999-2012.
- García-Heredia JM, Díaz-Moreno I, Nieto PM, Orzáez M, Kocanis S, Teixeira M, Pérez-Payá E, Díaz-Quintana A & De la Rosa MA (2010) Nitration of tyrosine 74 prevents human cytochrome *c* to play a key role in apoptosis signaling by blocking caspase-9 activation. *Biochim Biophys Acta - Bioenergetics* 1797, 981-993.
- García-Heredia JM, Díaz-Quintana A, Salzano M, Orzáez M, Pérez-Payá E, Teixeira M, De la Rosa MA & Díaz-Moreno I (2011) Tyrosine phosphorylation turns alkaline transition into a biologically relevant process and makes human cytochrome *c* behave as an anti-apoptotic switch. *J Biol Inorg Chem* 16, 1155-1168.



- García-Heredia JM, Díaz-Moreno I, Díaz-Quintana A, Orzáez M, Navarro JA, Hervás M & De la Rosa MA (2012) Specific nitration of tyrosines 46 and 48 makes cytochrome *c* assemble a non-functional apoptosome. *FEBS Lett* 586, 154-158.
- Grzesiek S & Bax A (1993) Amino acid type determination in the sequential assignment procedure of uniformly  $^{13}\text{C}/^{15}\text{N}$ -enriched proteins. *J Biomol NMR* 3, 185-204.
- Güntert P, Mumenthaler C & Wüthrich K (1997) Torsion angle dynamics for NMR structure calculation with the new program Dyana1. *J Mol Biol* 273, 283-298.
- Hüttemann M, Helling S, Sanderson TH, Sinkler C, Samavati L, Mahapatra G, Varughese A, Lu G, Liu J, Ramzan R, *et al.* (2012a) Regulation of mitochondrial respiration and apoptosis through cell signaling: Cytochrome *c* oxidase and cytochrome *c* in ischemia/reperfusion injury and inflammation. *Biochim Biophys Acta - Bioenergetics* 1817, 598-609.
- Hüttemann M, Lee I, Grossman LI, Doan JW & Sanderson TH (2012b) Phosphorylation of mammalian cytochrome *c* and cytochrome *c* oxidase in the regulation of cell destiny: Respiration, apoptosis, and human disease. In *Mitochondrial Oxidative Phosphorylation*. Springer New York.
- Jeng WY, Chen CY, Chang HC & Chuang WJ (2002) Expression and characterization of recombinant human cytochrome *c* in *E. coli*. *J Bioenerg Biomembr* 34, 423-431.
- Kay LE, Torchia DA & Bax A (1989) Backbone dynamics of proteins as studied by  $^{15}\text{N}$  inverse detected heteronuclear NMR spectroscopy: application to staphylococcal nuclease. *Biochemistry* 28, 8972-8979.
- Kay LE, Xu G, Singer AU, Muhandiram, DR & Forman-Kay, JD (1993) A gradient-enhanced HCCH-TOCSY experiment for recording

side-chain  $^1\text{H}$  and  $^{13}\text{C}$  correlation in  $\text{H}_2\text{O}$  samples of proteins. *J Magn Reson* 101, 333-337.

- Keller R (2004) The computer aided resonance assignment tutorial.
- Khoury GA, Baliban RC & Floudas CA (2011) Proteome-wide post-translational modification statistics: frequency analysis and curation of the swiss-prot database. *Sci Rep* 1, 1-5.
- Koradi R, Billeter M & Wuthrich K (1996) MOLMOL: a program for display and analysis of macromolecular structures. *J Mol Graph* 14, 51-55, 29-32.
- Krishna MMG, Lin Y, Rumbley JN & Walter Englander S (2003) Cooperative omega loops in cytochrome *c*: role in folding and function. *J Mol Biol* 331, 29-36.
- Lee I, Salomon AR, Yu K, Doan JW, Grossman LI & Hüttemann M (2006) New prospects for an old enzyme: Mammalian cytochrome *c* is tyrosine-phosphorylated in vivo. *Biochemistry* 45, 9121-9128.
- Maity H, Maity M, Krishna MMG, Mayne L & Englander SW (2005) Protein folding: The stepwise assembly of foldon units. *Proc Natl Acad Sci USA* 102, 4741-4746.
- Marion D, Driscoll PC, Kay LE, Wingfield PT, Bax A, Gronenborn AM & Clore GM (1989a) Overcoming the overlap problem in the assignment of  $^1\text{H}$  NMR spectra of larger proteins by use of three-dimensional heteronuclear  $^1\text{H}$ - $^{15}\text{N}$  Hartmann-Hahn-multiple quantum coherence and nuclear Overhauser-multiple quantum coherence spectroscopy: application to interleukin 1 beta. *Biochemistry* 28, 6150-6156.
- Marion D, Kay LE, Sparks SW, Torchia DA & Bax A (1989b) Three-dimensional heteronuclear NMR of nitrogen- $^{15}$  labeled proteins. *J Am Chem Soc* 111, 1515-1517.

- Martínez-Fábregas J, Díaz-Moreno I, González-Arzola K, Janocha S, Navarro JA, Hervás M, Bernhardt R, Velázquez-Campoy A, Díaz-Quintana A & De la Rosa MA (2014a) Structural and functional analysis of novel human cytochrome *c* targets in apoptosis. *Mol Cell Proteomics* 13, 1439-1456.
- Martínez-Fábregas J, Díaz-Moreno I, González-Arzola K, Díaz-Quintana A & De la Rosa MA (2014b) A common signalosome for programmed cell death in humans and plants. *Cell Death Dis* 5, e1314.
- Moreno-Beltrán B, Díaz-Moreno I, González-Arzola K, Guerra-Castellano A, Velázquez-Campoy A, De la Rosa MA & Díaz-Quintana A (2015a) Respiratory complexes III and IV can each bind two molecules of cytochrome *c* at low ionic strength. *FEBS Lett* 589, 476-483.
- Moreno-Beltrán B, González-Arzola K, Martínez-Fábregas J, Díaz-Moreno I & De la Rosa MA (2015b) Cytochrome *c*-based signalosome. In *Redox proteins in supercomplexes and signalosomes*. Taylor and Francis Editorial Group.
- Olteanu A, Patel CN, Dedmon MM, Kennedy S, Linhoff MW, Minder CM, Potts PR, Deshmukh M & Pielak GJ (2003) Stability and apoptotic activity of recombinant human cytochrome *c*. *Biochem Biophys Res Commun* 312, 733-740.
- Pecina P, Borisenko GG, Belikova NA, Tyurina YY, Pecinova A, Lee I, Samhan-Arias AK, Przyklenk K, Kagan VE & Hüttemann M (2010) Phosphomimetic substitution of cytochrome *c* tyrosine 48 decreases respiration and binding to cardiolipin and abolishes ability to trigger downstream caspase activation. *Biochemistry* 49, 6705-6714.
- Pettersen EF, Goddard TD, Huang CC, Couch GS, Greenblatt DM, Meng EC & Ferrin TE (2004) UCSF Chimera—A visualization system for exploratory research and analysis. *J Comput Chem* 25, 1605-1612.

- Piotto M, Saudek V & Sklenar V (1992) Gradient-tailored excitation for single-quantum NMR spectroscopy of aqueous solutions. *J Biomol NMR* 2, 661-665.
- Ryckaert JP, Ciccotti G & Berendsen HJC (1977) Numerical integration of the cartesian equations of motion of a system with constraints: Molecular dynamics of n-Alkanes. *J Comp Phys* 23.
- Sreerama N & Woody RW (2000) Estimation of protein secondary structure from circular dichroism spectra: Comparison of CONTIN, SELCON, and CDSSTR methods with an expanded reference set. *Anal Biochem* 287, 252-260.
- Sreerama N & Woody RW (2004) Computation and analysis of protein circular dichroism spectra. In *Methods in Enzymology*. Academic Press.
- Song B-J, Akbar M, Abdelmegeed MA, Byun K, Lee B, Yoon SK & Hardwick JP (2014) Mitochondrial dysfunction and tissue injury by alcohol, high fat, nonalcoholic substances and pathological conditions through post-translational protein modifications. *Redox Biol* 3, 109-123.
- Xie J, Supekova L & Schultz PG (2007) A genetically encoded metabolically stable analogue of phosphotyrosine in *Escherichia coli*. *ACS Chem Biol* 2, 474-478.
- Yu H, Lee I, Salomon AR, Yu K & Hüttemann M (2008) Mammalian liver cytochrome *c* is tyrosine-48 phosphorylated in vivo, inhibiting mitochondrial respiration. *Biochim Biophys Acta - Bioenergetics* 1777, 1066-1071.
- Zhao X, León IR, Bak S, Mogensen M, Wrzesinski K, Højlund K & Jensen ON (2011) Phosphoproteome analysis of functional mitochondria isolated from resting human muscle reveals extensive phosphorylation of inner membrane protein complexes and enzymes. *Mol Cell Proteomics* 10, 1-14.

- Zuiderweg ER & Fesik SW (1989) Heteronuclear three-dimensional NMR spectroscopy of the inflammatory protein C5a. *Biochemistry* 28, 2387-2391.
- Zuiderweg ER & Fesik SW (1988) Heteronuclear 3-dimensional NMR spectroscopy. A strategy for the simplification of homonuclear two-dimensional NMR spectra. *J Magn Reson* 78, 588-593

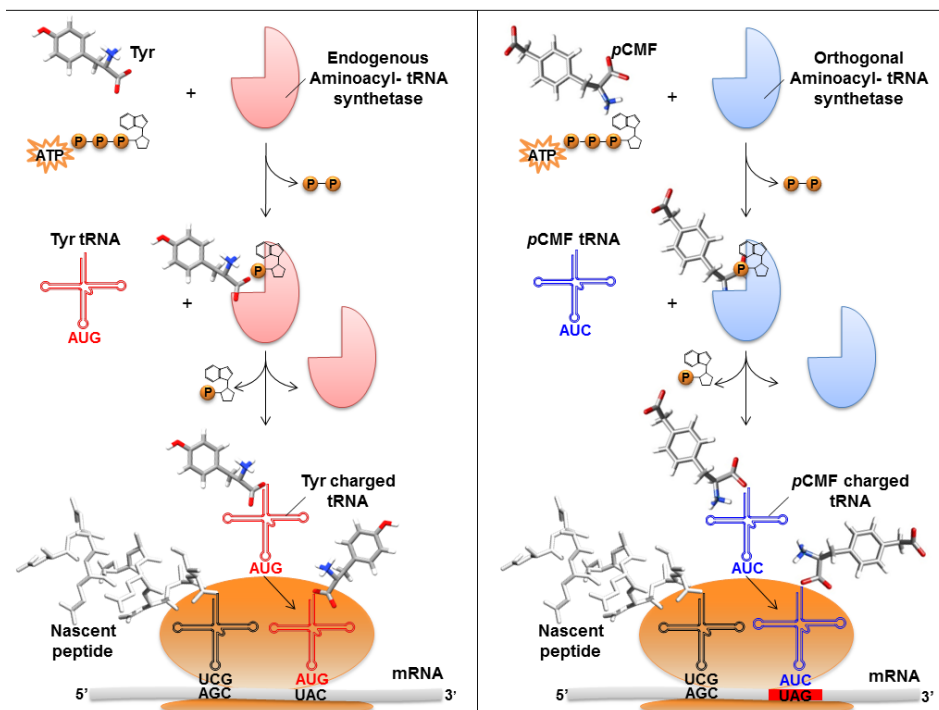


**Figure 1.** Comparison between the molecular pathways that incorporate the canonical amino acid Tyr (left panel) and the non-canonical *p*CMF residue (right panel) during protein synthesis. The biological inclusion of *p*CMF is achieved by using an evolved suppressor tRNA<sub>AUC</sub> (*p*CMF tRNA) that acts as an AMBER suppressor tRNA along with an orthogonal aminoacyl-tRNA synthetase. The Figure shows the punctual mutation of a specific Tyr encoding mRNA triplet (UAC) by the AMBER stop codon (UAG).

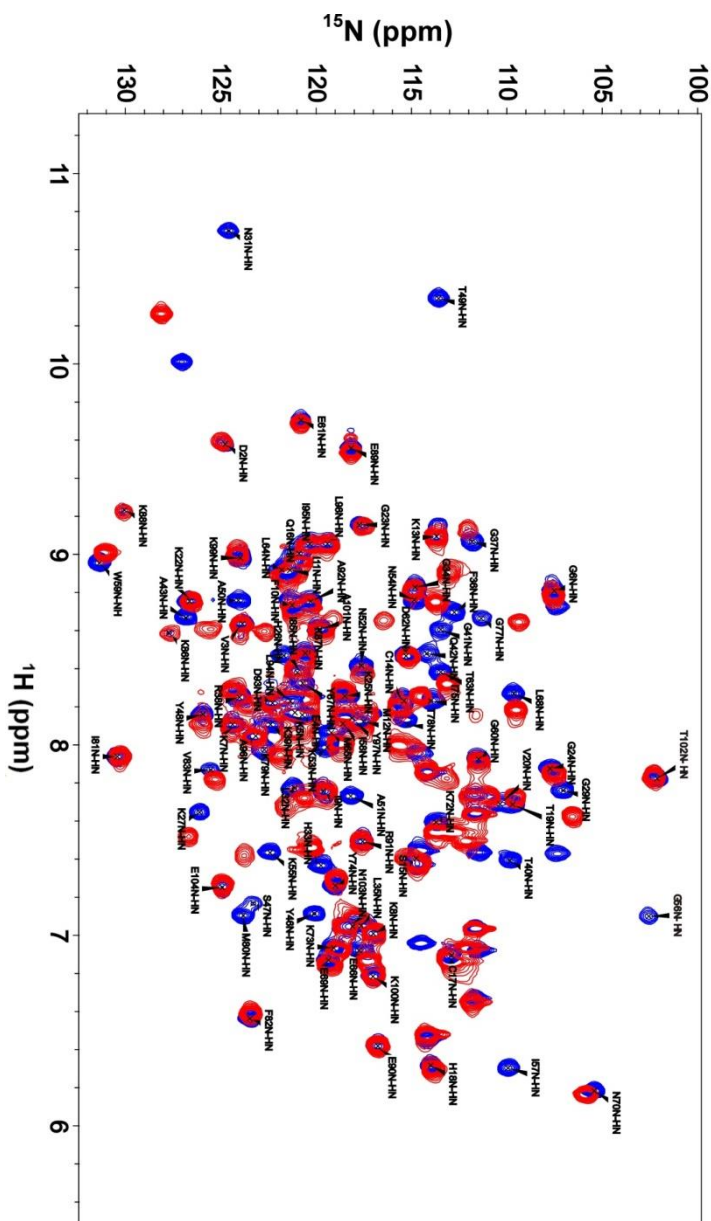


**Figure 2.** Superimposition of the  $[^1\text{H}, ^{15}\text{N}]$  HSQC spectra of uniformly  $^{15}\text{N}$ -labeled forms of the wild-type and Y48pCMF hCc species. Wild-type hCc is colored in blue, whereas Y48pCMF hCc in red. Backbone amide resonances of wild-type hCc are displayed (Jeng *et al.*, 2002).

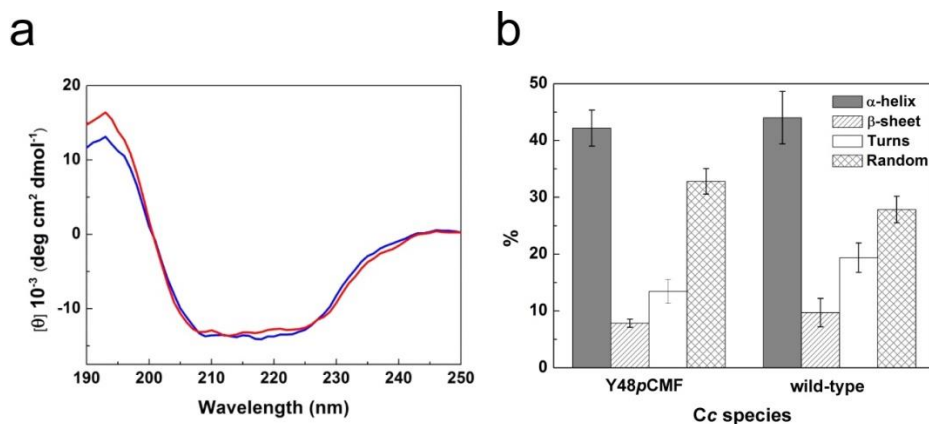


**Figure 3.** Comparison of CD spectra and secondary structure elements between the reduced forms of the wild-type and Y48pCMF hCc species. a) Superimposition of the Far-UV spectra. Wild-type hCc is colored in blue, whereas Y48pCMF hCc in red. b) Analysis of the diverse secondary structure elements for the wild-type and Y48pCMF hCc species by CD Pro Software Package.



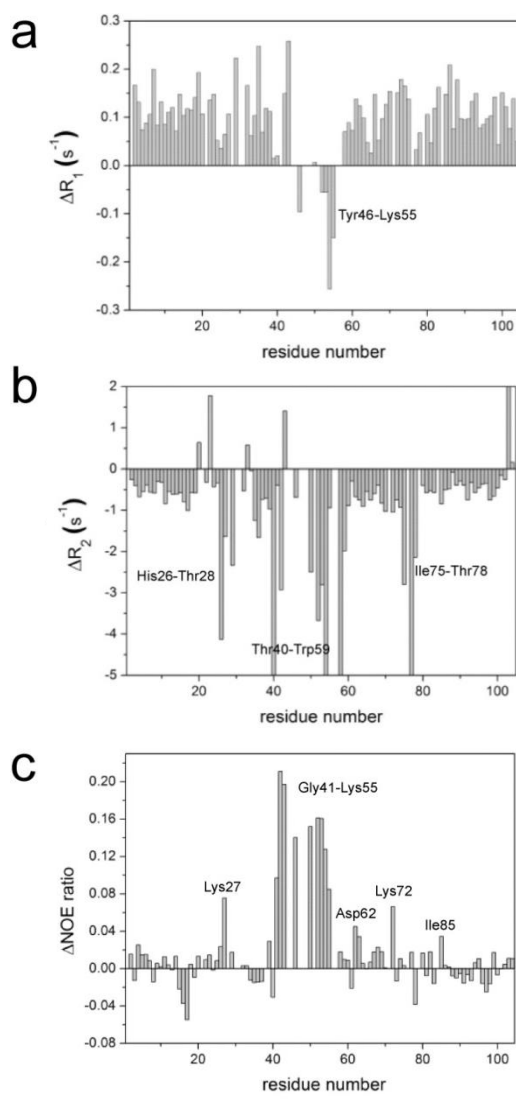


**Figure 4.** The differences between the experimental values of the relaxation rates  $R_1$  (a),  $R_2$  (b) and NOE (c) between the reduced forms of the wild-type and Y48pCMF hCc species, plotted as a function of the residue number. Gaps in the data result from overlapping resonances, broadened resonances beyond the detection limit and unassigned resonances. More affected regions are highlighted.

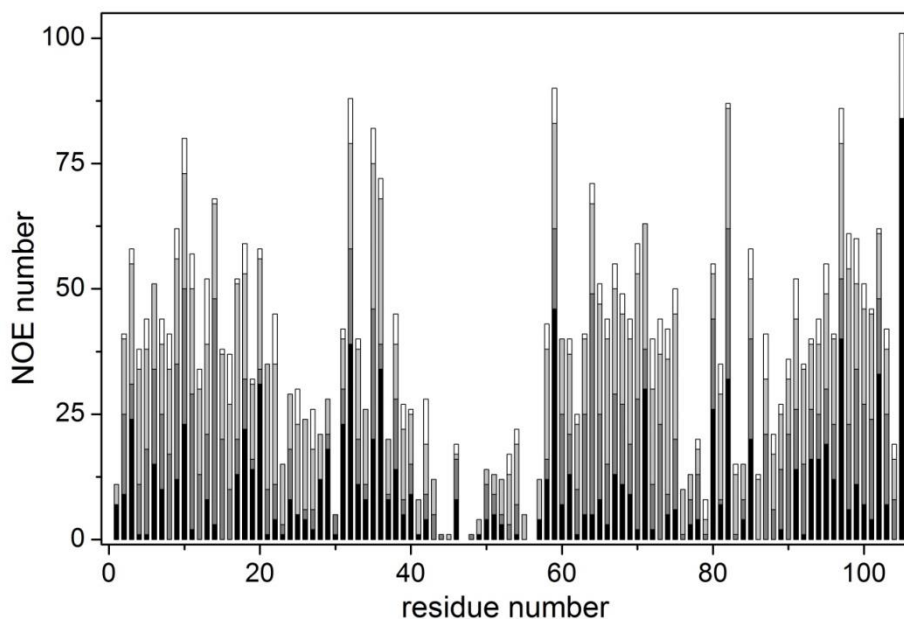


**Figure 5.** Number of experimental meaningful NOEs per residue used for the structure calculation of Y48pCMF hCc. White bars indicate intra-residue NOEs; light gray, sequential NOEs; dark gray and black, medium and long range NOEs, respectively. Residue 105 corresponds to the heme group.

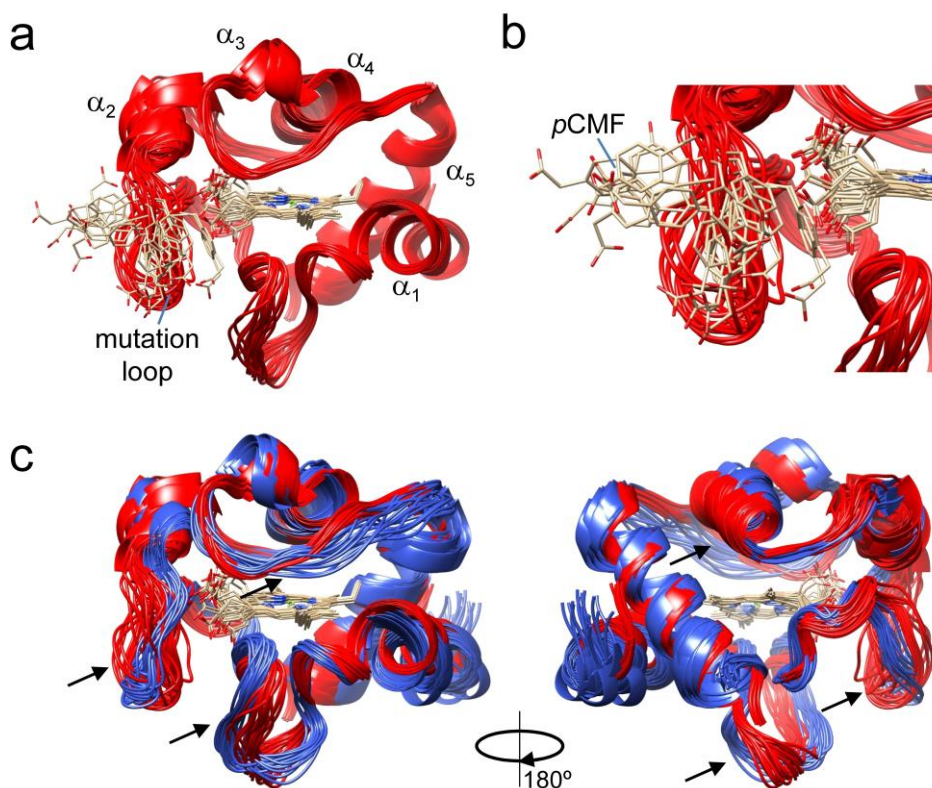


**Figure 6.** NMR solution structure of Y48pCMF hCc. a) Ribbon representation of the best 20 conformers of Y48pCMF hCc. The heme group and the side chain of the pCMF48 is shown for all conformers. Ribbons are colored in red and atoms from the heme group and pCMF by CPK color scheme. The five helices are indicated, as well as the mutation-containing loop. b) A close-up of the mutation-containing loop. The non-canonical pCMF48 adopts multiple orientations. c) Comparison between the NMR solution structures of the wild-type (Jeng *et al.*, 2002) and Y48pCMF hCc species. The ribbon of the wild-type form is colored in blue. Arrows indicate the regions with substantial structural changes. Protein structures were represented by Chimera (Pettersen *et al.*, 2004).

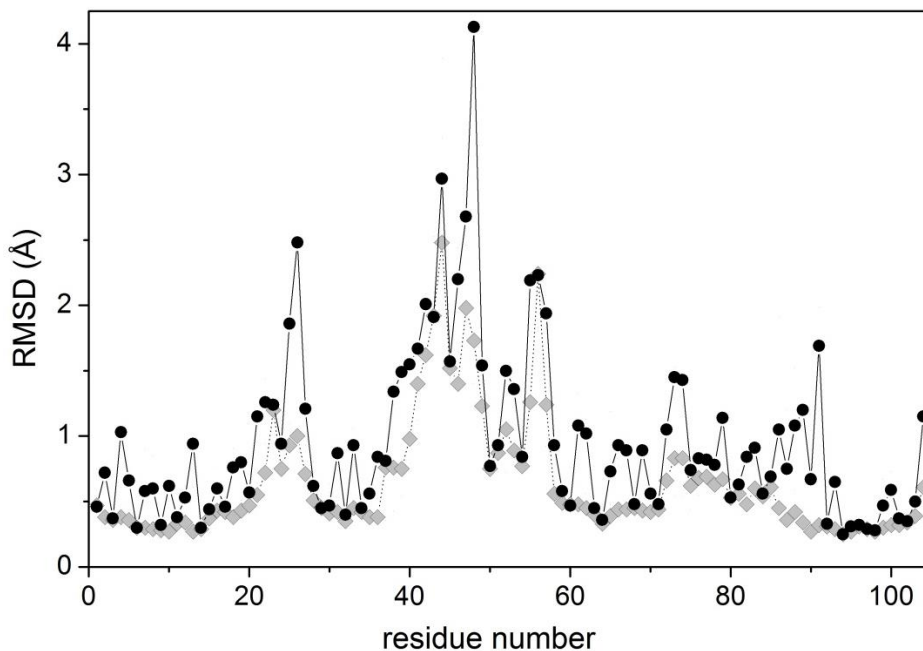


**Figure 7.** The RMSD values per residue of the best 20 conformers of the Y48pCMF hCc mutant to the mean structure. Backbone atoms are represented as gray rhombs and heavy atoms, as black circles. The RMSD calculations and the generation of the mean structure were performed by Molmol (Koradi *et al.*, 1996).

**Table 1.** Comprehensive  $^{15}\text{N}$ -relaxation parameters of the wild-type and Y48pCMF hCc species.

	wild-type hCc	Y48pCMF hCc	Difference
$R_1$ ( $\text{s}^{-1}$ )	$2.26 \pm 0.08$	$2.15 \pm 0.07$	0.11
$R_2$ ( $\text{s}^{-1}$ )	$8.53 \pm 0.46$	$9.14 \pm 0.48$	0.61
$R_2/R_1$ ( $\text{s}^{-1}$ )	$3.77 \pm 0.23$	$4.25 \pm 0.23$	0.48
NOE ratio	$0.80 \pm 0.03$	$0.80 \pm 0.02$	0.00
$\tau_c$ (ns)	$6.33 \pm 0.28$	$6.89 \pm 0.25$	0.56

**Table 2.** NMR statistics of the Y48pCMF hCc structure

<b>NMR distance and dihedral constraints</b>	
Distance constraints	
Total meaningful NOE	2,176
Intra-residue	362
Inter-residue	1,814
Sequential ( $ i - j  = 1$ )	769
Medium-range ( $ i - j  \leq 5$ )	562
Long-range ( $ i - j  > 5$ )	483
Total dihedral angle restraints	
$\phi$	71
$\psi$	71
<b>Structure statistics</b>	
Violations	
Target function	$0.73 \pm 0.18$
RMSD of upper limits (Å)	$0.0059 \pm 0.0014$
RMSD of torsion angles (°)	$0.3336 \pm 0.0973$
Max. distance constraint violation (Å)	0.29
Max. dihedral angle violation (°)	3.79
RMSD of minimized 20 conformers to the mean (Å)	
Backbone	$0.87 \pm 0.16$
Heavy atoms	$1.33 \pm 0.24$

## **XII. APPENDIX III**





## Dataset

1. **Moreno-Beltrán, B** *et al.* (2012) NMR Assignment of *Arabidopsis thaliana* cytochrome *c* in its reduced state. BMRB Entry 18828 (Released).



```

save assigned_chem_shift_list_1
  _Assigned_chem_shift_list.Sf_category          assigned_chemical_shifts
  _Assigned_chem_shift_list.Sf_framecode        assigned_chem_shift_list_1
  _Assigned_chem_shift_list.Entry_ID           18828
  _Assigned_chem_shift_list.ID                 1
  _Assigned_chem_shift_list.Sample_condition_list_ID 1
  _Assigned_chem_shift_list.Sample_condition_list_label $AtCc_cond
  _Assigned_chem_shift_list.Chem_shift_reference_ID 1
  _Assigned_chem_shift_list.Chem_shift_reference_label $DSS
  _Assigned_chem_shift_list.Chem_shift_1H_err .
  _Assigned_chem_shift_list.Chem_shift_13C_err .
  _Assigned_chem_shift_list.Chem_shift_15N_err .
  _Assigned_chem_shift_list.Chem_shift_31P_err .
  _Assigned_chem_shift_list.Chem_shift_2H_err .
  _Assigned_chem_shift_list.Chem_shift_19F_err .
  _Assigned_chem_shift_list.Error_derivation_method .
  _Assigned_chem_shift_list.Details .
  _Assigned_chem_shift_list.Text_data_format .
  _Assigned_chem_shift_list.Text_data .

loop
  _Chem_shift_experiment.Experiment_ID
  _Chem_shift_experiment.Experiment_name
  _Chem_shift_experiment.Sample_ID
  _Chem_shift_experiment.Sample_label
  _Chem_shift_experiment.Sample_state
  _Chem_shift_experiment.Entry_ID
  _Chem_shift_experiment.Assigned_chem_shift_list_ID

  1 '2D 1H-15N HSQC' . . . 18828 1
  2 '3D 1H-15N NOESY' . . . 18828 1
  3 '3D 1H-15N TOCSY' . . . 18828 1

stop_

loop
  _Atom_chem_shift.ID
  _Atom_chem_shift.Assembly_atom_ID
  _Atom_chem_shift.Entity_assembly_ID
  _Atom_chem_shift.Entity_ID
  _Atom_chem_shift.Comp_index_ID
  _Atom_chem_shift.Seq_ID
  _Atom_chem_shift.Comp_ID
  _Atom_chem_shift.Atom_ID
  _Atom_chem_shift.Atom_type
  _Atom_chem_shift.Atom_isotope_number
  _Atom_chem_shift.Val
  _Atom_chem_shift.Val_err
  _Atom_chem_shift.Assign_fig_of_merit
  _Atom_chem_shift.Ambiguity_code
  _Atom_chem_shift.Occupancy
  _Atom_chem_shift.Resonance_ID
  _Atom_chem_shift.Auth_entity_assembly_ID
  _Atom_chem_shift.Auth_asym_ID
  _Atom_chem_shift.Auth_seq_ID
  _Atom_chem_shift.Auth_comp_ID
  _Atom_chem_shift.Auth_atom_ID
  _Atom_chem_shift.Details
  _Atom_chem_shift.Entry_ID
  _Atom_chem_shift.Assigned_chem_shift_list_ID

  1 . 1 1 3 3 PHE H H 1 8.823 0.001 . 1 . . . . 3 PHE H . 18828 1
  2 . 1 1 3 3 PHE N N 15 121.960 0.001 . 1 . . . . 3 PHE N . 18828 1
  3 . 1 1 4 4 ASP H H 1 7.889 0.001 . 1 . . . . 4 ASP H . 18828 1
  4 . 1 1 4 4 ASP N N 15 118.261 0.001 . 1 . . . . 4 ASP N . 18828 1
  5 . 1 1 5 5 GLU H H 1 7.343 0.001 . 1 . . . . 5 GLU H . 18828 1
  6 . 1 1 5 5 GLU N N 15 116.346 0.001 . 1 . . . . 5 GLU N . 18828 1
  7 . 1 1 6 6 ALA H H 1 7.301 0.001 . 1 . . . . 6 ALA H . 18828 1
  8 . 1 1 6 6 ALA N N 15 125.155 0.001 . 1 . . . . 6 ALA N . 18828 1
  9 . 1 1 9 9 GLY H H 1 8.592 0.001 . 1 . . . . 9 GLY H . 18828 1
  10 . 1 1 9 9 GLY N N 15 110.759 0.001 . 1 . . . . 9 GLY N . 18828 1
  11 . 1 1 10 10 ASN H H 1 10.166 0.001 . 1 . . . . 10 ASN H . 18828 1
  12 . 1 1 10 10 ASN HD21 H 1 7.104 0.001 . 1 . . . . 10 ASN HD21 . 18828 1
  13 . 1 1 10 10 ASN HD22 H 1 7.903 0.001 . 1 . . . . 10 ASN HD22 . 18828 1
  14 . 1 1 10 10 ASN N N 15 124.108 0.001 . 1 . . . . 10 ASN N . 18828 1
  15 . 1 1 10 10 ASN ND2 N 15 114.007 0.005 . 1 . . . . 10 ASN ND2 . 18828 1
  16 . 1 1 12 12 LYS H H 1 7.839 0.001 . 1 . . . . 12 LYS H . 18828 1
  17 . 1 1 12 12 LYS N N 15 119.662 0.001 . 1 . . . . 12 LYS N . 18828 1
  18 . 1 1 13 13 ALA H H 1 7.098 0.001 . 1 . . . . 13 ALA H . 18828 1

```

19	.	1	1	13	13 ALA N	N	15	122.999	0.001	.	1	.	.	.	.	13 ALA N	.	18828	1
20	.	1	1	14	14 GLY H	H	1	8.518	0.001	.	1	.	.	.	.	14 GLY H	.	18828	1
21	.	1	1	14	14 GLY N	N	15	106.441	0.001	.	1	.	.	.	.	14 GLY N	.	18828	1
22	.	1	1	15	15 GLU H	H	1	7.988	0.001	.	1	.	.	.	.	15 GLU H	.	18828	1
23	.	1	1	15	15 GLU N	N	15	124.686	0.001	.	1	.	.	.	.	15 GLU N	.	18828	1
24	.	1	1	16	16 LYS H	H	1	6.744	0.001	.	1	.	.	.	.	16 LYS H	.	18828	1
25	.	1	1	16	16 LYS N	N	15	117.355	0.001	.	1	.	.	.	.	16 LYS N	.	18828	1
26	.	1	1	17	17 ILE H	H	1	7.468	0.001	.	1	.	.	.	.	17 ILE H	.	18828	1
27	.	1	1	17	17 ILE N	N	15	120.342	0.001	.	1	.	.	.	.	17 ILE N	.	18828	1
28	.	1	1	18	18 PHE H	H	1	8.789	0.001	.	1	.	.	.	.	18 PHE H	.	18828	1
29	.	1	1	18	18 PHE N	N	15	121.409	0.001	.	1	.	.	.	.	18 PHE N	.	18828	1
30	.	1	1	19	19 ARG H	H	1	8.667	0.001	.	1	.	.	.	.	19 ARG H	.	18828	1
31	.	1	1	19	19 ARG N	N	15	118.614	0.001	.	1	.	.	.	.	19 ARG N	.	18828	1
32	.	1	1	20	20 THR H	H	1	7.736	0.001	.	1	.	.	.	.	20 THR H	.	18828	1
33	.	1	1	20	20 THR N	N	15	108.909	0.001	.	1	.	.	.	.	20 THR N	.	18828	1
34	.	1	1	21	21 LYS H	H	1	8.840	0.001	.	1	.	.	.	.	21 LYS H	.	18828	1
35	.	1	1	21	21 LYS N	N	15	117.805	0.001	.	1	.	.	.	.	21 LYS N	.	18828	1
36	.	1	1	22	22 CYS H	H	1	8.013	0.001	.	1	.	.	.	.	22 CYS H	.	18828	1
37	.	1	1	22	22 CYS N	N	15	115.392	0.001	.	1	.	.	.	.	22 CYS N	.	18828	1
38	.	1	1	23	23 ALA H	H	1	7.291	0.001	.	1	.	.	.	.	23 ALA H	.	18828	1
39	.	1	1	23	23 ALA N	N	15	120.944	0.001	.	1	.	.	.	.	23 ALA N	.	18828	1
40	.	1	1	24	24 GLN H	H	1	8.818	0.001	.	1	.	.	.	.	24 GLN H	.	18828	1
41	.	1	1	24	24 GLN HE21	H	1	6.937	0.001	.	1	.	.	.	.	24 GLN HE21	.	18828	1
42	.	1	1	24	24 GLN HE22	H	1	7.578	0.001	.	1	.	.	.	.	24 GLN HE22	.	18828	1
43	.	1	1	24	24 GLN N	N	15	115.860	0.001	.	1	.	.	.	.	24 GLN N	.	18828	1
44	.	1	1	24	24 GLN NE2	N	15	111.441	0.004	.	1	.	.	.	.	24 GLN NE2	.	18828	1
45	.	1	1	25	25 CYS H	H	1	6.789	0.001	.	1	.	.	.	.	25 CYS H	.	18828	1
46	.	1	1	25	25 CYS N	N	15	113.172	0.001	.	1	.	.	.	.	25 CYS N	.	18828	1
47	.	1	1	26	26 HIS H	H	1	6.256	0.001	.	1	.	.	.	.	26 HIS H	.	18828	1
48	.	1	1	26	26 HIS HD1	H	1	9.492	0.001	.	1	.	.	.	.	26 HIS HD1	.	18828	1
49	.	1	1	26	26 HIS N	N	15	113.816	0.001	.	1	.	.	.	.	26 HIS N	.	18828	1
50	.	1	1	26	26 HIS ND1	N	15	129.797	0.001	.	1	.	.	.	.	26 HIS ND1	.	18828	1
51	.	1	1	27	27 THR H	H	1	7.234	0.001	.	1	.	.	.	.	27 THR H	.	18828	1
52	.	1	1	27	27 THR N	N	15	109.480	0.001	.	1	.	.	.	.	27 THR N	.	18828	1
53	.	1	1	28	28 VAL H	H	1	7.763	0.001	.	1	.	.	.	.	28 VAL H	.	18828	1
54	.	1	1	28	28 VAL N	N	15	111.233	0.001	.	1	.	.	.	.	28 VAL N	.	18828	1
55	.	1	1	29	29 GLU H	H	1	8.107	0.001	.	1	.	.	.	.	29 GLU H	.	18828	1
56	.	1	1	29	29 GLU N	N	15	120.358	0.001	.	1	.	.	.	.	29 GLU N	.	18828	1
57	.	1	1	30	30 LYS H	H	1	8.924	0.001	.	1	.	.	.	.	30 LYS H	.	18828	1
58	.	1	1	30	30 LYS N	N	15	127.085	0.001	.	1	.	.	.	.	30 LYS N	.	18828	1
59	.	1	1	31	31 GLY H	H	1	9.057	0.001	.	1	.	.	.	.	31 GLY H	.	18828	1
60	.	1	1	31	31 GLY N	N	15	115.424	0.001	.	1	.	.	.	.	31 GLY N	.	18828	1
61	.	1	1	32	32 ALA H	H	1	7.084	0.001	.	1	.	.	.	.	32 ALA H	.	18828	1
62	.	1	1	32	32 ALA N	N	15	120.697	0.001	.	1	.	.	.	.	32 ALA N	.	18828	1
63	.	1	1	33	33 GLY H	H	1	8.085	0.001	.	1	.	.	.	.	33 GLY H	.	18828	1
64	.	1	1	33	33 GLY N	N	15	105.141	0.001	.	1	.	.	.	.	33 GLY N	.	18828	1
65	.	1	1	34	34 HIS H	H	1	8.198	0.001	.	1	.	.	.	.	34 HIS H	.	18828	1
66	.	1	1	34	34 HIS N	N	15	119.674	0.001	.	1	.	.	.	.	34 HIS N	.	18828	1
67	.	1	1	35	35 LYS H	H	1	7.556	0.001	.	1	.	.	.	.	35 LYS H	.	18828	1
68	.	1	1	35	35 LYS N	N	15	125.179	0.001	.	1	.	.	.	.	35 LYS N	.	18828	1
69	.	1	1	36	36 GLN H	H	1	8.272	0.001	.	1	.	.	.	.	36 GLN H	.	18828	1
70	.	1	1	36	36 GLN HE21	H	1	7.155	0.001	.	1	.	.	.	.	36 GLN HE21	.	18828	1
71	.	1	1	36	36 GLN HE22	H	1	7.724	0.001	.	1	.	.	.	.	36 GLN HE22	.	18828	1
72	.	1	1	36	36 GLN N	N	15	122.946	0.001	.	1	.	.	.	.	36 GLN N	.	18828	1
73	.	1	1	36	36 GLN NE2	N	15	111.240	0.001	.	1	.	.	.	.	36 GLN NE2	.	18828	1
74	.	1	1	37	37 GLY H	H	1	7.647	0.001	.	1	.	.	.	.	37 GLY H	.	18828	1
75	.	1	1	37	37 GLY N	N	15	104.501	0.001	.	1	.	.	.	.	37 GLY N	.	18828	1
76	.	1	1	39	39 ASN H	H	1	10.862	0.001	.	1	.	.	.	.	39 ASN H	.	18828	1
77	.	1	1	39	39 ASN HD21	H	1	7.101	0.001	.	1	.	.	.	.	39 ASN HD21	.	18828	1
78	.	1	1	39	39 ASN HD22	H	1	7.671	0.001	.	1	.	.	.	.	39 ASN HD22	.	18828	1
79	.	1	1	39	39 ASN N	N	15	124.542	0.001	.	1	.	.	.	.	39 ASN N	.	18828	1
80	.	1	1	39	39 ASN ND2	N	15	115.206	0.004	.	1	.	.	.	.	39 ASN ND2	.	18828	1
81	.	1	1	40	40 LEU H	H	1	8.080	0.001	.	1	.	.	.	.	40 LEU H	.	18828	1
82	.	1	1	40	40 LEU N	N	15	122.870	0.001	.	1	.	.	.	.	40 LEU N	.	18828	1
83	.	1	1	41	41 ASN H	H	1	7.750	0.001	.	1	.	.	.	.	41 ASN H	.	18828	1
84	.	1	1	41	41 ASN HD21	H	1	6.858	0.001	.	1	.	.	.	.	41 ASN HD21	.	18828	1
85	.	1	1	41	41 ASN HD22	H	1	7.742	0.001	.	1	.	.	.	.	41 ASN HD22	.	18828	1
86	.	1	1	41	41 ASN N	N	15	119.715	0.001	.	1	.	.	.	.	41 ASN N	.	18828	1
87	.	1	1	41	41 ASN ND2	N	15	112.930	0.008	.	1	.	.	.	.	41 ASN ND2	.	18828	1
88	.	1	1	42	42 GLY H	H	1	9.763	0.001	.	1	.	.	.	.	42 GLY H	.	18828	1
89	.	1	1	42	42 GLY N	N	15	115.383	0.001	.	1	.	.	.	.	42 GLY N	.	18828	1
90	.	1	1	43	43 LEU H	H	1	7.055	0.001	.	1	.	.	.	.	43 LEU H	.	18828	1
91	.	1	1	43	43 LEU N	N	15	117.700	0.001	.	1	.	.	.	.	43 LEU N	.	18828	1
92	.	1	1	44	44 PHE H	H	1	8.287	0.001	.	1	.	.	.	.	44 PHE H	.	18828	1
93	.	1	1	44	44 PHE N	N	15	113.030	0.001	.	1	.	.	.	.	44 PHE N	.	18828	1
94	.	1	1	45	45 GLY H	H	1	9.374	0.001	.	1	.	.	.	.	45 GLY H	.	18828	1
95	.	1	1	45	45 GLY N	N	15	114.443	0.001	.	1	.	.	.	.	45 GLY N	.	18828	1
96	.	1	1	46	46 ARG H	H	1	8.191	0.001	.	1	.	.	.	.	46 ARG H	.	18828	1
97	.	1	1	46	46 ARG HE	H	1	6.954	0.001	.	1	.	.	.	.	46 ARG HE	.	18828	1
98	.	1	1	46	46 ARG N	N	15	123.275	0.001	.	1	.	.	.	.	46 ARG N	.	18828	1
99	.	1	1	46	46 ARG NE	N	15	121.139	0.001	.	1	.	.	.	.	46 ARG NE	.	18828	1
100	.	1	1	47	47 GLN H	H	1	8.419	0.001	.	1	.	.	.	.	47 GLN H	.	18828	1
101	.	1	1	47	47 GLN HE21	H	1	6.813	0.001	.	1	.	.	.	.	47 GLN HE21	.	18828	1

102	. 1 1	47	47	GLN	HE22	H	1	7.714	0.001	. 1	. . . . .	47	GLN	HE22	. 18828	1
103	. 1 1	47	47	GLN	N	N	15	123.859	0.001	. 1	. . . . .	47	GLN	N	. 18828	1
104	. 1 1	47	47	GLN	NE2	N	15	113.813	0.004	. 1	. . . . .	47	GLN	NE2	. 18828	1
105	. 1 1	48	48	SER	H	H	1	8.608	0.001	. 1	. . . . .	48	SER	H	. 18828	1
106	. 1 1	48	48	SER	N	N	15	129.167	0.001	. 1	. . . . .	48	SER	N	. 18828	1
107	. 1 1	49	49	GLY	H	H	1	7.671	0.001	. 1	. . . . .	49	GLY	H	. 18828	1
108	. 1 1	49	49	GLY	N	N	15	103.843	0.001	. 1	. . . . .	49	GLY	N	. 18828	1
109	. 1 1	50	50	THR	H	H	1	7.534	0.001	. 1	. . . . .	50	THR	H	. 18828	1
110	. 1 1	50	50	THR	N	N	15	113.113	0.001	. 1	. . . . .	50	THR	N	. 18828	1
111	. 1 1	51	51	THR	H	H	1	7.891	0.001	. 1	. . . . .	51	THR	H	. 18828	1
112	. 1 1	51	51	THR	N	N	15	123.899	0.001	. 1	. . . . .	51	THR	N	. 18828	1
113	. 1 1	53	53	GLY	H	H	1	8.947	0.001	. 1	. . . . .	53	GLY	H	. 18828	1
114	. 1 1	53	53	GLY	N	N	15	110.195	0.001	. 1	. . . . .	53	GLY	N	. 18828	1
115	. 1 1	54	54	TYR	H	H	1	6.988	0.001	. 1	. . . . .	54	TYR	H	. 18828	1
116	. 1 1	54	54	TYR	N	N	15	119.351	0.001	. 1	. . . . .	54	TYR	N	. 18828	1
117	. 1 1	55	55	SER	H	H	1	7.144	0.001	. 1	. . . . .	55	SER	H	. 18828	1
118	. 1 1	55	55	SER	N	N	15	123.280	0.001	. 1	. . . . .	55	SER	N	. 18828	1
119	. 1 1	56	56	TYR	H	H	1	8.088	0.001	. 1	. . . . .	56	TYR	H	. 18828	1
120	. 1 1	56	56	TYR	N	N	15	125.725	0.001	. 1	. . . . .	56	TYR	N	. 18828	1
121	. 1 1	57	57	SER	H	H	1	10.898	0.001	. 1	. . . . .	57	SER	H	. 18828	1
122	. 1 1	57	57	SER	N	N	15	118.911	0.001	. 1	. . . . .	57	SER	N	. 18828	1
123	. 1 1	58	58	ALA	H	H	1	8.842	0.001	. 1	. . . . .	58	ALA	H	. 18828	1
124	. 1 1	58	58	ALA	N	N	15	123.986	0.001	. 1	. . . . .	58	ALA	N	. 18828	1
125	. 1 1	59	59	ALA	H	H	1	8.028	0.001	. 1	. . . . .	59	ALA	H	. 18828	1
126	. 1 1	59	59	ALA	N	N	15	119.436	0.001	. 1	. . . . .	59	ALA	N	. 18828	1
127	. 1 1	60	60	ASN	H	H	1	8.346	0.001	. 1	. . . . .	60	ASN	H	. 18828	1
128	. 1 1	60	60	ASN	HD21	H	1	7.455	0.001	. 1	. . . . .	60	ASN	HD21	. 18828	1
129	. 1 1	60	60	ASN	HD22	H	1	8.695	0.001	. 1	. . . . .	60	ASN	HD22	. 18828	1
130	. 1 1	60	60	ASN	N	N	15	118.629	0.001	. 1	. . . . .	60	ASN	N	. 18828	1
131	. 1 1	60	60	ASN	ND2	N	15	107.218	0.001	. 1	. . . . .	60	ASN	ND2	. 18828	1
132	. 1 1	61	61	LYS	H	H	1	7.765	0.001	. 1	. . . . .	61	LYS	H	. 18828	1
133	. 1 1	61	61	LYS	N	N	15	117.955	0.001	. 1	. . . . .	61	LYS	N	. 18828	1
134	. 1 1	62	62	SER	H	H	1	8.599	0.001	. 1	. . . . .	62	SER	H	. 18828	1
135	. 1 1	62	62	SER	N	N	15	113.957	0.001	. 1	. . . . .	62	SER	N	. 18828	1
136	. 1 1	63	63	MET	H	H	1	7.513	0.001	. 1	. . . . .	63	MET	H	. 18828	1
137	. 1 1	63	63	MET	N	N	15	120.042	0.001	. 1	. . . . .	63	MET	N	. 18828	1
138	. 1 1	64	64	ALA	H	H	1	6.949	0.001	. 1	. . . . .	64	ALA	H	. 18828	1
139	. 1 1	64	64	ALA	N	N	15	118.102	0.001	. 1	. . . . .	64	ALA	N	. 18828	1
140	. 1 1	65	65	VAL	H	H	1	7.732	0.001	. 1	. . . . .	65	VAL	H	. 18828	1
141	. 1 1	65	65	VAL	N	N	15	117.485	0.001	. 1	. . . . .	65	VAL	N	. 18828	1
142	. 1 1	66	66	ASN	H	H	1	8.479	0.001	. 1	. . . . .	66	ASN	H	. 18828	1
143	. 1 1	66	66	ASN	HD21	H	1	6.718	0.001	. 1	. . . . .	66	ASN	HD21	. 18828	1
144	. 1 1	66	66	ASN	HD22	H	1	7.278	0.001	. 1	. . . . .	66	ASN	HD22	. 18828	1
145	. 1 1	66	66	ASN	N	N	15	125.014	0.001	. 1	. . . . .	66	ASN	N	. 18828	1
146	. 1 1	66	66	ASN	ND2	N	15	112.162	0.003	. 1	. . . . .	66	ASN	ND2	. 18828	1
147	. 1 1	67	67	TRP	H	H	1	9.826	0.001	. 1	. . . . .	67	TRP	H	. 18828	1
148	. 1 1	67	67	TRP	HE1	H	1	9.619	0.001	. 1	. . . . .	67	TRP	HE1	. 18828	1
149	. 1 1	67	67	TRP	N	N	15	128.100	0.001	. 1	. . . . .	67	TRP	N	. 18828	1
150	. 1 1	67	67	TRP	NE1	N	15	125.481	0.001	. 1	. . . . .	67	TRP	NE1	. 18828	1
151	. 1 1	68	68	GLU	H	H	1	7.986	0.001	. 1	. . . . .	68	GLU	H	. 18828	1
152	. 1 1	68	68	GLU	N	N	15	118.330	0.001	. 1	. . . . .	68	GLU	N	. 18828	1
153	. 1 1	69	69	GLU	H	H	1	10.624	0.001	. 1	. . . . .	69	GLU	H	. 18828	1
154	. 1 1	69	69	GLU	N	N	15	122.306	0.001	. 1	. . . . .	69	GLU	N	. 18828	1
155	. 1 1	70	70	LYS	H	H	1	8.750	0.001	. 1	. . . . .	70	LYS	H	. 18828	1
156	. 1 1	70	70	LYS	N	N	15	113.872	0.001	. 1	. . . . .	70	LYS	N	. 18828	1
157	. 1 1	71	71	THR	H	H	1	7.318	0.001	. 1	. . . . .	71	THR	H	. 18828	1
158	. 1 1	71	71	THR	N	N	15	108.998	0.001	. 1	. . . . .	71	THR	N	. 18828	1
159	. 1 1	72	72	LEU	H	H	1	8.775	0.001	. 1	. . . . .	72	LEU	H	. 18828	1
160	. 1 1	72	72	LEU	N	N	15	121.861	0.001	. 1	. . . . .	72	LEU	N	. 18828	1
161	. 1 1	73	73	TYR	H	H	1	8.297	0.001	. 1	. . . . .	73	TYR	H	. 18828	1
162	. 1 1	73	73	TYR	N	N	15	119.521	0.001	. 1	. . . . .	73	TYR	N	. 18828	1
163	. 1 1	74	74	ASP	H	H	1	6.946	0.001	. 1	. . . . .	74	ASP	H	. 18828	1
164	. 1 1	74	74	ASP	N	N	15	117.056	0.001	. 1	. . . . .	74	ASP	N	. 18828	1
165	. 1 1	75	75	TYR	H	H	1	8.181	0.001	. 1	. . . . .	75	TYR	H	. 18828	1
166	. 1 1	75	75	TYR	N	N	15	122.818	0.001	. 1	. . . . .	75	TYR	N	. 18828	1
167	. 1 1	76	76	LEU	H	H	1	8.066	0.001	. 1	. . . . .	76	LEU	H	. 18828	1
168	. 1 1	76	76	LEU	N	N	15	110.802	0.001	. 1	. . . . .	76	LEU	N	. 18828	1
169	. 1 1	77	77	LEU	H	H	1	6.478	0.001	. 1	. . . . .	77	LEU	H	. 18828	1
170	. 1 1	77	77	LEU	N	N	15	119.352	0.001	. 1	. . . . .	77	LEU	N	. 18828	1
171	. 1 1	78	78	ASN	H	H	1	5.995	0.001	. 1	. . . . .	78	ASN	H	. 18828	1
172	. 1 1	78	78	ASN	HD21	H	1	6.613	0.001	. 1	. . . . .	78	ASN	HD21	. 18828	1
173	. 1 1	78	78	ASN	HD22	H	1	7.484	0.001	. 1	. . . . .	78	ASN	HD22	. 18828	1
174	. 1 1	78	78	ASN	N	N	15	105.159	0.001	. 1	. . . . .	78	ASN	N	. 18828	1
175	. 1 1	78	78	ASN	ND2	N	15	111.316	0.002	. 1	. . . . .	78	ASN	ND2	. 18828	1
176	. 1 1	80	80	LYS	H	H	1	7.497	0.001	. 1	. . . . .	80	LYS	H	. 18828	1
177	. 1 1	80	80	LYS	N	N	15	113.179	0.001	. 1	. . . . .	80	LYS	N	. 18828	1
178	. 1 1	81	81	LYS	H	H	1	6.871	0.001	. 1	. . . . .	81	LYS	H	. 18828	1
179	. 1 1	81	81	LYS	N	N	15	117.569	0.001	. 1	. . . . .	81	LYS	N	. 18828	1
180	. 1 1	82	82	TYR	H	H	1	7.416	0.001	. 1	. . . . .	82	TYR	H	. 18828	1
181	. 1 1	82	82	TYR	N	N	15	120.650	0.001	. 1	. . . . .	82	TYR	N	. 18828	1
182	. 1 1	83	83	ILE	H	H	1	7.956	0.001	. 1	. . . . .	83	ILE	H	. 18828	1
183	. 1 1	83	83	ILE	N	N	15	112.869	0.001	. 1	. . . . .	83	ILE	N	. 18828	1
184	. 1 1	85	85	GLY	H	H	1	8.570	0.001	. 1	. . . . .	85	GLY	H	. 18828	1

185	. 1 1	85	85	GLY	N	N 15	110.965	0.001	. 1	. . . . .	85	GLY	N	. 18828	1
186	. 1 1	86	86	THR	H	H 1	8.153	0.001	. 1	. . . . .	86	THR	H	. 18828	1
187	. 1 1	86	86	THR	N	N 15	115.546	0.001	. 1	. . . . .	86	THR	N	. 18828	1
188	. 1 1	87	87	LYS	H	H 1	8.083	0.001	. 1	. . . . .	87	LYS	H	. 18828	1
189	. 1 1	87	87	LYS	N	N 15	121.928	0.001	. 1	. . . . .	87	LYS	N	. 18828	1
190	. 1 1	88	88	MET	H	H 1	7.266	0.001	. 1	. . . . .	88	MET	H	. 18828	1
191	. 1 1	88	88	MET	N	N 15	123.253	0.001	. 1	. . . . .	88	MET	N	. 18828	1
192	. 1 1	89	89	VAL	H	H 1	7.339	0.001	. 1	. . . . .	89	VAL	H	. 18828	1
193	. 1 1	89	89	VAL	N	N 15	128.097	0.001	. 1	. . . . .	89	VAL	N	. 18828	1
194	. 1 1	90	90	PHE	H	H 1	6.561	0.001	. 1	. . . . .	90	PHE	H	. 18828	1
195	. 1 1	90	90	PHE	N	N 15	123.897	0.001	. 1	. . . . .	90	PHE	N	. 18828	1
196	. 1 1	93	93	LEU	H	H 1	8.266	0.001	. 1	. . . . .	93	LEU	H	. 18828	1
197	. 1 1	93	93	LEU	N	N 15	123.664	0.001	. 1	. . . . .	93	LEU	N	. 18828	1
198	. 1 1	94	94	LYS	H	H 1	8.305	0.001	. 1	. . . . .	94	LYS	H	. 18828	1
199	. 1 1	94	94	LYS	N	N 15	122.207	0.001	. 1	. . . . .	94	LYS	N	. 18828	1
200	. 1 1	95	95	LYS	H	H 1	9.210	0.001	. 1	. . . . .	95	LYS	H	. 18828	1
201	. 1 1	95	95	LYS	N	N 15	121.897	0.001	. 1	. . . . .	95	LYS	N	. 18828	1
202	. 1 1	97	97	GLN	H	H 1	8.758	0.001	. 1	. . . . .	97	GLN	H	. 18828	1
203	. 1 1	97	97	GLN	HE21	H 1	6.852	0.001	. 1	. . . . .	97	GLN	HE21	. 18828	1
204	. 1 1	97	97	GLN	HE22	H 1	8.627	0.001	. 1	. . . . .	97	GLN	HE22	. 18828	1
205	. 1 1	97	97	GLN	N	N 15	114.402	0.001	. 1	. . . . .	97	GLN	N	. 18828	1
206	. 1 1	97	97	GLN	NE2	N 15	119.296	0.007	. 1	. . . . .	97	GLN	NE2	. 18828	1
207	. 1 1	98	98	ASP	H	H 1	6.553	0.001	. 1	. . . . .	98	ASP	H	. 18828	1
208	. 1 1	98	98	ASP	N	N 15	115.633	0.001	. 1	. . . . .	98	ASP	N	. 18828	1
209	. 1 1	99	99	ARG	H	H 1	7.420	0.001	. 1	. . . . .	99	ARG	H	. 18828	1
210	. 1 1	99	99	ARG	N	N 15	116.756	0.001	. 1	. . . . .	99	ARG	N	. 18828	1
211	. 1 1	100	100	ALA	H	H 1	9.078	0.001	. 1	. . . . .	100	ALA	H	. 18828	1
212	. 1 1	100	100	ALA	N	N 15	121.633	0.001	. 1	. . . . .	100	ALA	N	. 18828	1
213	. 1 1	101	101	ASP	H	H 1	9.014	0.001	. 1	. . . . .	101	ASP	H	. 18828	1
214	. 1 1	101	101	ASP	N	N 15	121.739	0.001	. 1	. . . . .	101	ASP	N	. 18828	1
215	. 1 1	102	102	LEU	H	H 1	8.379	0.001	. 1	. . . . .	102	LEU	H	. 18828	1
216	. 1 1	102	102	LEU	N	N 15	121.426	0.001	. 1	. . . . .	102	LEU	N	. 18828	1
217	. 1 1	103	103	ILE	H	H 1	8.924	0.001	. 1	. . . . .	103	ILE	H	. 18828	1
218	. 1 1	103	103	ILE	N	N 15	120.687	0.001	. 1	. . . . .	103	ILE	N	. 18828	1
219	. 1 1	104	104	ALA	H	H 1	8.113	0.001	. 1	. . . . .	104	ALA	H	. 18828	1
220	. 1 1	104	104	ALA	N	N 15	121.585	0.001	. 1	. . . . .	104	ALA	N	. 18828	1
221	. 1 1	105	105	TYR	H	H 1	8.221	0.001	. 1	. . . . .	105	TYR	H	. 18828	1
222	. 1 1	105	105	TYR	N	N 15	117.374	0.001	. 1	. . . . .	105	TYR	N	. 18828	1
223	. 1 1	106	106	LEU	H	H 1	9.226	0.001	. 1	. . . . .	106	LEU	H	. 18828	1
224	. 1 1	106	106	LEU	N	N 15	120.278	0.001	. 1	. . . . .	106	LEU	N	. 18828	1
225	. 1 1	107	107	LYS	H	H 1	8.501	0.001	. 1	. . . . .	107	LYS	H	. 18828	1
226	. 1 1	107	107	LYS	N	N 15	123.078	0.001	. 1	. . . . .	107	LYS	N	. 18828	1
227	. 1 1	108	108	GLU	H	H 1	6.746	0.001	. 1	. . . . .	108	GLU	H	. 18828	1
228	. 1 1	108	108	GLU	N	N 15	115.299	0.001	. 1	. . . . .	108	GLU	N	. 18828	1
229	. 1 1	109	109	GLY	H	H 1	8.885	0.001	. 1	. . . . .	109	GLY	H	. 18828	1
230	. 1 1	109	109	GLY	N	N 15	106.157	0.001	. 1	. . . . .	109	GLY	N	. 18828	1
231	. 1 1	110	110	THR	H	H 1	7.513	0.001	. 1	. . . . .	110	THR	H	. 18828	1
232	. 1 1	110	110	THR	N	N 15	106.151	0.001	. 1	. . . . .	110	THR	N	. 18828	1
233	. 1 1	111	111	ALA	H	H 1	6.597	0.001	. 1	. . . . .	111	ALA	H	. 18828	1
234	. 1 1	111	111	ALA	N	N 15	129.851	0.001	. 1	. . . . .	111	ALA	N	. 18828	1

stop\_

save\_

## Dataset

2. **Moreno-Beltrán, B** *et al.* (2015) NMR Assignment of *Homo sapiens* cytochrome *c* in its oxidized state. BMRB Entry 26578 (Entry on Hold).





```

loop_
  _Atom_chem_shift.ID
  _Atom_chem_shift.Assembly_atom_ID
  _Atom_chem_shift.Entity_assembly_ID
  _Atom_chem_shift.Entity_ID
  _Atom_chem_shift.Comp_index_ID
  _Atom_chem_shift.Seq_ID
  _Atom_chem_shift.Comp_ID
  _Atom_chem_shift.Atom_ID
  _Atom_chem_shift.Atom_type
  _Atom_chem_shift.Atom_isotope_number
  _Atom_chem_shift.Val
  _Atom_chem_shift.Val_err
  _Atom_chem_shift.Assign_fig_of_merit
  _Atom_chem_shift.Ambiguity_code
  _Atom_chem_shift.Occupancy
  _Atom_chem_shift.Resonance_ID
  _Atom_chem_shift.Auth_entity_assembly_ID
  _Atom_chem_shift.Auth_asym_ID
  _Atom_chem_shift.Auth_seq_ID
  _Atom_chem_shift.Auth_comp_ID
  _Atom_chem_shift.Auth_atom_ID
  _Atom_chem_shift.PDB_Record_ID
  _Atom_chem_shift.PDB_model_num
  _Atom_chem_shift.PDB_strand_ID
  _Atom_chem_shift.PDB_ins_code
  _Atom_chem_shift.PDB_residue_no
  _Atom_chem_shift.PDB_residue_name
  _Atom_chem_shift.PDB_atom_name
  _Atom_chem_shift.Original_PDB_strand_ID
  _Atom_chem_shift.Original_PDB_residue_no
  _Atom_chem_shift.Original_PDB_residue_name
  _Atom_chem_shift.Original_PDB_atom_name
  _Atom_chem_shift.Details
  _Atom_chem_shift.Entry_ID
  _Atom_chem_shift.Assigned_chem_shift_list_ID

```

1	.	1	1	3	3	VAL	H	H	1	9.454	0.001	.	1	.	.	.	.
2	VAL	H	.	.	.	.	.	.	.	.	26578	1	.	.	.	.	.
2	.	1	1	3	3	VAL	N	N	15	124.899	0.001	.	1	.	.	.	.
2	VAL	N	.	.	.	.	.	.	.	.	26578	1	.	.	.	.	.
3	.	1	1	4	4	GLU	H	H	1	8.041	0.001	.	1	.	.	.	.
4	GLU	H	.	.	.	.	.	.	.	.	26578	1	.	.	.	.	.
4	.	1	1	4	4	GLU	N	N	15	120.426	0.001	.	1	.	.	.	.
4	GLU	N	.	.	.	.	.	.	.	.	26578	1	.	.	.	.	.
5	.	1	1	5	5	LYS	H	H	1	8.037	0.001	.	1	.	.	.	.
5	LYS	H	.	.	.	.	.	.	.	.	26578	1	.	.	.	.	.
6	.	1	1	5	5	LYS	N	N	15	121.250	0.001	.	1	.	.	.	.
5	LYS	N	.	.	.	.	.	.	.	.	26578	1	.	.	.	.	.
7	.	1	1	6	6	GLY	H	H	1	8.586	0.001	.	1	.	.	.	.
6	GLY	H	.	.	.	.	.	.	.	.	26578	1	.	.	.	.	.
8	.	1	1	6	6	GLY	N	N	15	107.020	0.001	.	1	.	.	.	.
6	GLY	N	.	.	.	.	.	.	.	.	26578	1	.	.	.	.	.
9	.	1	1	7	7	LYS	H	H	1	7.962	0.001	.	1	.	.	.	.
7	LYS	H	.	.	.	.	.	.	.	.	26578	1	.	.	.	.	.
10	.	1	1	7	7	LYS	N	N	15	124.147	0.001	.	1	.	.	.	.
7	LYS	N	.	.	.	.	.	.	.	.	26578	1	.	.	.	.	.
11	.	1	1	8	8	LYS	H	H	1	6.921	0.001	.	1	.	.	.	.
8	LYS	H	.	.	.	.	.	.	.	.	26578	1	.	.	.	.	.
12	.	1	1	8	8	LYS	N	N	15	117.319	0.001	.	1	.	.	.	.
8	LYS	N	.	.	.	.	.	.	.	.	26578	1	.	.	.	.	.
13	.	1	1	9	9	ILE	H	H	1	7.553	0.001	.	1	.	.	.	.
9	ILE	H	.	.	.	.	.	.	.	.	26578	1	.	.	.	.	.
14	.	1	1	9	9	ILE	N	N	15	119.082	0.001	.	1	.	.	.	.
9	ILE	N	.	.	.	.	.	.	.	.	26578	1	.	.	.	.	.
15	.	1	1	10	10	PHE	H	H	1	8.420	0.001	.	1	.	.	.	.
10	PHE	H	.	.	.	.	.	.	.	.	26578	1	.	.	.	.	.
16	.	1	1	10	10	PHE	N	N	15	120.609	0.001	.	1	.	.	.	.
10	PHE	N	.	.	.	.	.	.	.	.	26578	1	.	.	.	.	.
17	.	1	1	11	11	ILE	H	H	1	8.953	0.001	.	1	.	.	.	.
11	ILE	H	.	.	.	.	.	.	.	.	26578	1	.	.	.	.	.
18	.	1	1	11	11	ILE	N	N	15	121.849	0.001	.	1	.	.	.	.
11	ILE	N	.	.	.	.	.	.	.	.	26578	1	.	.	.	.	.
19	.	1	1	12	12	MET	H	H	1	7.996	0.001	.	1	.	.	.	.
12	MET	H	.	.	.	.	.	.	.	.	26578	1	.	.	.	.	.
20	.	1	1	12	12	MET	N	N	15	117.403	0.001	.	1	.	.	.	.
12	MET	N	.	.	.	.	.	.	.	.	26578	1	.	.	.	.	.
21	.	1	1	13	13	LYS	H	H	1	8.546	0.001	.	1	.	.	.	.
13	LYS	H	.	.	.	.	.	.	.	.	26578	1	.	.	.	.	.
22	.	1	1	13	13	LYS	N	N	15	112.645	0.001	.	1	.	.	.	.
13	LYS	N	.	.	.	.	.	.	.	.	26578	1	.	.	.	.	.
23	.	1	1	14	14	CYS	H	H	1	7.904	0.001	.	1	.	.	.	.
14	CYS	H	.	.	.	.	.	.	.	.	26578	1	.	.	.	.	.

14	24	CYS	N	1	1	14	14	CYS	N	N	15	114.418	0.001	26578	1	1			
	25	SER	H	1	1	15	15	SER	H	H	1	8.041	0.001	26578	1	1			
15	26	SER	N	1	1	15	15	SER	N	N	15	116.401	0.001	26578	1	1			
	27	GLN	H	1	1	16	16	GLN	H	H	1	9.994	0.001	26578	1	1			
16	28	GLN	HE21	1	1	16	16	GLN	HE21	H	1	6.783	0.001	26578	1	1			
	29	GLN	HE22	1	1	16	16	GLN	HE22	H	1	7.477	0.001	26578	1	1			
16	30	GLN	N	1	1	16	16	GLN	N	N	15	122.814	0.001	26578	1	1			
	31	GLN	NE2	1	1	16	16	GLN	NE2	N	15	111.320	0.002	26578	1	1			
16	32	CYS	H	1	1	17	17	CYS	H	H	1	9.397	0.001	26578	1	1			
17	33	CYS	N	1	1	17	17	CYS	N	N	15	113.534	0.001	26578	1	1			
	34	HIS	H	1	1	18	18	HIS	H	H	1	10.728	0.001	26578	1	1			
18	35	HIS	N	1	1	18	18	HIS	N	N	15	118.287	0.001	26578	1	1			
	36	THR	H	1	1	19	19	THR	H	H	1	10.450	0.001	26578	1	1			
19	37	THR	N	1	1	19	19	THR	N	N	15	113.616	0.001	26578	1	1			
	38	VAL	H	1	1	20	20	VAL	H	H	1	8.880	0.001	26578	1	1			
20	39	VAL	N	1	1	20	20	VAL	N	N	15	112.013	0.001	26578	1	1			
	40	LYS	H	1	1	22	22	LYS	H	H	1	9.031	0.001	26578	1	1			
22	41	LYS	N	1	1	22	22	LYS	N	N	15	126.771	0.001	26578	1	1			
	42	GLY	H	1	1	23	23	GLY	H	H	1	9.318	0.001	26578	1	1			
23	43	GLY	N	1	1	23	23	GLY	N	N	15	117.787	0.001	26578	1	1			
	44	GLY	H	1	1	24	24	GLY	H	H	1	8.224	0.001	26578	1	1			
24	45	GLY	N	1	1	24	24	GLY	N	N	15	107.900	0.001	26578	1	1			
	46	LYS	H	1	1	25	25	LYS	H	H	1	8.801	0.001	26578	1	1			
25	47	LYS	N	1	1	25	25	LYS	N	N	15	118.895	0.001	26578	1	1			
	48	HIS	H	1	1	26	26	HIS	H	H	1	8.779	0.001	26578	1	1			
26	49	HIS	N	1	1	26	26	HIS	N	N	15	122.060	0.001	26578	1	1			
	50	LYS	H	1	1	27	27	LYS	H	H	1	8.099	0.001	26578	1	1			
27	51	LYS	N	1	1	27	27	LYS	N	N	15	126.145	0.001	26578	1	1			
	52	GLY	H	1	1	29	29	GLY	H	H	1	7.193	0.001	26578	1	1			
29	53	GLY	N	1	1	29	29	GLY	N	N	15	103.736	0.001	26578	1	1			
	54	ASN	H	1	1	31	31	ASN	H	H	1	11.645	0.001	26578	1	1			
31	55	ASN	HD21	1	1	31	31	ASN	HD21	H	1	8.078	0.001	26578	1	1			
	56	ASN	HD22	1	1	31	31	ASN	HD22	H	1	8.898	0.001	26578	1	1			
31	57	ASN	N	1	1	31	31	ASN	N	N	15	127.501	0.001	26578	1	1			
	58	ASN	ND2	1	1	31	31	ASN	ND2	N	15	115.345	0.003	26578	1	1			
31	59	LEU	H	1	1	32	32	LEU	H	H	1	9.502	0.001	26578	1	1			
	60	LEU	N	1	1	32	32	LEU	N	N	15	122.148	0.001	26578	1	1			
32	61	HIS	H	1	1	33	33	HIS	H	H	1	8.119	0.001	26578	1	1			
	62	HIS	N	1	1	33	33	HIS	N	N	15	120.266	0.001	26578	1	1			
33	63	GLY	H	1	1	34	34	GLY	H	H	1	8.959	0.001	26578	1	1			
	64	GLY	N	1	1	34	34	GLY	N	N	15	115.097	0.001	26578	1	1			



54	106	ASN	HD21	1	1	54	54	ASN	HD21	H	1	6.897	0.001	26578	1	1			
	107	ASN	HD22	1	1	54	54	ASN	HD22	H	1	7.427	0.001	26578	1	1			
54	108	ASN	HD22	1	1	54	54	ASN	N	N	15	113.081	0.001	26578	1	1			
54	109	ASN	N	1	1	54	54	ASN	ND2	N	15	112.161	0.001	26578	1	1			
54	110	ASN	ND2	1	1	55	55	LYS	H	H	1	6.987	0.001	26578	1	1			
55	111	LYS	H	1	1	55	55	LYS	N	N	15	121.530	0.001	26578	1	1			
55	112	LYS	N	1	1	56	56	GLY	H	H	1	7.752	0.001	26578	1	1			
56	113	GLY	H	1	1	56	56	GLY	N	N	15	103.167	0.001	26578	1	1			
56	114	GLY	N	1	1	57	57	ILE	H	H	1	6.463	0.001	26578	1	1			
57	115	ILE	H	1	1	57	57	ILE	N	N	15	110.660	0.001	26578	1	1			
57	116	ILE	N	1	1	58	58	ILE	H	H	1	8.164	0.001	26578	1	1			
58	117	ILE	H	1	1	58	58	ILE	N	N	15	119.269	0.001	26578	1	1			
58	118	ILE	N	1	1	59	59	TRP	H	H	1	8.643	0.001	26578	1	1			
59	119	TRP	H	1	1	59	59	TRP	HE1	H	1	9.497	0.001	26578	1	1			
59	120	TRP	HE1	1	1	59	59	TRP	N	N	15	130.596	0.001	26578	1	1			
59	121	TRP	N	1	1	59	59	TRP	NE1	N	15	125.473	0.001	26578	1	1			
59	122	TRP	NE1	1	1	60	60	GLY	H	H	1	7.682	0.001	26578	1	1			
60	123	GLY	H	1	1	60	60	GLY	N	N	15	111.288	0.001	26578	1	1			
60	124	GLY	N	1	1	61	61	GLU	H	H	1	9.540	0.001	26578	1	1			
61	125	GLU	H	1	1	61	61	GLU	N	N	15	120.579	0.001	26578	1	1			
61	126	GLU	N	1	1	62	62	ASP	H	H	1	8.335	0.001	26578	1	1			
62	127	ASP	H	1	1	62	62	ASP	N	N	15	115.286	0.001	26578	1	1			
62	128	ASP	N	1	1	63	63	THR	H	H	1	8.227	0.001	26578	1	1			
63	129	THR	H	1	1	63	63	THR	N	N	15	113.073	0.001	26578	1	1			
63	130	THR	N	1	1	64	64	LEU	H	H	1	8.513	0.001	26578	1	1			
64	131	LEU	H	1	1	64	64	LEU	N	N	15	120.582	0.001	26578	1	1			
64	132	LEU	N	1	1	65	65	MET	H	H	1	7.668	0.001	26578	1	1			
65	133	MET	H	1	1	65	65	MET	N	N	15	118.953	0.001	26578	1	1			
65	134	MET	N	1	1	66	66	GLU	H	H	1	6.796	0.001	26578	1	1			
66	135	GLU	H	1	1	66	66	GLU	N	N	15	117.722	0.001	26578	1	1			
66	136	GLU	N	1	1	67	67	TYR	H	H	1	8.099	0.001	26578	1	1			
67	137	TYR	H	1	1	67	67	TYR	N	N	15	121.308	0.001	26578	1	1			
67	138	TYR	N	1	1	68	68	LEU	H	H	1	8.007	0.001	26578	1	1			
68	139	LEU	H	1	1	68	68	LEU	N	N	15	110.992	0.001	26578	1	1			
68	140	LEU	N	1	1	69	69	GLU	H	H	1	6.747	0.001	26578	1	1			
69	141	GLU	H	1	1	69	69	GLU	N	N	15	118.836	0.001	26578	1	1			
69	142	GLU	N	1	1	70	70	ASN	H	H	1	6.638	0.001	26578	1	1			
70	143	ASN	H	1	1	70	70	ASN	HD21	H	1	6.904	0.001	26578	1	1			
70	144	ASN	HD21	1	1	70	70	ASN	HD22	H	1	7.881	0.001	26578	1	1			
70	145	ASN	HD22	1	1	70	70	ASN	N	N	15	105.368	0.001	26578	1	1			
70	146	ASN	N	1	1	70	70	ASN	ND2	N	15	112.340	0.001	26578	1	1			
70	146	ASN	ND2	1	1	70	70	ASN	ND2	N	15	112.340	0.001	26578	1	1			

147	.	1	1	72	72	LYS	H	H	1	9.327	0.001	.	1	.	.	.	.
72	LYS	H	.	.	.	.	.	.	.	.	.	26578	1	.	.	.	.
148	.	1	1	72	72	LYS	N	N	15	115.751	0.001	.	1	.	.	.	.
72	LYS	N	.	.	.	.	.	.	.	.	.	26578	1	.	.	.	.
149	.	1	1	73	73	LYS	H	H	1	7.773	0.001	.	1	.	.	.	.
73	LYS	H	.	.	.	.	.	.	.	.	.	26578	1	.	.	.	.
150	.	1	1	73	73	LYS	N	N	15	119.376	0.001	.	1	.	.	.	.
73	LYS	N	.	.	.	.	.	.	.	.	.	26578	1	.	.	.	.
151	.	1	1	74	74	TYR	H	H	1	8.089	0.001	.	1	.	.	.	.
74	TYR	H	.	.	.	.	.	.	.	.	.	26578	1	.	.	.	.
152	.	1	1	74	74	TYR	N	N	15	120.499	0.001	.	1	.	.	.	.
74	TYR	N	.	.	.	.	.	.	.	.	.	26578	1	.	.	.	.
153	.	1	1	75	75	ILE	H	H	1	9.377	0.001	.	1	.	.	.	.
75	ILE	H	.	.	.	.	.	.	.	.	.	26578	1	.	.	.	.
154	.	1	1	75	75	ILE	N	N	15	114.999	0.001	.	1	.	.	.	.
75	ILE	N	.	.	.	.	.	.	.	.	.	26578	1	.	.	.	.
155	.	1	1	77	77	GLY	H	H	1	9.140	0.001	.	1	.	.	.	.
77	GLY	H	.	.	.	.	.	.	.	.	.	26578	1	.	.	.	.
156	.	1	1	77	77	GLY	N	N	15	112.120	0.001	.	1	.	.	.	.
77	GLY	N	.	.	.	.	.	.	.	.	.	26578	1	.	.	.	.
157	.	1	1	78	78	THR	H	H	1	9.001	0.001	.	1	.	.	.	.
78	THR	H	.	.	.	.	.	.	.	.	.	26578	1	.	.	.	.
158	.	1	1	78	78	THR	N	N	15	115.318	0.001	.	1	.	.	.	.
78	THR	N	.	.	.	.	.	.	.	.	.	26578	1	.	.	.	.
159	.	1	1	79	79	LYS	H	H	1	8.233	0.001	.	1	.	.	.	.
79	LYS	H	.	.	.	.	.	.	.	.	.	26578	1	.	.	.	.
160	.	1	1	79	79	LYS	N	N	15	123.039	0.001	.	1	.	.	.	.
79	LYS	N	.	.	.	.	.	.	.	.	.	26578	1	.	.	.	.
161	.	1	1	80	80	MET	H	H	1	9.174	0.001	.	1	.	.	.	.
80	MET	H	.	.	.	.	.	.	.	.	.	26578	1	.	.	.	.
162	.	1	1	80	80	MET	N	N	15	123.254	0.001	.	1	.	.	.	.
80	MET	N	.	.	.	.	.	.	.	.	.	26578	1	.	.	.	.
163	.	1	1	81	81	ILE	H	H	1	8.440	0.001	.	1	.	.	.	.
81	ILE	H	.	.	.	.	.	.	.	.	.	26578	1	.	.	.	.
164	.	1	1	81	81	ILE	N	N	15	135.513	0.001	.	1	.	.	.	.
81	ILE	N	.	.	.	.	.	.	.	.	.	26578	1	.	.	.	.
165	.	1	1	82	82	PHE	H	H	1	9.031	0.001	.	1	.	.	.	.
82	PHE	H	.	.	.	.	.	.	.	.	.	26578	1	.	.	.	.
166	.	1	1	82	82	PHE	N	N	15	126.565	0.001	.	1	.	.	.	.
82	PHE	N	.	.	.	.	.	.	.	.	.	26578	1	.	.	.	.
167	.	1	1	83	83	VAL	H	H	1	8.003	0.001	.	1	.	.	.	.
83	VAL	H	.	.	.	.	.	.	.	.	.	26578	1	.	.	.	.
168	.	1	1	83	83	VAL	N	N	15	127.001	0.001	.	1	.	.	.	.
83	VAL	N	.	.	.	.	.	.	.	.	.	26578	1	.	.	.	.
169	.	1	1	85	85	ILE	H	H	1	7.870	0.001	.	1	.	.	.	.
85	ILE	H	.	.	.	.	.	.	.	.	.	26578	1	.	.	.	.
170	.	1	1	85	85	ILE	N	N	15	120.180	0.001	.	1	.	.	.	.
85	ILE	N	.	.	.	.	.	.	.	.	.	26578	1	.	.	.	.
171	.	1	1	86	86	LYS	H	H	1	8.232	0.001	.	1	.	.	.	.
86	LYS	H	.	.	.	.	.	.	.	.	.	26578	1	.	.	.	.
172	.	1	1	86	86	LYS	N	N	15	127.669	0.001	.	1	.	.	.	.
86	LYS	N	.	.	.	.	.	.	.	.	.	26578	1	.	.	.	.
173	.	1	1	87	87	LYS	H	H	1	8.188	0.001	.	1	.	.	.	.
87	LYS	H	.	.	.	.	.	.	.	.	.	26578	1	.	.	.	.
174	.	1	1	87	87	LYS	N	N	15	120.154	0.001	.	1	.	.	.	.
87	LYS	N	.	.	.	.	.	.	.	.	.	26578	1	.	.	.	.
175	.	1	1	88	88	LYS	H	H	1	8.734	0.001	.	1	.	.	.	.
88	LYS	H	.	.	.	.	.	.	.	.	.	26578	1	.	.	.	.
176	.	1	1	88	88	LYS	N	N	15	129.999	0.001	.	1	.	.	.	.
88	LYS	N	.	.	.	.	.	.	.	.	.	26578	1	.	.	.	.
177	.	1	1	89	89	GLU	H	H	1	9.281	0.001	.	1	.	.	.	.
89	GLU	H	.	.	.	.	.	.	.	.	.	26578	1	.	.	.	.
178	.	1	1	89	89	GLU	N	N	15	117.939	0.001	.	1	.	.	.	.
89	GLU	N	.	.	.	.	.	.	.	.	.	26578	1	.	.	.	.
179	.	1	1	90	90	GLU	H	H	1	6.175	0.001	.	1	.	.	.	.
90	GLU	H	.	.	.	.	.	.	.	.	.	26578	1	.	.	.	.
180	.	1	1	90	90	GLU	N	N	15	116.411	0.001	.	1	.	.	.	.
90	GLU	N	.	.	.	.	.	.	.	.	.	26578	1	.	.	.	.
181	.	1	1	91	91	ARG	H	H	1	7.136	0.001	.	1	.	.	.	.
91	ARG	H	.	.	.	.	.	.	.	.	.	26578	1	.	.	.	.
182	.	1	1	91	91	ARG	N	N	15	117.033	0.001	.	1	.	.	.	.
91	ARG	N	.	.	.	.	.	.	.	.	.	26578	1	.	.	.	.
183	.	1	1	92	92	ALA	H	H	1	8.350	0.001	.	1	.	.	.	.
92	ALA	H	.	.	.	.	.	.	.	.	.	26578	1	.	.	.	.
184	.	1	1	92	92	ALA	N	N	15	119.991	0.001	.	1	.	.	.	.
92	ALA	N	.	.	.	.	.	.	.	.	.	26578	1	.	.	.	.
185	.	1	1	93	93	ASP	H	H	1	8.034	0.001	.	1	.	.	.	.
93	ASP	H	.	.	.	.	.	.	.	.	.	26578	1	.	.	.	.
186	.	1	1	93	93	ASP	N	N	15	122.088	0.001	.	1	.	.	.	.
93	ASP	N	.	.	.	.	.	.	.	.	.	26578	1	.	.	.	.
187	.	1	1	94	94	LEU	H	H	1	7.783	0.001	.	1	.	.	.	.
94	LEU	H	.	.	.	.	.	.	.	.	.	26578	1	.	.	.	.

	188	.	1	1	94	94	LEU	N	N	15	120.831	0.001	.	1	.	.	.	.
.	94	LEU	N	.	.	.	.	.	.	.	.	26578	1	.	.	.	.	.
.	189	.	1	1	95	95	ILE	H	H	1	8.453	0.001	.	1	.	.	.	.
.	95	ILE	H	.	.	.	.	.	.	.	.	26578	1	.	.	.	.	.
.	190	.	1	1	95	95	ILE	N	N	15	119.688	0.001	.	1	.	.	.	.
.	95	ILE	N	.	.	.	.	.	.	.	.	26578	1	.	.	.	.	.
.	191	.	1	1	96	96	ALA	H	H	1	7.731	0.001	.	1	.	.	.	.
.	96	ALA	H	.	.	.	.	.	.	.	.	26578	1	.	.	.	.	.
.	192	.	1	1	96	96	ALA	N	N	15	122.619	0.001	.	1	.	.	.	.
.	96	ALA	N	.	.	.	.	.	.	.	.	26578	1	.	.	.	.	.
.	193	.	1	1	97	97	TYR	H	H	1	7.869	0.001	.	1	.	.	.	.
.	97	TYR	H	.	.	.	.	.	.	.	.	26578	1	.	.	.	.	.
.	194	.	1	1	97	97	TYR	N	N	15	117.863	0.001	.	1	.	.	.	.
.	97	TYR	N	.	.	.	.	.	.	.	.	26578	1	.	.	.	.	.
.	195	.	1	1	98	98	LEU	H	H	1	8.706	0.001	.	1	.	.	.	.
.	98	LEU	H	.	.	.	.	.	.	.	.	26578	1	.	.	.	.	.
.	196	.	1	1	98	98	LEU	N	N	15	118.879	0.001	.	1	.	.	.	.
.	98	LEU	N	.	.	.	.	.	.	.	.	26578	1	.	.	.	.	.
.	197	.	1	1	99	99	LYS	H	H	1	8.794	0.001	.	1	.	.	.	.
.	99	LYS	H	.	.	.	.	.	.	.	.	26578	1	.	.	.	.	.
.	198	.	1	1	99	99	LYS	N	N	15	123.829	0.001	.	1	.	.	.	.
.	99	LYS	N	.	.	.	.	.	.	.	.	26578	1	.	.	.	.	.
.	199	.	1	1	100	100	LYS	H	H	1	6.696	0.001	.	1	.	.	.	.
.	100	LYS	H	.	.	.	.	.	.	.	.	26578	1	.	.	.	.	.
.	200	.	1	1	100	100	LYS	N	N	15	116.963	0.001	.	1	.	.	.	.
.	100	LYS	N	.	.	.	.	.	.	.	.	26578	1	.	.	.	.	.
.	201	.	1	1	101	101	ALA	H	H	1	8.594	0.001	.	1	.	.	.	.
.	101	ALA	H	.	.	.	.	.	.	.	.	26578	1	.	.	.	.	.
.	202	.	1	1	101	101	ALA	N	N	15	119.590	0.001	.	1	.	.	.	.
.	101	ALA	N	.	.	.	.	.	.	.	.	26578	1	.	.	.	.	.
.	203	.	1	1	102	102	THR	H	H	1	7.882	0.001	.	1	.	.	.	.
.	102	THR	H	.	.	.	.	.	.	.	.	26578	1	.	.	.	.	.
.	204	.	1	1	102	102	THR	N	N	15	102.092	0.001	.	1	.	.	.	.
.	102	THR	N	.	.	.	.	.	.	.	.	26578	1	.	.	.	.	.
.	205	.	1	1	103	103	ASN	H	H	1	7.087	0.001	.	1	.	.	.	.
.	103	ASN	H	.	.	.	.	.	.	.	.	26578	1	.	.	.	.	.
.	206	.	1	1	103	103	ASN	HD21	H	1	6.364	0.001	.	1	.	.	.	.
.	103	ASN	HD21	.	.	.	.	.	.	.	.	26578	1	.	.	.	.	.
.	207	.	1	1	103	103	ASN	HD22	H	1	7.852	0.001	.	1	.	.	.	.
.	103	ASN	HD22	.	.	.	.	.	.	.	.	26578	1	.	.	.	.	.
.	208	.	1	1	103	103	ASN	N	N	15	118.492	0.001	.	1	.	.	.	.
.	103	ASN	N	.	.	.	.	.	.	.	.	26578	1	.	.	.	.	.
.	209	.	1	1	103	103	ASN	ND2	N	15	114.131	0.001	.	1	.	.	.	.
.	103	ASN	ND2	.	.	.	.	.	.	.	.	26578	1	.	.	.	.	.
.	210	.	1	1	104	104	GLU	H	H	1	7.372	0.001	.	1	.	.	.	.
.	104	GLU	H	.	.	.	.	.	.	.	.	26578	1	.	.	.	.	.
.	211	.	1	1	104	104	GLU	N	N	15	125.094	0.001	.	1	.	.	.	.
.	104	GLU	N	.	.	.	.	.	.	.	.	26578	1	.	.	.	.	.
.	stop_	.	.	.	.	.	.	.	.	.	.	.	.	.	.	.	.	.

save\_

## Dataset

3. **Moreno-Beltrán, B** *et al.* (2015). NMR Assignment of the Y48pCMF variant of *Homo sapiens* cytochrome *c* in its reduced state. BMRB and PDB entries (in preparation).





```

loop_
  _Atom_chem_shift.ID
  _Atom_chem_shift.Val
  _Atom_chem_shift.Val_err
  _Atom_chem_shift.Atom_ID
  _Atom_chem_shift.Comp_index_ID
  _Atom_chem_shift.Comp_ID

```

269	7.810	0.004	H	102	THR
270	101.974	0.000	N	102	THR
273	8.709	0.002	H	6	GLY
274	107.193	0.000	N	6	GLY
277	46.479	0.000	CA	6	GLY
279	174.012	0.000	C	6	GLY
280	8.563	0.001	H	77	GLY
281	108.831	0.000	N	77	GLY
284	44.314	0.000	CA	77	GLY
286	174.866	0.000	C	77	GLY
287	7.548	0.002	H	29	GLY
288	106.150	0.000	N	29	GLY
289	7.730	0.000	H	24	GLY
290	107.042	0.000	N	24	GLY
291	9.462	0.009	H	89	GLU
292	117.925	0.000	N	89	GLU
295	28.814	0.000	CB	89	GLU
298	7.856	0.003	H	81	ILE
299	130.146	0.000	N	81	ILE
302	59.285	0.030	CA	81	ILE
303	34.612	0.000	CB	81	ILE
305	173.220	0.000	C	81	ILE
306	9.040	0.007	H	41	GLY
307	111.811	0.000	N	41	GLY
310	46.409	0.000	CA	41	GLY
312	174.720	0.000	C	41	GLY
313	7.739	0.003	H	83	VAL
314	125.079	0.000	N	83	VAL
317	64.273	0.000	CA	83	VAL
318	31.352	0.000	CB	83	VAL
320	8.545	0.002	H	26	HIS
321	122.465	0.000	N	26	HIS
324	30.173	0.000	CB	26	HIS
326	175.081	0.000	C	26	HIS
327	9.619	0.003	H	61	GLU
328	120.606	0.000	N	61	GLU
330	62.088	0.000	CA	61	GLU
331	29.364	0.000	CB	61	GLU
333	177.011	0.000	C	61	GLU
334	6.092	0.005	H	70	ASN
335	105.553	0.000	N	70	ASN
338	51.365	0.000	CA	70	ASN
339	36.797	0.000	CB	70	ASN
341	172.247	0.000	C	70	ASN
342	8.945	0.001	H	99	LYS
343	123.889	0.000	N	99	LYS
346	31.869	0.000	CB	99	LYS
347	59.190	0.000	CA	99	LYS
349	176.653	0.000	C	99	LYS
350	8.569	0.000	H	3	VAL
351	123.739	0.000	N	3	VAL
354	31.965	0.000	CB	3	VAL
355	65.946	0.000	CA	3	VAL
357	177.302	0.000	C	3	VAL
358	8.147	0.002	H	39	LYS
359	123.290	0.000	N	39	LYS
362	33.682	0.000	CB	39	LYS
363	55.199	0.000	CA	39	LYS
365	172.219	0.000	C	39	LYS
366	8.039	0.004	H	7	LYS
367	124.124	0.005	N	7	LYS
369	59.052	0.000	CA	7	LYS
370	32.105	0.000	CB	7	LYS
372	177.457	0.000	C	7	LYS
373	8.215	0.001	H	38	ARG
374	124.035	0.000	N	38	ARG
376	55.764	0.000	CA	38	ARG
377	32.411	0.000	CB	38	ARG
379	174.415	0.000	C	38	ARG
380	7.974	0.002	H	96	ALA
381	123.001	0.000	N	96	ALA
382	54.933	0.000	CA	96	ALA
383	16.970	0.000	CB	96	ALA
387	180.700	0.000	C	96	ALA
388	8.063	0.002	H	43	ALA

389	125.825	0.000	N	43	ALA
392	49.991	0.000	CA	43	ALA
393	18.488	0.000	CB	43	ALA
395	175.308	0.000	C	43	ALA
396	7.439	0.002	H	27	LYS
397	126.571	0.000	N	27	LYS
401	175.781	0.000	C	27	LYS
402	55.066	0.000	CA	27	LYS
403	30.731	0.000	CB	27	LYS
404	8.717	0.003	H	22	LYS
405	126.123	0.000	N	22	LYS
408	57.749	0.000	CA	22	LYS
409	30.941	0.000	CB	22	LYS
411	8.518	0.001	H	86	LYS
412	127.466	0.000	N	86	LYS
415	32.343	0.000	CB	86	LYS
416	58.619	0.000	CA	86	LYS
418	178.442	0.000	C	86	LYS
419	8.507	0.000	H	50	ALA
420	125.381	0.000	N	50	ALA
421	6.529	0.006	H	82	PHE
422	123.143	0.000	N	82	PHE
425	56.578	0.004	CA	82	PHE
426	40.644	0.000	CB	82	PHE
428	174.333	0.000	C	82	PHE
429	9.541	0.000	H	2	ASP
430	124.691	0.000	N	2	ASP
434	175.662	0.000	C	2	ASP
435	52.772	0.000	CA	2	ASP
436	7.157	0.008	H	104	GLU
437	124.633	0.000	N	104	GLU
440	57.673	0.000	CA	104	GLU
441	30.937	0.000	CB	104	GLU
443	180.562	0.000	C	104	GLU
444	7.384	0.001	H	80	MET
445	123.515	0.000	N	80	MET
448	27.552	0.000	CB	80	MET
449	55.863	0.000	CA	80	MET
451	171.833	0.000	C	80	MET
454	8.982	0.002	H	98	LEU
455	119.118	0.000	N	98	LEU
458	57.650	0.000	CA	98	LEU
459	41.645	0.000	CB	98	LEU
461	179.188	0.000	C	98	LEU
462	8.974	0.001	H	95	ILE
463	120.159	0.000	N	95	ILE
466	66.222	0.000	CA	95	ILE
467	37.668	0.000	CB	95	ILE
469	176.351	0.000	C	95	ILE
470	8.668	0.001	H	92	ALA
471	120.161	0.000	N	92	ALA
474	55.281	0.000	CA	92	ALA
475	17.539	0.000	CB	92	ALA
477	181.044	0.000	C	92	ALA
478	8.879	0.004	H	16	GLN
479	120.608	0.000	N	16	GLN
482	57.938	0.000	CA	16	GLN
483	27.900	0.000	CB	16	GLN
485	176.559	0.000	C	16	GLN
486	8.834	0.002	H	11	ILE
487	121.053	0.002	N	11	ILE
490	65.622	0.000	CA	11	ILE
491	37.617	0.000	CB	11	ILE
493	178.867	0.000	C	11	ILE
494	8.809	0.005	H	64	LEU
495	121.355	0.000	N	64	LEU
499	42.355	0.000	CB	64	LEU
500	58.314	0.000	CA	64	LEU
502	178.628	0.000	C	64	LEU
503	7.889	0.002	H	32	LEU
504	121.653	0.000	N	32	LEU
507	53.287	0.000	CA	32	LEU
508	42.520	0.000	CB	32	LEU
510	174.533	0.000	C	32	LEU
511	8.635	0.001	H	10	PHE
512	120.908	0.000	N	10	PHE
515	62.164	0.000	CA	10	PHE
516	39.377	0.000	CB	10	PHE
518	178.820	0.000	C	10	PHE
519	8.539	0.002	H	101	ALA
520	119.416	0.000	N	101	ALA
523	54.401	0.000	CA	101	ALA
524	18.353	0.000	CB	101	ALA

526	179.576	0.000	C	101	ALA
527	8.368	0.000	H	87	LYS
528	120.309	0.000	N	87	LYS
531	56.865	0.000	CA	87	LYS
532	32.531	0.000	CB	87	LYS
534	177.569	0.000	C	87	LYS
535	8.327	0.001	H	85	ILE
536	120.758	0.000	N	85	ILE
538	59.390	0.000	CA	85	ILE
539	39.528	0.000	CB	85	ILE
541	175.103	0.000	C	85	ILE
542	8.153	0.001	H	93	ASP
543	122.101	0.000	N	93	ASP
546	39.552	0.000	CB	93	ASP
547	58.147	0.000	CA	93	ASP
549	177.634	0.000	C	93	ASP
550	8.083	0.003	H	4	GLU
551	120.310	0.000	N	4	GLU
554	58.963	0.000	CA	4	GLU
555	28.479	0.000	CB	4	GLU
557	180.515	0.000	C	4	GLU
558	7.988	0.002	H	58	ILE
559	121.053	0.000	N	58	ILE
562	8.931	0.000	H	59	TRP
563	130.896	0.006	N	59	TRP
566	57.229	0.000	CA	59	TRP
567	29.908	0.000	CB	59	TRP
569	175.793	0.000	C	59	TRP
570	7.634	0.001	H	55	LYS
571	121.354	0.000	N	55	LYS
574	56.818	0.000	CA	55	LYS
575	31.536	0.000	CB	55	LYS
577	177.422	0.000	C	55	LYS
578	7.445	0.002	H	33	HIS
579	119.860	0.000	N	33	HIS
582	60.491	0.000	CA	33	HIS
583	28.223	0.000	CB	33	HIS
585	176.992	0.000	C	33	HIS
586	7.661	0.001	H	46	TYR
587	120.307	0.000	N	46	TYR
589	57.515	0.000	CA	46	TYR
590	39.539	0.000	CB	46	TYR
592	174.910	0.000	C	46	TYR
593	7.681	0.003	H	9	ILE
594	119.269	0.000	N	9	ILE
597	65.105	0.000	CA	9	ILE
598	37.562	0.000	CB	9	ILE
600	177.006	0.000	C	9	ILE
601	8.152	0.001	H	53	LYS
602	120.164	0.000	N	53	LYS
603	8.096	0.002	H	5	LYS
604	121.058	0.000	N	5	LYS
607	32.454	0.000	CB	5	LYS
608	59.459	0.000	CA	5	LYS
610	180.515	0.000	C	5	LYS
611	8.183	0.001	H	94	LEU
612	121.208	0.000	N	94	LEU
615	41.711	0.000	CB	94	LEU
616	58.295	0.000	CA	94	LEU
618	178.395	0.000	C	94	LEU
619	8.170	0.000	H	67	TYR
620	120.608	0.000	N	67	TYR
623	40.118	0.000	CB	67	TYR
624	59.911	0.000	CA	67	TYR
626	176.312	0.000	C	67	TYR
627	6.223	0.000	H	18	HIS
628	113.603	0.000	N	18	HIS
631	31.916	0.000	CB	18	HIS
632	53.514	0.000	CA	18	HIS
634	173.588	0.000	C	18	HIS
635	6.347	0.005	H	90	GLU
636	116.437	0.000	N	90	GLU
639	58.277	0.000	CA	90	GLU
640	29.990	0.000	CB	90	GLU
642	178.730	0.000	C	90	GLU
643	8.553	0.000	H	54	ASN
644	116.286	0.000	N	54	ASN
645	53.488	0.000	CA	54	ASN
646	38.101	0.000	CB	54	ASN
649	175.501	0.000	C	54	ASN
650	8.130	0.003	H	14	CYS
651	115.390	0.000	N	14	CYS
654	36.784	0.000	CB	14	CYS

655	54.119	0.000	CA	14	CYS
657	177.723	0.000	C	14	CYS
658	8.189	0.001	H	75	ILE
659	114.346	0.000	N	75	ILE
662	37.615	0.000	CB	75	ILE
663	58.474	0.000	CA	75	ILE
665	179.773	0.000	C	75	ILE
666	8.763	0.001	H	34	GLY
667	114.645	0.000	N	34	GLY
670	45.713	0.000	CA	34	GLY
672	174.473	0.000	C	34	GLY
673	8.396	0.001	H	62	ASP
674	114.943	0.000	N	62	ASP
677	57.208	0.000	CA	62	ASP
678	39.477	0.000	CB	62	ASP
680	179.228	0.000	C	62	ASP
681	8.694	0.000	H	36	PHE
682	113.600	0.000	N	36	PHE
685	36.223	0.000	CB	36	PHE
686	59.702	0.000	CA	36	PHE
688	176.553	0.000	C	36	PHE
689	9.016	0.004	H	13	LYS
690	113.452	0.000	N	13	LYS
693	57.260	0.000	CA	13	LYS
694	35.199	0.000	CB	13	LYS
696	177.353	0.000	C	13	LYS
697	8.839	0.001	H	37	GLY
698	112.857	0.000	N	37	GLY
701	44.455	0.000	CA	37	GLY
703	173.382	0.000	C	37	GLY
704	9.078	0.001	H	23	GLY
705	117.177	0.000	N	23	GLY
708	44.906	0.000	CA	23	GLY
710	174.531	0.000	C	23	GLY
711	8.246	0.002	H	63	THR
712	112.857	0.000	N	63	THR
715	68.918	0.000	CB	63	THR
716	63.601	0.000	CA	63	THR
718	177.971	0.000	C	63	THR
719	8.108	0.002	H	68	LEU
720	109.278	0.000	N	68	LEU
723	55.211	0.000	CA	68	LEU
724	41.188	0.000	CB	68	LEU
726	176.652	0.000	C	68	LEU
727	7.839	0.002	H	60	GLY
728	111.218	0.000	N	60	GLY
731	44.214	0.000	CA	60	GLY
733	171.636	0.000	C	60	GLY
734	7.636	0.002	H	19	THR
735	109.280	0.000	N	19	THR
738	58.557	0.000	CA	19	THR
739	71.176	0.000	CB	19	THR
741	174.026	0.000	C	19	THR
742	7.675	0.000	H	20	VAL
743	110.620	0.000	N	20	VAL
746	33.427	0.000	CB	20	VAL
747	60.794	0.000	CA	20	VAL
749	173.470	0.000	C	20	VAL
750	7.804	0.003	H	40	THR
751	113.158	0.000	N	40	THR
755	7.922	0.000	H	78	THR
756	115.541	0.000	N	78	THR
758	67.910	0.005	CB	78	THR
759	61.759	0.000	CA	78	THR
761	173.114	0.000	C	78	THR
762	8.286	0.001	H	52	ASN
763	117.178	0.000	N	52	ASN
766	55.769	0.000	CA	52	ASN
768	8.222	0.001	H	25	LYS
769	118.452	0.000	N	25	LYS
771	55.712	0.000	CA	25	LYS
772	32.861	0.000	CB	25	LYS
774	178.209	0.000	C	25	LYS
775	8.089	0.005	H	97	TYR
776	118.224	0.000	N	97	TYR
779	61.456	0.000	CA	97	TYR
780	36.943	0.000	CB	97	TYR
781	8.047	0.008	H	12	MET
782	117.328	0.000	N	12	MET
785	58.560	0.000	CA	12	MET
786	33.675	0.000	CB	12	MET
788	177.972	0.000	C	12	MET
789	8.084	0.000	H	42	GLN

790	117.180	0.000	N	42	GLN
792	54.615	0.000	CA	42	GLN
793	28.977	0.000	CB	42	GLN
795	175.152	0.000	C	42	GLN
796	7.934	0.002	H	65	MET
797	118.519	0.000	N	65	MET
800	57.910	0.000	CA	65	MET
801	31.019	0.000	CB	65	MET
803	177.782	0.000	C	65	MET
804	7.423	0.001	H	91	ARG
805	117.405	0.000	N	91	ARG
808	31.106	0.000	CB	91	ARG
809	61.182	0.000	CA	91	ARG
811	177.430	0.000	C	91	ARG
812	7.219	0.000	H	74	TYR
813	118.674	0.000	N	74	TYR
816	39.536	0.000	CB	74	TYR
817	60.721	0.000	CA	74	TYR
819	175.794	0.000	C	74	TYR
820	6.968	0.007	H	103	ASN
821	118.372	0.000	N	103	ASN
824	52.469	0.000	CA	103	ASN
825	41.376	0.000	CB	103	ASN
827	173.663	0.000	C	103	ASN
828	7.010	0.002	H	35	LEU
829	117.774	0.000	N	35	LEU
831	57.459	0.000	CA	35	LEU
832	43.808	0.000	CB	35	LEU
834	176.507	0.000	C	35	LEU
835	6.958	0.000	H	8	LYS
836	116.732	0.000	N	8	LYS
839	31.815	0.000	CB	8	LYS
840	59.322	0.000	CA	8	LYS
841	6.855	0.000	H	73	LYS
842	118.522	0.000	N	73	LYS
845	32.899	0.000	CB	73	LYS
846	57.407	0.000	CA	73	LYS
848	176.890	0.000	C	73	LYS
849	6.795	0.001	H	66	GLU
850	117.027	0.000	N	66	GLU
853	29.676	0.000	CB	66	GLU
854	58.103	0.000	CA	66	GLU
856	178.928	0.000	C	66	GLU
857	6.724	0.006	H	100	LYS
858	116.726	0.000	N	100	LYS
861	57.655	0.000	CA	100	LYS
862	33.175	0.000	CB	100	LYS
864	178.363	0.000	C	100	LYS
865	6.783	0.001	H	69	GLU
866	119.118	0.000	N	69	GLU
869	58.526	0.000	CA	69	GLU
870	29.549	0.000	CB	69	GLU
872	176.033	0.000	C	69	GLU
873	6.805	0.004	H	17	CYS
874	112.857	0.000	N	17	CYS
877	53.967	0.000	CA	17	CYS
878	38.172	0.000	CB	17	CYS
880	171.419	0.000	C	17	CYS
881	7.297	0.005	H	15	SER
882	114.347	0.000	N	15	SER
885	62.483	0.000	CB	15	SER
886	60.587	0.000	CA	15	SER
888	174.272	0.000	C	15	SER
889	7.457	0.001	H	72	LYS
890	113.454	0.000	N	72	LYS
893	57.046	0.000	CA	72	LYS
894	31.565	0.000	CB	72	LYS
896	177.234	0.000	C	72	LYS
897	9.151	0.004	H	88	LYS
898	129.999	0.000	N	88	LYS
901	60.314	0.000	CA	88	LYS
902	32.083	0.000	CB	88	LYS
904	177.664	0.000	C	88	LYS
905	69.403	0.000	CB	102	THR
906	61.954	0.000	CA	102	THR
908	172.872	0.000	C	102	THR
909	40.882	0.000	CA	29	GLY
913	169.328	0.000	C	29	GLY
915	44.146	0.000	CA	24	GLY
917	172.234	0.000	C	24	GLY
918	59.760	0.000	CA	89	GLU
919	177.911	0.000	C	89	GLU
920	174.444	0.000	C	83	VAL

921	55.813	0.000	CA	26	HIS
922	177.538	0.000	C	22	LYS
925	53.813	0.000	CA	50	ALA
926	17.942	0.000	CB	50	ALA
927	178.430	0.000	C	50	ALA
931	176.278	0.000	C	97	TYR
933	179.228	0.000	C	8	LYS
934	61.920	0.000	CA	40	THR
935	68.539	0.000	CB	40	THR
937	177.676	0.000	C	53	LYS
938	32.296	0.000	CB	53	LYS
939	58.402	0.000	CA	53	LYS
972	3.860	0.002	HA	69	GLU
973	1.920	0.001	HB2	69	GLU
974	36.287	0.000	CG	69	GLU
975	2.016	0.002	HG2	69	GLU
976	2.075	0.001	HG3	69	GLU
1179	3.795	0.000	HA	101	ALA
1180	4.767	0.000	HA	103	ASN
1181	4.157	0.001	HA	102	THR
1182	3.976	0.002	HA	100	LYS
1183	2.549	0.002	HA	99	LYS
1184	3.334	0.001	HA	98	LEU
1185	4.197	0.000	HA	97	TYR
1186	4.026	0.002	HA	96	ALA
1187	3.609	0.002	HA	95	ILE
1188	4.205	0.002	HA	94	LEU
1189	4.208	0.003	HA	93	ASP
1190	3.970	0.001	HA	92	ALA
1191	3.740	0.002	HA	91	ARG
1192	4.198	0.001	HA	90	GLU
1193	3.899	0.000	HA	89	GLU
1194	4.247	0.001	HA	87	LYS
1195	3.972	0.002	HA	86	LYS
1196	4.136	0.001	HA	85	ILE
1197	4.327	0.000	HA	82	PHE
1198	4.231	0.003	HA	74	TYR
1199	3.790	0.001	HA	73	LYS
1200	3.715	0.001	HA	72	LYS
1201	3.899	0.000	HA	5	LYS
1202	4.008	0.003	HA	4	GLU
1203	2.986	0.000	HA	68	LEU
1204	3.550	0.000	HA	3	VAL
1205	4.775	0.000	HA	2	ASP
1206	3.501	0.001	HA	67	TYR
1207	3.958	0.001	HA	66	GLU
1208	4.354	0.000	HA	42	GLN
1209	3.896	0.000	HA	65	MET
1210	4.233	0.004	HA	64	LEU
1211	4.847	0.001	HA	39	LYS
1212	4.449	0.000	HA	38	ARG
1213	4.116	0.001	HA	63	THR
1214	4.334	0.000	HA	62	ASP
1215	3.858	0.001	HA	61	GLU
1216	3.848	0.000	HA	36	PHE
1217	3.527	0.000	HA	35	LEU
1218	4.829	0.003	HA	59	TRP
1219	3.707	0.002	HA	33	HIS
1220	4.413	0.000	HA	19	THR
1221	3.867	0.005	HA	32	LEU
1222	3.622	0.000	HA	18	HIS
1223	4.084	0.000	HA	17	CYS
1224	4.192	0.000	HA	26	HIS
1225	3.909	0.000	HA	16	GLN
1226	3.833	0.002	HA	25	LYS
1227	5.296	0.000	HA	14	CYS
1228	3.052	0.000	HA	22	LYS
1229	4.935	0.001	HA	13	LYS
1230	3.485	0.001	HA	81	ILE
1231	4.219	0.001	HA	12	MET
1232	2.934	0.000	HA	80	MET
1233	3.973	0.000	HA	10	PHE
1234	3.719	0.000	HA	9	ILE
1235	4.389	0.000	HA	54	ASN
1236	3.815	0.000	HA	8	LYS
1237	2.714	0.002	HB2	103	ASN
1238	1.482	0.004	HB2	99	LYS
1239	2.216	0.001	HB2	98	LEU
1240	3.582	0.001	HB2	97	TYR
1241	2.250	0.002	HB2	94	LEU
1242	2.083	0.002	HB2	91	ARG
1243	2.022	0.000	HB2	82	PHE
1244	1.588	0.001	HB2	68	LEU

1245	2.735	0.000	HB2	2	ASP
1246	3.216	0.000	HB2	67	TYR
1247	2.181	0.000	HB2	42	GLN
1248	2.356	0.000	HB2	65	MET
1249	1.991	0.000	HB2	64	LEU
1250	3.185	0.000	HB2	36	PHE
1251	2.086	0.008	HB2	35	LEU
1252	3.739	0.005	HB2	59	TRP
1253	1.326	0.002	HB2	32	LEU
1254	0.996	0.000	HB2	18	HIS
1255	1.392	0.000	HB2	17	CYS
1256	2.194	0.000	HB2	16	GLN
1257	1.756	0.000	HB2	14	CYS
1258	1.206	0.000	HB2	22	LYS
1259	-0.261	0.000	HB2	80	MET
1260	29.202	0.000	CD	73	LYS
1261	1.461	0.000	QB	73	LYS
1263	41.769	0.000	CE	73	LYS
1264	24.651	0.000	CG	73	LYS
1265	1.642	0.002	HB3	100	LYS
1266	1.673	0.001	HB2	100	LYS
1267	41.733	0.000	CE	100	LYS
1270	4.095	0.003	HA3	6	GLY
1271	4.428	0.001	HA3	37	GLY
1272	4.110	0.001	HA3	60	GLY
1273	3.713	0.002	HA3	24	GLY
1274	3.740	0.001	HA3	23	GLY
1275	3.478	0.000	HA2	6	GLY
1276	3.432	0.001	HA2	37	GLY
1277	3.832	0.005	HA2	60	GLY
1278	3.054	0.003	HA2	24	GLY
1279	3.441	0.001	HA2	23	GLY
1280	0.460	0.003	QB	101	ALA
1282	1.314	0.002	QB	96	ALA
1283	2.604	0.002	QB	93	ASP
1284	1.426	0.002	QB	92	ALA
1286	1.920	0.002	QB	89	GLU
1288	1.699	0.001	QB	86	LYS
1289	1.852	0.000	QB	8	LYS
1291	1.706	0.005	QB	5	LYS
1296	2.084	0.000	QB	38	ARG
1298	2.113	0.003	QB	61	GLU
1306	2.685	0.000	QB	54	ASN
1307	4.625	0.000	HB	102	THR
1308	1.955	0.001	HB	95	ILE
1309	1.356	0.001	HB	85	ILE
1310	1.961	0.001	HB	81	ILE
1311	4.339	0.001	HB	63	THR
1312	4.356	0.000	HB	19	THR
1313	2.004	0.000	HB	9	ILE
1314	2.097	0.000	HB	3	VAL
1315	1.607	0.001	HB3	69	GLU
1316	2.387	0.002	HB3	103	ASN
1317	1.249	0.002	HB3	99	LYS
1318	1.264	0.002	HB3	98	LEU
1319	3.044	0.000	HB3	97	TYR
1320	1.746	0.002	HB3	94	LEU
1321	1.830	0.001	HB3	91	ARG
1322	0.423	0.000	HB3	82	PHE
1323	-2.814	0.000	HB3	80	MET
1324	0.983	0.005	HB3	68	LEU
1325	2.562	0.000	HB3	67	TYR
1326	2.031	0.000	HB3	65	MET
1327	1.156	0.000	HB3	64	LEU
1328	2.438	0.001	HB3	59	TRP
1329	0.660	0.003	HB3	18	HIS
1330	0.427	0.000	HB3	17	CYS
1331	1.939	0.000	HB3	16	GLN
1332	1.059	0.000	HB3	14	CYS
1333	2.370	0.000	HB3	2	ASP
1334	1.832	0.000	HB3	42	GLN
1335	2.770	0.000	HB3	36	PHE
1336	1.456	0.002	HB3	35	LEU
1337	0.997	0.002	HB3	32	LEU
1338	0.425	0.000	HB3	22	LYS
1342	42.313	0.000	CB	2	ASP
1344	3.728	0.001	HA	53	LYS
1347	24.108	0.000	CG	53	LYS
1348	29.089	0.000	CD	53	LYS
1349	41.778	0.000	CE	53	LYS
1351	21.342	0.000	CG2	19	THR
1352	0.989	0.002	QG2	19	THR
1353	21.945	0.000	CG2	102	THR

1354	0.896	0.002	QG2	102	THR
1355	2.705	0.000	HB2	62	ASP
1356	2.626	0.000	HB3	62	ASP
1357	21.577	0.000	CG2	3	VAL
1358	21.697	0.000	CG1	3	VAL
1359	0.988	0.000	QG1	3	VAL
1360	0.954	0.000	QG2	3	VAL
1361	36.428	0.000	CG	89	GLU
1363	37.068	0.000	CG	61	GLU
1364	2.376	0.003	HG2	61	GLU
1365	2.306	0.001	HG3	61	GLU
1366	2.320	0.001	HG2	89	GLU
1367	2.253	0.001	HG3	89	GLU
1368	35.918	0.000	CG	4	GLU
1369	2.053	0.001	HB2	4	GLU
1370	2.021	0.002	HB3	4	GLU
1371	2.231	0.001	HG2	4	GLU
1372	2.208	0.002	HG3	4	GLU
1373	36.943	0.000	CG	90	GLU
1374	1.999	0.002	HB2	90	GLU
1375	1.919	0.001	HB3	90	GLU
1376	35.887	0.000	CG	66	GLU
1377	1.874	0.002	HG2	66	GLU
1378	1.853	0.002	HG3	66	GLU
1379	1.590	0.001	HB2	66	GLU
1380	1.453	0.002	HB3	66	GLU
1381	26.036	0.041	CG1	81	ILE
1382	16.961	0.000	CG2	81	ILE
1383	10.665	0.000	CD1	81	ILE
1384	1.118	0.001	HG13	81	ILE
1385	1.348	0.005	HG12	81	ILE
1386	0.667	0.001	QG2	81	ILE
1387	0.618	0.001	QD1	81	ILE
1388	14.288	0.000	CD1	95	ILE
1389	17.883	0.000	CG2	95	ILE
1390	31.889	0.000	CG1	95	ILE
1391	1.884	0.001	HG12	95	ILE
1392	0.956	0.001	HG13	95	ILE
1393	1.115	0.001	QG2	95	ILE
1394	0.882	0.001	QD1	95	ILE
1395	26.889	0.000	CG1	85	ILE
1396	18.367	0.000	CG2	85	ILE
1397	14.053	0.000	CD1	85	ILE
1398	1.174	0.001	HG13	85	ILE
1399	1.616	0.001	HG12	85	ILE
1400	0.933	0.002	QG2	85	ILE
1401	0.892	0.001	QD1	85	ILE
1402	28.101	0.000	CG1	9	ILE
1403	18.364	0.000	CG2	9	ILE
1404	14.027	0.000	CD1	9	ILE
1405	1.152	0.004	HG13	9	ILE
1406	1.810	0.002	HG12	9	ILE
1407	1.064	0.002	QG2	9	ILE
1408	1.003	0.001	QD1	9	ILE
1409	2.969	0.000	HB2	26	HIS
1410	2.859	0.000	HB3	26	HIS
1411	2.822	0.001	HB2	33	HIS
1412	2.770	0.002	HB3	33	HIS
1413	24.548	0.000	CG	99	LYS
1414	29.179	0.000	CD	99	LYS
1415	41.722	0.000	CE	99	LYS
1416	0.712	0.001	HG2	99	LYS
1417	0.246	0.003	HG3	99	LYS
1418	1.180	0.002	HD3	99	LYS
1419	1.233	0.001	HD2	99	LYS
1420	2.631	0.002	QE	99	LYS
1421	41.608	0.000	CE	39	LYS
1422	25.303	0.000	CG	39	LYS
1423	29.200	0.000	CD	39	LYS
1424	1.670	0.000	HB2	39	LYS
1425	1.475	0.000	HB3	39	LYS
1426	1.503	0.000	QD	39	LYS
1427	1.322	0.001	QG	39	LYS
1428	2.799	0.002	QE	39	LYS
1429	26.072	0.000	CG	38	ARG
1430	45.037	0.000	CD	38	ARG
1431	3.169	0.000	HD2	38	ARG
1432	3.080	0.000	HD3	38	ARG
1433	2.143	0.000	HG2	38	ARG
1434	1.833	0.000	HG3	38	ARG
1435	41.566	0.000	CE	22	LYS
1436	28.870	0.000	CD	22	LYS
1437	24.010	0.000	CG	22	LYS



1438	2.769	0.002	QE	22	LYS
1439	1.339	0.000	QD	22	LYS
1440	0.851	0.001	HG2	22	LYS
1441	0.686	0.001	HG3	22	LYS
1442	24.348	0.000	CG	86	LYS
1444	41.883	0.000	CE	86	LYS
1445	2.831	0.000	QE	86	LYS
1446	29.648	0.000	CD	86	LYS
1447	25.694	0.000	CG	98	LEU
1448	22.455	0.000	CD2	98	LEU
1449	25.508	0.000	CD1	98	LEU
1450	2.106	0.001	HG	98	LEU
1452	33.202	0.000	CG	16	GLN
1453	2.604	0.000	HG2	16	GLN
1454	2.444	0.000	HG3	16	GLN
1455	26.849	0.000	CG	64	LEU
1456	24.353	0.000	CD1	64	LEU
1457	24.438	0.000	CD2	64	LEU
1458	0.637	0.004	QQD	64	LEU
1459	0.373	0.006	HG	64	LEU
1460	24.726	0.000	CG	32	LEU
1461	23.361	0.000	CD1	32	LEU
1462	20.335	0.000	CD2	32	LEU
1463	0.379	0.000	HG	32	LEU
1464	-0.761	0.002	QD2	32	LEU
1465	-0.869	0.004	QD1	32	LEU
1466	3.005	0.000	HB2	10	PHE
1467	2.890	0.000	HB3	10	PHE
1468	25.344	0.000	CG	87	LYS
1469	29.020	0.000	CD	87	LYS
1470	41.848	0.000	CE	87	LYS
1471	1.539	0.002	HG2	87	LYS
1472	1.391	0.002	HG3	87	LYS
1473	1.641	0.001	QD	87	LYS
1474	2.913	0.001	QE	87	LYS
1475	1.600	0.001	QD	53	LYS
1476	1.444	0.001	QG	53	LYS
1477	2.839	0.001	QE	53	LYS
1478	41.739	0.000	CE	5	LYS
1479	26.024	0.000	CG	5	LYS
1480	28.801	0.000	CD	5	LYS
1482	1.458	0.005	HG2	5	LYS
1483	1.304	0.000	HG3	5	LYS
1484	2.883	0.002	QE	5	LYS
1485	28.716	0.000	CG	94	LEU
1486	27.558	0.000	CD1	94	LEU
1487	24.198	0.000	CD2	94	LEU
1488	1.415	0.002	HG	94	LEU
1489	26.428	0.000	CD	13	LYS
1490	29.458	0.000	CG	13	LYS
1491	42.303	0.000	CE	13	LYS
1492	2.399	0.000	HB2	13	LYS
1493	2.221	0.000	HB3	13	LYS
1494	1.671	0.001	QD	13	LYS
1495	1.908	0.001	HG2	13	LYS
1496	1.785	0.001	HG3	13	LYS
1497	3.103	0.001	HE2	13	LYS
1498	3.069	0.001	HE3	13	LYS
1499	23.584	0.000	CG2	63	THR
1500	1.276	0.002	QG2	63	THR
1501	25.795	0.000	CG	68	LEU
1502	0.967	0.001	HG	68	LEU
1503	21.682	0.000	CD1	68	LEU
1504	21.583	0.000	CD2	68	LEU
1505	0.215	0.004	QQD	68	LEU
1506	24.281	0.000	CG	25	LYS
1507	28.514	0.000	CD	25	LYS
1508	41.714	0.000	CE	25	LYS
1509	2.797	0.000	QE	25	LYS
1510	1.451	0.000	QD	25	LYS
1511	1.216	0.000	QG	25	LYS
1512	31.430	0.000	CG	12	MET
1513	2.136	0.003	HB3	12	MET
1514	2.250	0.002	HB2	12	MET
1515	2.731	0.002	HG2	12	MET
1516	2.575	0.003	HG3	12	MET
1517	33.733	0.000	CG	42	GLN
1518	2.145	0.000	HG3	42	GLN
1519	2.206	0.000	HG2	42	GLN
1520	32.089	0.000	CG	65	MET
1521	2.766	0.000	HG2	65	MET
1522	2.542	0.001	HG3	65	MET
1523	43.817	0.005	CD	91	ARG

1524	29.904	0.000	CG	91	ARG
1526	3.113	0.001	HB2	74	TYR
1527	3.001	0.000	HB3	74	TYR
1528	26.652	0.000	CG	35	LEU
1529	26.583	0.000	CD1	35	LEU
1530	23.869	0.000	CD2	35	LEU
1531	1.115	0.008	HG	35	LEU
1533	41.830	0.000	CE	8	LYS
1534	25.179	0.000	CG	8	LYS
1535	29.001	0.000	CD	8	LYS
1537	2.884	0.001	QE	8	LYS
1538	2.713	0.001	QE	73	LYS
1539	1.515	0.000	QD	73	LYS
1540	24.236	0.000	CG	100	LYS
1541	29.587	0.000	CD	100	LYS
1542	2.885	0.003	QE	100	LYS
1543	24.417	0.000	CG	72	LYS
1544	29.146	0.000	CD	72	LYS
1545	41.563	0.000	CE	72	LYS
1546	1.507	0.001	HB2	72	LYS
1547	1.398	0.001	HB3	72	LYS
1548	2.701	0.001	QE	72	LYS
1549	1.383	0.001	QD	72	LYS
1550	1.158	0.003	HG2	72	LYS
1551	1.084	0.001	HG3	72	LYS
1552	3.765	0.001	HA	20	VAL
1553	21.700	0.000	CG1	20	VAL
1554	18.074	0.000	CG2	20	VAL
1555	1.426	0.000	HB	20	VAL
1556	-0.138	0.001	QG1	20	VAL
1557	0.278	0.001	QG2	20	VAL
1558	1.673	0.003	HB	83	VAL
1559	3.286	0.001	HA	83	VAL
1560	19.775	0.000	CG1	83	VAL
1561	19.675	0.000	CG2	83	VAL
1562	0.613	0.002	QQG	83	VAL
1563	1.290	0.000	QB	43	ALA
1564	4.463	0.002	HA	40	THR
1565	22.233	0.000	CG2	40	THR
1566	4.214	0.001	HB	40	THR
1567	0.825	0.003	QG2	40	THR
1568	4.067	0.001	HA	75	ILE
1569	27.194	0.000	CG1	75	ILE
1570	17.807	0.000	CG2	75	ILE
1571	12.517	0.000	CD1	75	ILE
1572	1.770	0.003	HB	75	ILE
1574	0.603	0.000	QG2	75	ILE
1575	0.777	0.000	QD1	75	ILE
1576	0.627	0.004	QG1	75	ILE
1577	4.226	0.001	HA	78	THR
1578	18.913	0.000	CG2	78	THR
1579	4.135	0.001	HA	104	GLU
1580	35.972	0.000	CG	104	GLU
1583	1.886	0.001	HB2	104	GLU
1584	1.810	0.001	HB3	104	GLU
1585	3.316	0.002	HA	11	ILE
1586	28.669	0.000	CG1	11	ILE
1587	16.179	0.000	CG2	11	ILE
1588	12.748	0.000	CD1	11	ILE
1589	1.862	0.002	HB	11	ILE
1590	1.773	0.002	HG12	11	ILE
1591	1.181	0.002	HG13	11	ILE
1592	0.804	0.000	QG2	11	ILE
1593	0.740	0.000	QD1	11	ILE
1594	3.847	0.002	HA3	34	GLY
1595	3.638	0.001	HA2	34	GLY
1596	0.572	0.002	QD2	35	LEU
1597	0.704	0.001	QD1	35	LEU
1598	3.704	0.001	HA3	29	GLY
1599	-0.072	0.002	HA2	29	GLY
1600	4.370	0.000	HA	27	LYS
1601	3.700	0.001	HA3	41	GLY
1602	3.591	0.001	HA2	41	GLY
1603	4.536	0.000	HA	43	ALA
1604	4.192	0.000	HA	46	TYR
1605	2.720	0.000	QB	46	TYR
1606	1.360	0.002	QB	50	ALA
1607	4.166	0.001	HA	50	ALA
1608	4.329	0.000	HA	52	ASN
1609	39.253	0.000	CB	52	ASN
1610	2.825	0.001	HB3	52	ASN
1611	2.949	0.002	HB2	52	ASN
1612	4.131	0.001	HA	70	ASN

1613	2.682	0.002	QB	70	ASN
1614	2.316	0.001	HG2	90	GLU
1615	2.253	0.001	HG3	90	GLU
1616	0.672	0.000	QG2	78	THR
1617	4.167	0.001	HB	78	THR
1618	3.721	0.000	HA2	77	GLY
1619	3.852	0.001	HA3	77	GLY
1620	1.001	0.001	QQD	94	LEU
1621	1.019	0.001	QD1	98	LEU
1622	0.544	0.001	QD2	98	LEU
1623	2.169	0.002	QG	104	GLU
1624	3.266	0.001	HD2	91	ARG
1625	3.179	0.001	HD3	91	ARG
1626	1.706	0.001	HG2	91	ARG
1627	1.180	0.001	HG3	91	ARG
1628	58.867	0.000	CA	58	ILE
1629	38.504	0.000	CB	58	ILE
1630	177.495	0.000	C	58	ILE
1631	4.082	0.000	HA	58	ILE
1632	1.491	0.000	HB	58	ILE
1633	12.387	0.000	CD1	58	ILE
1634	17.084	0.000	CG2	58	ILE
1635	27.350	0.000	CG1	58	ILE
1636	1.351	0.001	HG12	58	ILE
1637	0.834	0.003	HG13	58	ILE
1638	0.613	0.002	QG2	58	ILE
1639	0.616	0.001	QD1	58	ILE
1644	3.860	0.000	HB2	15	SER
1645	3.621	0.000	HB3	15	SER
1646	3.768	0.006	HA	15	SER
1647	1.353	0.001	HG3	8	LYS
1648	1.531	0.001	HG2	8	LYS
1649	1.591	0.002	QD	8	LYS
1650	2.160	0.002	HA	7	LYS
1651	41.814	0.000	CE	7	LYS
1652	24.023	0.000	CG	7	LYS
1653	29.272	0.000	CD	7	LYS
1655	1.670	0.002	HB2	7	LYS
1656	1.324	0.005	HB3	7	LYS
1657	0.986	0.002	QD	7	LYS
1658	1.536	0.001	QG	7	LYS
1660	24.155	0.000	CG	27	LYS
1661	29.035	0.000	CD	27	LYS
1662	41.341	0.000	CE	27	LYS
1663	1.671	0.000	HB2	27	LYS
1664	0.964	0.000	HB3	27	LYS
1665	1.235	0.000	HD2	27	LYS
1666	1.011	0.000	HD3	27	LYS
1667	0.954	0.000	QG	27	LYS
1668	2.386	0.000	QE	27	LYS
1669	1.563	0.000	HB2	25	LYS
1670	1.379	0.000	HB3	25	LYS
1671	1.813	0.001	HB2	53	LYS
1672	1.742	0.002	HB3	53	LYS
1673	4.032	0.002	HA	55	LYS
1674	24.386	0.000	CG	55	LYS
1675	28.097	0.000	CD	55	LYS
1676	1.858	0.001	HB2	55	LYS
1677	1.646	0.001	HB3	55	LYS
1678	1.516	0.000	QG	55	LYS
1679	1.199	0.003	QG	73	LYS
1680	3.562	0.001	HA	88	LYS
1681	24.802	0.000	CG	88	LYS
1682	29.271	0.000	CD	88	LYS
1683	41.650	0.000	CE	88	LYS
1684	1.781	0.001	HB2	88	LYS
1685	1.699	0.001	HB3	88	LYS
1686	1.321	0.001	QG	88	LYS
1687	2.857	0.000	QE	88	LYS
1688	1.538	0.001	QD	88	LYS
1689	1.789	0.000	HB2	87	LYS
1690	1.674	0.001	HB3	87	LYS
1691	1.261	0.000	HG2	100	LYS
1692	1.119	0.001	HG3	100	LYS
1693	1.606	0.002	QD	100	LYS
1747	54.344	0.000	CA	31	ASN
1748	4.023	0.002	HA	31	ASN
1749	39.785	0.000	CB	31	ASN
1750	2.013	0.004	HB2	31	ASN
1751	1.919	0.002	HB3	31	ASN
1752	3.752	0.000	HA3	1	GLY
1753	42.567	0.000	CA	1	GLY
1754	3.341	0.000	HA2	1	GLY

1755	168.239	0.000	C	1	GLY
1756	176.303	0.000	C	31	ASN
1757	4.134	0.002	HA	21	GLU
1758	56.452	0.000	CA	21	GLU
1759	29.646	0.000	CB	21	GLU
1760	35.631	0.000	CG	21	GLU
1761	1.698	0.002	HB3	21	GLU
1762	1.752	0.002	HB2	21	GLU
1763	2.066	0.003	QG	21	GLU
1764	177.538	0.000	C	21	GLU
1765	67.083	0.000	CA	28	THR
1766	4.017	0.001	HA	28	THR
1767	69.766	0.000	CB	28	THR
1768	22.205	0.000	CG2	28	THR
1769	4.101	0.008	HB	28	THR
1770	1.917	0.003	QG2	28	THR
1771	174.931	0.000	C	28	THR
1772	55.526	0.000	CA	79	LYS
1773	4.381	0.001	HA	79	LYS
1774	32.303	0.000	CB	79	LYS
1776	42.195	0.000	CE	79	LYS
1777	24.902	0.000	CG	79	LYS
1778	29.109	0.000	CD	79	LYS
1779	2.131	0.001	HB2	79	LYS
1780	2.072	0.001	HB3	79	LYS
1781	1.784	0.001	HG2	79	LYS
1782	1.605	0.000	HG3	79	LYS
1783	1.876	0.000	HD2	79	LYS
1784	1.792	0.000	HD3	79	LYS
1785	3.440	0.000	HE2	79	LYS
1786	3.233	0.000	HE3	79	LYS
1787	175.845	0.000	C	79	LYS
1788	38.366	0.000	CB	57	ILE
1789	1.471	0.001	HB	57	ILE
1790	58.621	0.000	CA	57	ILE
1791	4.042	0.001	HA	57	ILE
1792	12.910	0.000	CD1	57	ILE
1793	17.095	0.000	CG2	57	ILE
1794	27.181	0.000	CG1	57	ILE
1796	0.306	0.000	QG2	57	ILE
1797	-0.363	0.000	QD1	57	ILE
1798	173.923	0.000	C	57	ILE
1803	42.836	0.000	CA	84	GLY
1804	4.194	0.001	HA3	84	GLY
1805	2.851	0.001	HA2	84	GLY
1806	172.113	0.000	C	84	GLY
1807	64.021	0.000	CA	76	PRO
1808	4.477	0.001	HA	76	PRO
1809	31.137	0.000	CB	76	PRO
1810	27.154	0.000	CG	76	PRO
1811	49.303	0.009	CD	76	PRO
1812	2.110	0.001	HB2	76	PRO
1813	1.622	0.001	HB3	76	PRO
1814	1.846	0.000	HG2	76	PRO
1815	1.777	0.000	HG3	76	PRO
1816	3.330	0.001	HD2	76	PRO
1817	3.129	0.001	HD3	76	PRO
1818	178.583	0.000	C	76	PRO
1819	65.672	0.000	CA	71	PRO
1820	3.517	0.001	HA	71	PRO
1821	29.935	0.000	CB	71	PRO
1822	26.324	0.000	CG	71	PRO
1823	48.776	0.000	CD	71	PRO
1824	2.674	0.003	HD3	71	PRO
1825	2.971	0.002	HD2	71	PRO
1826	0.605	0.000	HG2	71	PRO
1827	-0.006	0.001	HG3	71	PRO
1828	0.786	0.002	HB2	71	PRO
1829	0.277	0.002	HB3	71	PRO
1830	176.414	0.000	C	71	PRO
1831	45.350	0.000	CA	45	GLY
1832	4.098	0.001	HA3	45	GLY
1833	3.723	0.001	HA2	45	GLY
1834	173.301	0.000	C	45	GLY
1835	61.555	0.000	CA	49	THR
1836	4.330	0.001	HA	49	THR
1837	21.696	0.000	CG2	49	THR
1838	70.660	0.000	CB	49	THR
1839	4.445	0.000	HB	49	THR
1840	1.377	0.000	QG2	49	THR
1841	1.253	0.000	QB	51	ALA
1842	18.249	0.000	CB	51	ALA
1843	53.932	0.000	CA	51	ALA

1844	3.993	0.001	HA	51	ALA
1845	6.957	0.000	HE21	16	GLN
1846	7.559	0.000	HE22	16	GLN
1849	10.179	0.000	HE1	59	TRP
1850	6.404	0.002	HD21	103	ASN
1851	7.807	0.001	HD22	103	ASN
1852	9.464	0.000	HD1	18	HIS
1853	7.660	0.002	HD22	70	ASN
1854	6.570	0.002	HD21	70	ASN
1855	6.491	0.000	HD2	97	TYR
1856	7.040	0.000	HD1	97	TYR
1857	5.457	0.000	HE2	97	TYR
1858	6.599	0.000	HE1	97	TYR
1859	6.856	0.000	HD2	10	PHE
1860	6.027	0.000	HE1	10	PHE
1861	6.928	0.000	HE2	10	PHE
1862	6.093	0.000	HZ	10	PHE
1863	0.010	0.004	HD2	18	HIS
1864	6.773	0.000	QE	36	PHE
1865	7.305	0.000	QD	36	PHE
1866	6.744	0.000	QD	46	TYR
1867	6.889	0.000	HD1	59	TRP
1868	7.472	0.005	HE3	59	TRP
1869	6.532	0.004	HZ3	59	TRP
1870	6.536	0.000	QE	67	TYR
1871	7.091	0.000	QD	67	TYR
1872	6.507	0.000	QE	74	TYR
1873	7.105	0.000	QD	74	TYR
1874	6.580	0.000	QD	82	PHE
1876	7.276	0.000	QE	82	PHE
1877	7.106	0.000	HZ	82	PHE
1878	111.391	0.000	NE2	16	GLN
1879	111.664	0.005	ND2	70	ASN
1880	111.964	0.000	ND2	54	ASN
1881	7.423	0.001	HD22	54	ASN
1882	6.854	0.000	HD21	54	ASN
1883	112.579	0.000	NE2	42	GLN
1884	7.470	0.000	HE22	42	GLN
1885	6.783	0.000	HE21	42	GLN
1886	114.098	0.000	ND2	103	ASN
1887	115.086	0.005	ND2	31	ASN
1888	7.325	0.000	HD21	31	ASN
1889	7.924	0.002	HD22	31	ASN
1890	127.918	0.000	NE1	59	TRP
1891	6.230	0.000	HE	38	ARG
1892	-3.750	0.000	HG3	80	MET
1893	-2.050	0.000	HG2	80	MET
1894	3.342	0.000	QM5	105	HEM
1895	9.530	0.008	HBM	105	HEM
1896	2.461	0.001	QT4	105	HEM
1897	6.272	0.000	HT4A	105	HEM
1898	3.735	0.000	QM3	105	HEM
1899	9.167	0.000	HAM	105	HEM
1900	1.380	0.000	QT2	105	HEM
1901	5.109	0.000	HT2A	105	HEM
1902	3.403	0.000	QM1	105	HEM
1903	8.884	0.000	HDM	105	HEM
1904	2.057	0.000	QM8	105	HEM
1905	4.062	0.000	HA71	105	HEM
1906	3.311	0.000	HA72	105	HEM
1907	999.000	0.000	QA7	105	HEM
1908	2.346	0.000	HB73	105	HEM
1909	3.001	0.000	HB74	105	HEM
1910	999.000	0.000	QB7	105	HEM
1911	9.571	0.000	HGM	105	HEM
1912	4.389	0.000	QA6	105	HEM
1913	999.000	0.000	HA62	105	HEM
1914	999.000	0.000	HA61	105	HEM
1915	3.680	0.000	HB63	105	HEM
1916	2.580	0.000	HB64	105	HEM
1917	999.000	0.000	QB6	105	HEM
1918	-3.429	0.000	QE	80	MET
1919	5.578	0.003	HH2	59	TRP
1920	6.956	0.002	HZ2	59	TRP
1921	0.381	0.000	HE1	18	HIS
3000	999.000	0.000	HD2	48	CMF
3001	999.000	0.000	HD1	48	CMF
3002	7.206	0.000	QD	48	CMF
3003	7.165	0.000	QE	48	CMF
3004	999.000	0.000	HB2	48	CMF
3005	999.000	0.000	HB3	48	CMF
3006	6.948	0.000	HD1	26	HIS
3008	6.730	0.003	HD2	26	HIS

3009	999.000	0.000	QHH	48	CMF
3010	175.638	0.000	C	40	THR
3011	178.294	0.000	C	44	PRO
3012	175.235	0.000	C	49	THR
3013	178.634	0.000	C	51	ALA
3014	176.255	0.000	C	52	ASN
3099	999.000	0.000	H	48	CMF
3100	6.206	0.000	HE	91	ARG
3101	6.579	0.000	H	47	SER
3102	4.151	0.000	HA	47	SER
3103	3.486	0.001	QB	47	SER
5000	3.590	0.000	HA	30	PRO
5001	1.230	0.000	QB	30	PRO
5002	0.733	0.000	QG	30	PRO
5003	2.540	0.001	HD2	30	PRO
5004	1.516	0.000	HD3	30	PRO
5011	6.704	0.000	QE	46	TYR
5020	10.198	0.000	H	31	ASN
5021	60.269	0.000	CA	30	PRO
5022	31.020	0.000	CB	30	PRO
5023	26.377	0.000	CG	30	PRO
5024	48.500	0.000	CD	30	PRO
5100	7.285	0.000	HE1	33	HIS
7000	0.752	0.005	HG12	57	ILE
7001	0.806	0.000	HG13	57	ILE
7002	7.076	0.000	HD1	10	PHE
7004	112.024	0.000	N	45	GLY
7005	8.831	0.000	H	45	GLY
8000	4.356	0.000	HA	44	PRO
8001	1.870	0.000	HB2	44	PRO
8002	2.147	0.000	HB3	44	PRO
8003	1.934	0.000	HG2	44	PRO
8004	2.064	0.000	HG3	44	PRO
8005	3.658	0.000	HD2	44	PRO
8006	3.949	0.000	HD3	44	PRO
8007	63.456	0.000	CA	44	PRO
8008	31.514	0.000	CB	44	PRO
8009	50.659	0.000	CD	44	PRO
8010	27.383	0.000	CG	44	PRO
8021	46.052	0.000	CA	56	GLY
8022	3.748	0.000	HA2	56	GLY
8023	3.637	0.000	HA3	56	GLY

stop\_



